Bright field

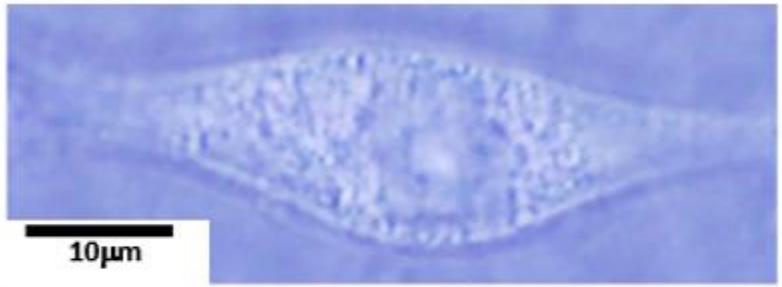

Raman imaging

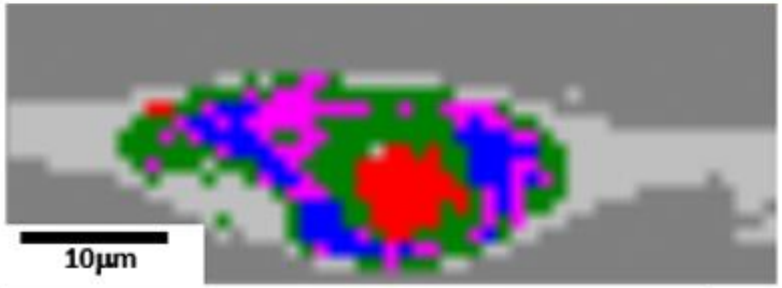

Fluorescence imaging of Oil Red O

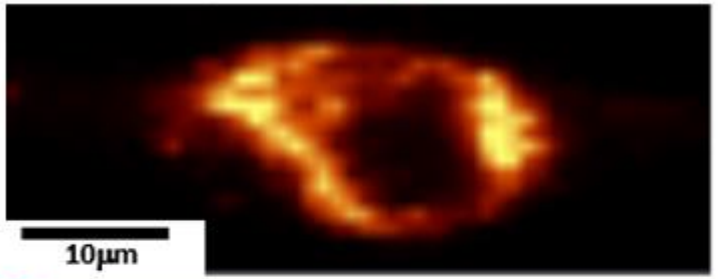

Bright field after lipid staining with Oil Red O

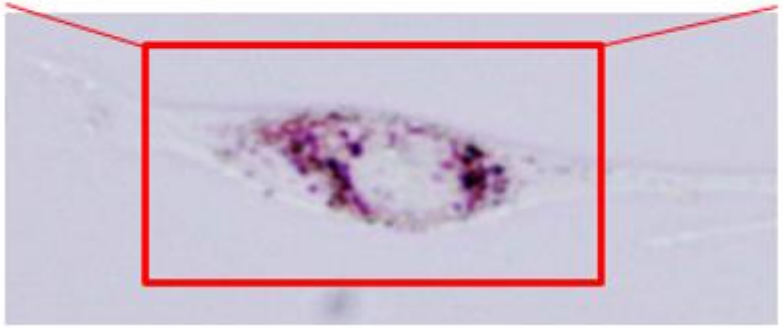

LINEAR AND NONLINEAR OPTICS IN CANCER RESEARCH. THE FUTURE OF MEDICAL DIAGNOSTICS

Halina Abramczyk
Lodz University of Technology, Laboratory of Laser Molecular Spectroscopy
Poland
http://mitr.p.lodz.pl/raman/

LODZ UNIVERSITY OF TECHNOLOGY, FACULTY OF CHEMISTRY , LABORATORY OF LASER MOLECULAR SPECTROSCOPY, LODZ, POLAND

mitr.p.lodz.pl/raman

Jacek Musiał[2] Radzislaw Kordek[2]
Alina Morawiec-Sztandera[2] Krystyna Fabianowska[2]
Eric Freysz[3] Lech Polis[4] Bartosz Polis[4]

[2]Medical University of Lodz, Department of Pathology, Chair of Oncology, Paderewskiego 4, 93-509 Lodz, Poland

[3] Laboratoire Ondes et Matière d'Aquitaine (LOMA), UMR 5798 Université Bordeaux 1, France

[4] Polish Mother's Memorial Hospital Research Institute, Department of Neurosurgery and Neurotraumatology, 3-338 Lodz, Poland

Lodz University of Technology, Faculty of Chemistry ,
Laboratory of Laser Molecular Spectroscopy, Lodz, Poland

COOPERATION WITH MEDICAL CENTERS

Uniwersytet Medyczny w Łodzi
Katedra Onkologii
Prof. dr hab. n med. Radzisław Kordek
Dr n med. Jacek Musiał

WSS i M. Kopernika w Łodzi
Prof. dr hab. n med. Z. Morawiec
Lekarz med. Marek Tazbir

mitr.p.lodz.pl/raman

Uniwersytecki Szpital Kliniczny im. WAM – Centralny Szpital Weteranów
Prof. dr hab. n. med. Adam Dziki

Uniwersytet Medyczny w Łodzi
Klinika Chirurgii Nowotworów Głowy i Szyi
Oddział Laryngologii Onkologicznej –
Regionalny Ośrodek Onkologiczny
Wojewódzkiego Szpitala Specjalistycznego i
m. Kopernika

Prof. dr hab. n med. Alina Morawiec-Sztandera
Dr n med. Izabela Niedźwiecka

Instytut Centrum Zdrowia Matki Polki w Łodzi
Prof. dr hab. n. med. Lech Polis
Dr n. med. Bartosz Polis

LABORATORY OF LASER MOLECULAR SPECTROSCOPY www.mitr.p.lodz.pl/raman

Laboratory of Raman spectroscopy

Ramanor U 1000 (Jobin Yvon), 488-514nm

Raman confocal microscope (Renishaw)

Laboratory of Raman imaging

Microscope Raman/AFM/SNOM/TERS

Laboratory of IR imaging

FTIR microscope (Agilent Technologies Cary 600 Series)

Laboratory of femtosecond spectroscopy

Millennia, Tsunami, Empower30, Spitfire Ace, Topas (Spectra Physics)

H. Abramczyk, B. Brozek-Pluska, *Chem. Rev.* 113 (2013) 5766-7581

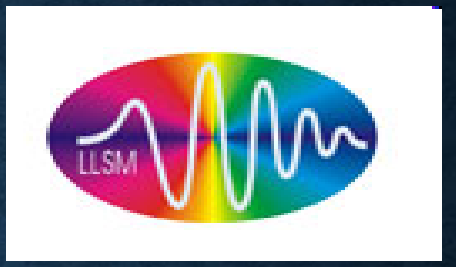

CHEMICAL REVIEWS

2013

IF = 41,298

Review

pubs.acs.org/CR

Raman Imaging in Biochemical and Biomedical Applications. Diagnosis and Treatment of Breast Cancer

Halina Abramczyk* and Beata Brozek-Pluska

Laboratory of Laser Molecular Spectroscopy, Institute of Applied Radiation Chemistry, Lodz University of Technology, Wroblewskiego 15, 93-590 Lodz, Poland

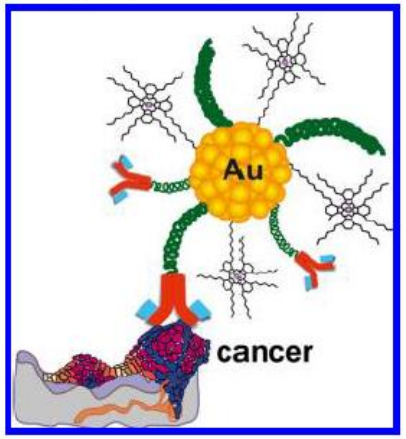

The field of cancer diagnostics has become so huge that it is impossible to touch the whole field in a single lecture. Therefore, I have selected only a few topics , giving preference only to those which were directly related to our personal contribution: The views expressed in this lecture are highly personal, in the sense that they are based either on my own laboratory work recently , or on the work I am familiar with

WHAT?

Human normal and cancerous breast tissue, brain, neck and head , intestine tissues

Cell human Lines: breast normal (MCF-10A,) and cancerous epithelial : (MCF-7, MDA-MB-231) and brain glial cells: NHA Astrocytes CC2565), astrocytoma (CCF-STTG1 (ATCC CLR1718) and glioblastoma (U87MG) (ATCC® HTB-14)

In vivo animal models (brain)

Drugs (temodal,erlotinib) and photosensitizers in cancer therapy

BIOMEDICAL APPLICATION

- High spatial resolution RAMAN IMAGING
- SNOM microscopy (far below the diffraction limit, SNOM)
- Strong signal enhancement enabling monitoring the genetic and immunological responses in biological systems (SERS COMBINED WITH NANOPARTICLES)
- Specificity of interactions (BIOCONJUGATES)
- AFM topography, stiffness, adhesion, Young modulus (AFM)
- High temporal resolution (FEMTOSECOND PUMP-PROBE SPECTROSCOPY)

Patients Statistics- breast

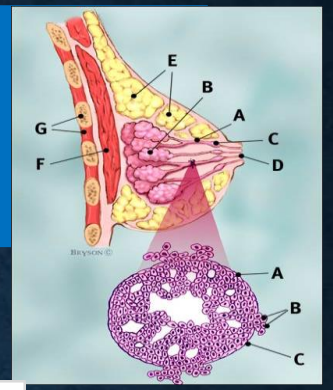

❖250 patients

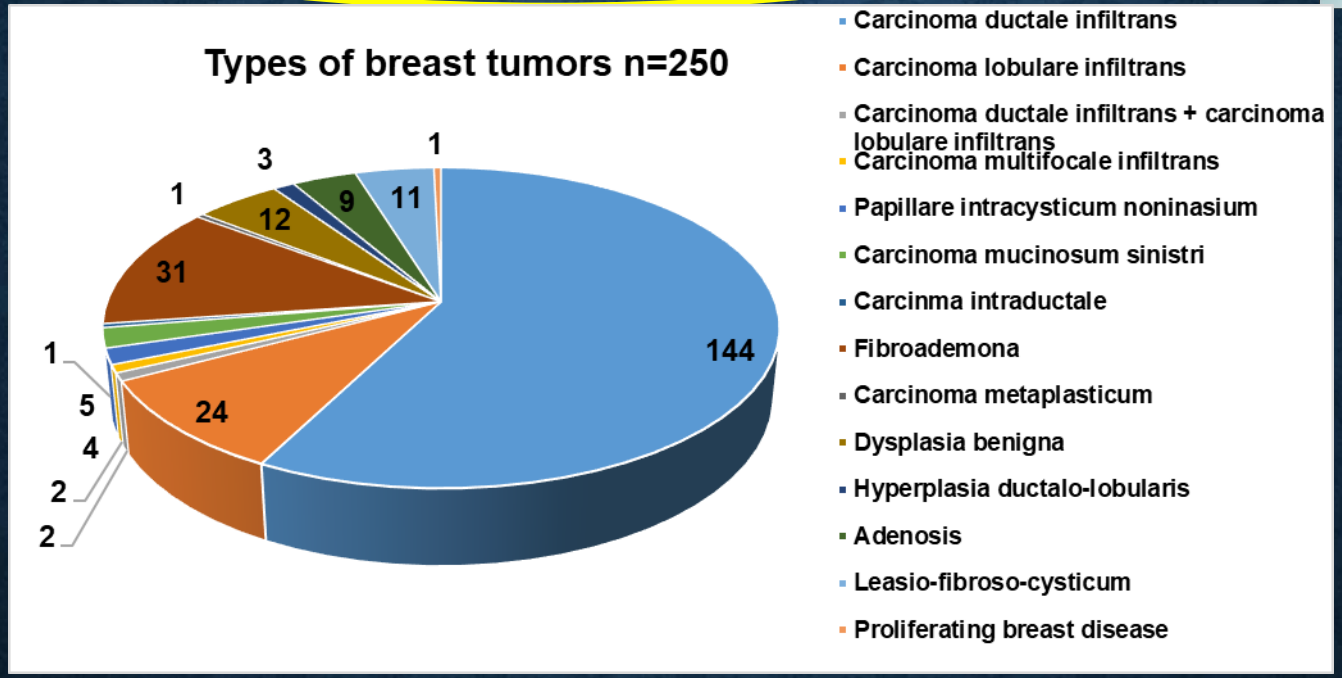

The pathology reports indicated that 70% of the cancer samples were ductal carcinomas; the remaining samples were lobular or untyped mammary carcinomas, metastases were found in 60% of patients

We will deal with epithelial cancer types. Most cancers have epithelial origin and they represent approximately 80-85% of all cancers.[38]

PATIENTS STATISTICS-BRAIN

42 patients

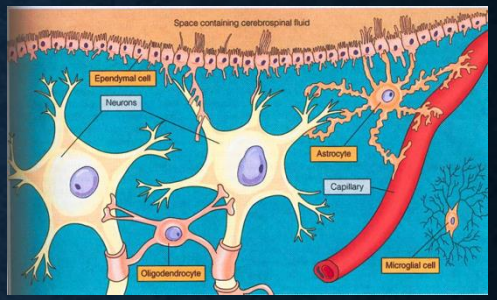

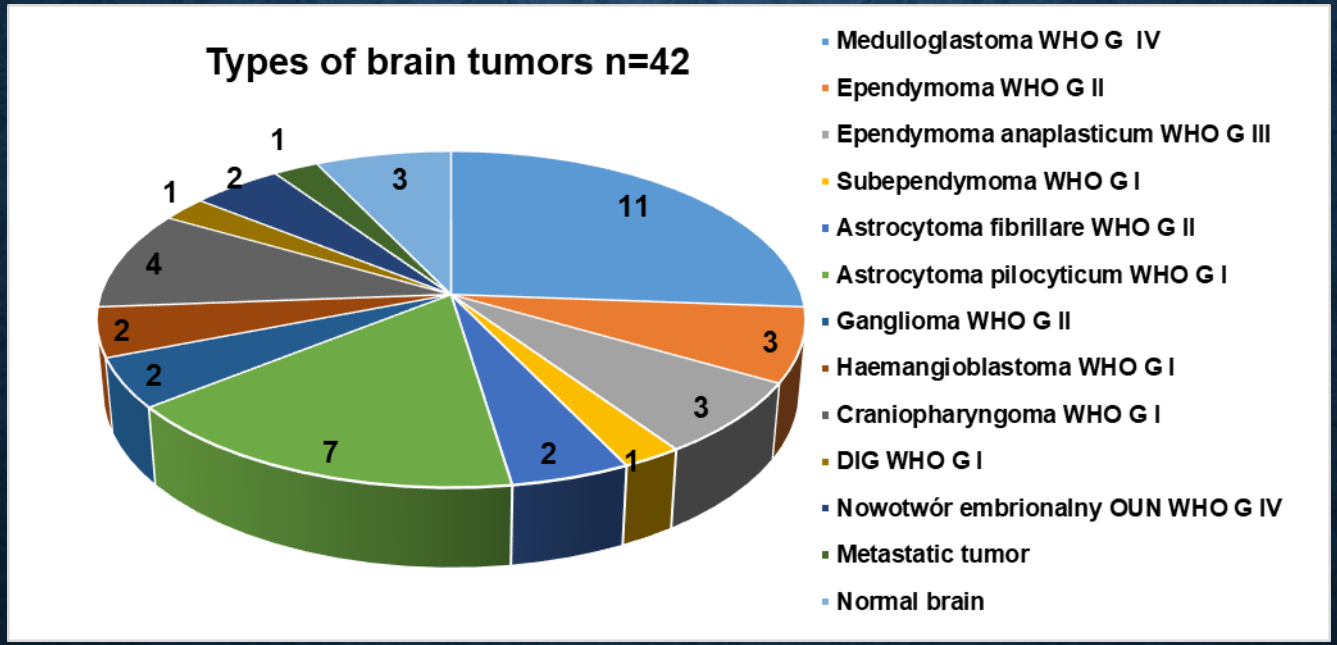

The epithelium cells cover the body and lines in the majority of organs, such as the milk ducts in the breast gland or the digestive tract and are involved in the absorption of food, although it is just only one of the many features of epithelia.[37] The cells lining the brain called ependymocytes, are a type of glial cells, covering the walls of the ventricular system of the brain: the brain ventricles and the central tube of the spinal cord. They are involved in the exchange of material between the cerebrospinal fluid and nervous tissue and, unlike epithelial cells, have no basal membrane. Despite these differences, for simplicity both groups will be called

PATIENTS STATISTICS- INTESTINE

40 patients

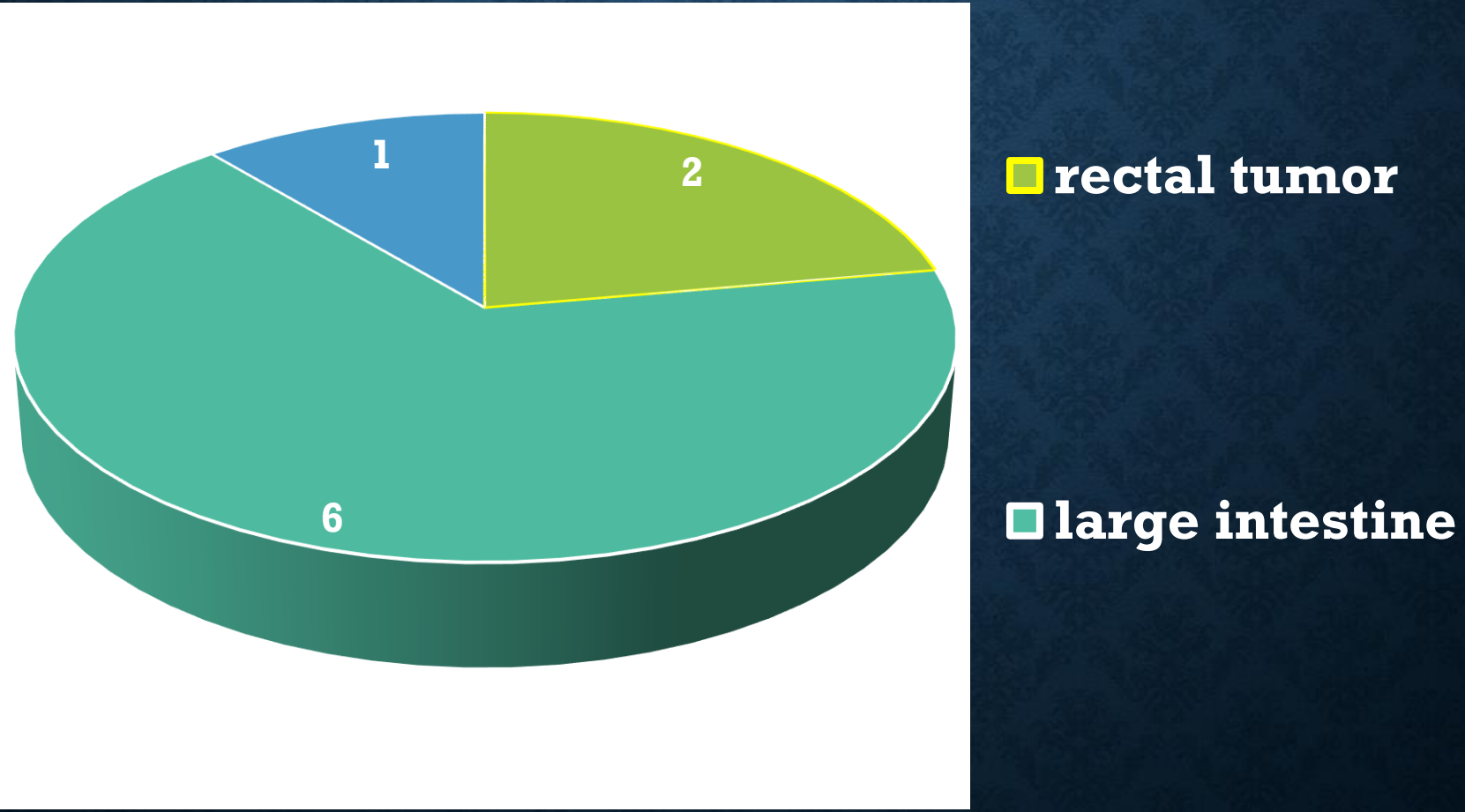

PATIENTS STATISTICS-HEAD AND NECK

14 patients

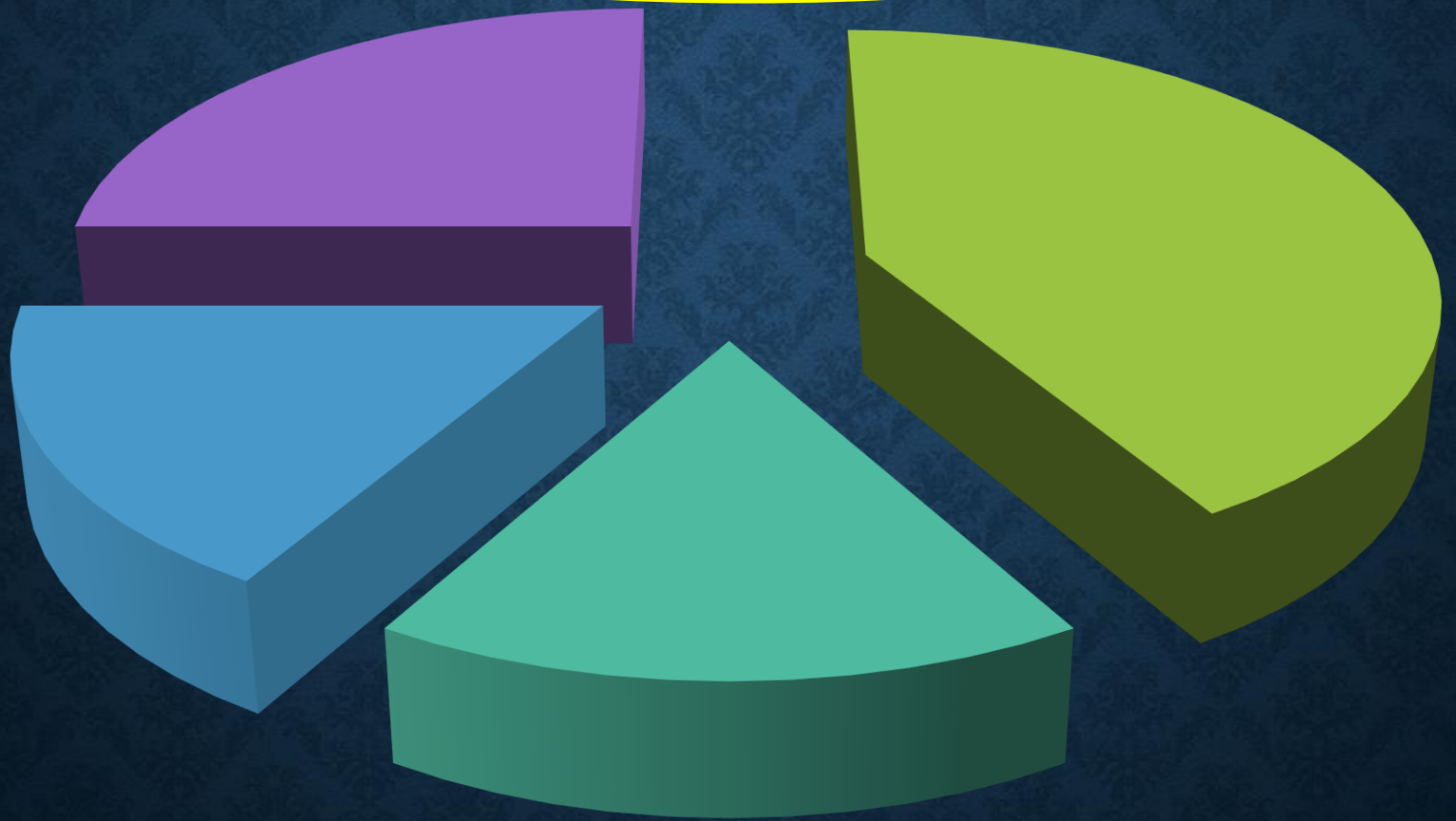

The epithelium cells cover the body and lines in the majority of organs, such as the milk ducts in the breast gland or the digestive tract and are involved in the absorption of food, although it is just only one of the many features of epithelia.[37] The cells lining the brain called ependymocytes, are a type of glial cells, covering the walls of the ventricular system of the brain: the brain ventricles and the central tube of the spinal cord. They are involved in the exchange of material between the cerebrospinal fluid and nervous tissue and, unlike epithelial cells, have no basal membrane. Despite these differences, for simplicity both groups will be called

LINEAR AND NONLINEAR OPTICS IN CANCER RESEARCH

$$P_i = \chi_{ij}^{(1)} E + \chi_{ijk}^{(2)} E_j E_k + \chi_{ijkl}^{(3)} E_j E_k E_l$$

- Nonlinear microscopy
- Basic principles The theoretical basis for non-linear microscopy was established in 1931 by Maria GöppertMayer, who mathematically showed the possibility for two-photon adsorption and its quadratic dependency on the intensity of light [175] (English translation: [176]). In 1977, with the development of more powerful light sources, this process could be utilized for image generation [177]. Along with the construction of pulsed lasers with high peak-powers, more nonlinear processes could be explored and employed.
- Nonlinear optics as a discipline is set apart from linear optics, the class of light-matter interactions behind everyday effects like rainbows, cameras, or telescopes that is also the basis of epifluorescence microscopy and CLSM. These interactions occur with natural, low
- light intensities and physical parameters describing them depend linearly on the incident light electric field amplitude (and therefore intensity). A much higher light intensity is needed to trigger light-matter interactions classified as nonlinear. In such processes, the induced polarization in a material with caused by the incident electric field (light) is no longer linearly dependent on the field amplitude.
- The theory behind nonlinear optics in general, and specifically coherent Raman scattering has been described in detail in textbooks [178], [179]. Briefly, the induced macroscopic polarization P of the electric dipoles in a material depends on the strength of the applied optical field E. For weak electric fields (compared to the fields binding electrons to the nucleus), this relation can be formulated in a linear dependence as:
- $P=\varepsilon\ \chi\ E$
- eq. 1 where ε is the electric permittivity in vacuum and χ the linear susceptibility of the material. For stronger fields, P can be expanded as a power series:
- $P=\varepsilon\ [\chi(1)\ E+\chi\ (2)EE+\chi\ (3)EEE+\cdots] = P1+P2+P3+\cdots$
- where χ is the nth order susceptibility. P is the nth order polarization. The physical processes occurring as result of the second-order polarization differ from the third-order polarization. There is a multitude of processes that can occur in the nonlinear regime. The following sections focus on processes originating due to P or P as they commonly occur in biological samples. Due to the applied nature of this thesis the mathematics behind solutions for the prediction of P or P are omitted. Coherent

Technique	Spatial resolution[a]	Penetration depth[b]	Sensitivity to detect molecular markers[c]	Data density per pixel[d]	Data acquisition speed[e]	Primary contrast
CLSM/RLSM	✓✓✓	✓	✓	✓	✓✓✓	scattering, fluorescence
OCT	✓✓	✓✓	✓	✓	✓✓✓	scattering, polarization
PAI	✓✓	✓✓✓	✓	✓	✓✓	absorption
TPEF[f]	✓✓✓	✓✓	✓✓	✓✓	✓✓	fluorescence
SHG[f]	✓✓✓	✓✓	✓✓	✓✓	✓✓	noncentrosymmetry of molecular assemblies
FLIM[f]	✓✓✓	✓✓	✓✓	✓✓	✓✓	fluorescence lifetimes
Raman	✓✓✓	✓	✓✓✓	✓✓✓	✓	molecular vibrations
SRS	✓✓✓	✓✓	✓✓	✓✓✓	✓✓	molecular vibrations
CARS	✓✓✓	✓✓	✓✓	✓✓	✓✓	molecular vibrations

"Chemical Fingerprint"

LINEAR AND NONLINEAR PHENOMENA

$$P_i = \chi_{ij}^{(1)} E + \chi_{ijk}^{(2)} E_j E_k + \chi_{ijkl}^{(3)} E_j E_k E_l$$

CONFOCAL RAMAN MICROSCOPY

SECOND HARMONIC GENERATION (SHG)

STIMULATED RAMAN SCATTERING

Pump-probe transient absorption
Femtosecond spectroscopy

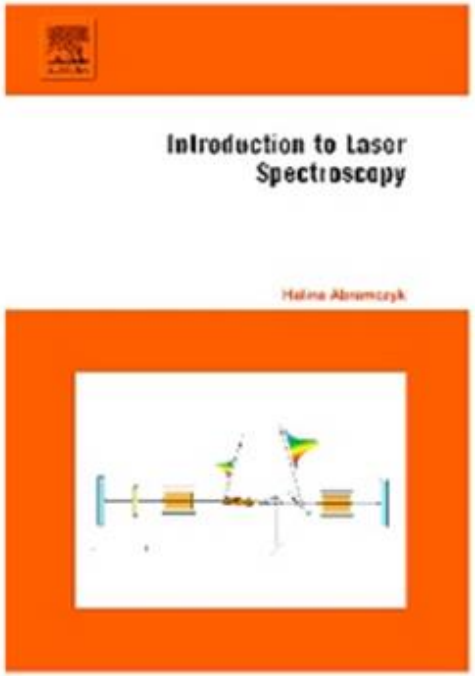

Introduction to Laser Spectroscopy

1st Edition

☆☆☆☆☆ Write a review

Authors: Halina Abramczyk

eBook ISBN: 9780080455259
Hardcover ISBN: 9780444516626

Imprint: Elsevier Science
Published Date: 6th May 2005

Page Count: 384

View on ScienceDirect ↗

Google Preview

HOW DOES RAMAN SPECTROSCOPY AND IMAGING BENEFIT CANCER RESEARCH?

•RAMAN BIOMARKERS OF CANCER

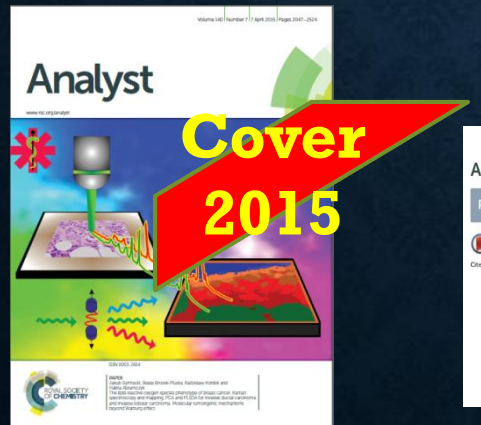

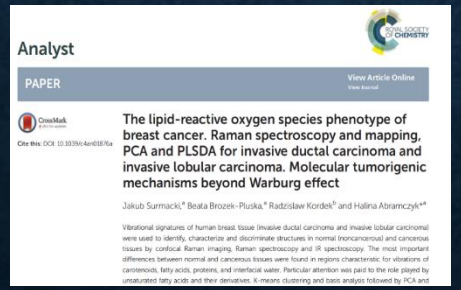
Analyst

PAPER

View Article Online

The lipid-reactive oxygen species phenotype of breast cancer. Raman spectroscopy and mapping, PCA and PLSDA for invasive ductal carcinoma and invasive lobular carcinoma. Molecular tumorigenic mechanisms beyond Warburg effect

Jakub Surmacki, Beata Brozek-Pluska, Radzisław Kordek and Halina Abramczyk

Surmacki J, Brozek-Pluska B, Kordek R, Abramczyk H, The lipid-reactive oxygen species phenotype of breast cancer. Raman spectroscopy and mapping, PCA and PLSDA for invasive ductal carcinoma and invasive lobular carcinoma. Molecular tumorigenic mechanisms beyond Warburg effect, Analyst, 2015, 140, 2121 – 2133, (IF=4.2)

HOW DOES RAMAN SPECTROSCOPY AND IMAGING BENEFIT CANCER RESEARCH?

•RAMAN OPTICAL BIOPSY

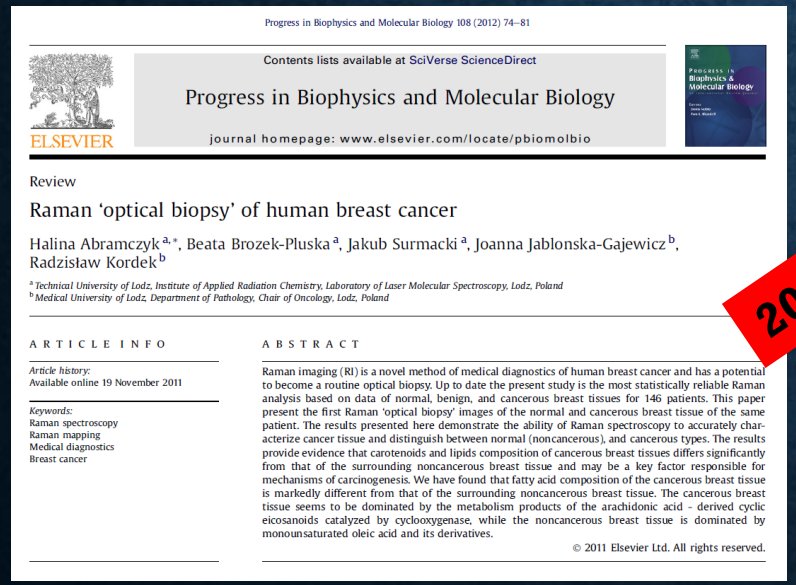

Progress in Biophysics and Molecular Biology 108 (2012) 74–81

Contents lists available at SciVerse ScienceDirect

Progress in Biophysics and Molecular Biology

journal homepage: www.elsevier.com/locate/pbiomolbio

Review

Raman 'optical biopsy' of human breast cancer

Halina Abramczyk [a,*], Beata Brozek-Pluska [a], Jakub Surmacki [a], Joanna Jablonska-Gajewicz [b], Radzisław Kordek [b]

[a] Technical University of Lodz, Institute of Applied Radiation Chemistry, Laboratory of Laser Molecular Spectroscopy, Lodz, Poland
[b] Medical University of Lodz, Department of Pathology, Chair of Oncology, Lodz, Poland

ARTICLE INFO

Article history:
Available online 19 November 2011

Keywords:
Raman spectroscopy
Raman mapping
Medical diagnostics
Breast cancer

ABSTRACT

Raman imaging (RI) is a novel method of medical diagnostics of human breast cancer and has a potential to become a routine optical biopsy. Up to date the present study is the most statistically reliable Raman analysis based on data of normal, benign, and cancerous breast tissues for 146 patients. This paper present the first Raman 'optical biopsy' images of the normal and cancerous breast tissue of the same patient. The results presented here demonstrate the ability of Raman spectroscopy to accurately characterize cancer tissue and distinguish between normal (noncancerous), and cancerous types. The results provide evidence that carotenoids and lipids composition of cancerous breast tissues differs significantly from that of the surrounding noncancerous breast tissue and may be a key factor responsible for mechanisms of carcinogenesis. We have found that fatty acid composition of the cancerous breast tissue is markedly different from that of the surrounding noncancerous breast tissue. The cancerous breast tissue seems to be dominated by the metabolism products of the arachidonic acid - derived cyclic eicosanoids catalyzed by cyclooxygenase, while the noncancerous breast tissue is dominated by monounsaturated oleic acid and its derivatives.

2012

H. Abramczyk, B. Brozek-Pluska, J. Surmacki, J. Jablonska-Gajewicz, R. Kordek, *PBMB* 108 (2012) 74-81

The completeness of the surgical resection is a key factor in the progress of patients with cancers. The safety margin can be positive which means that not all cancer cells have been removed in the surgery. Patients with a positive margin often require more surgery to make sure that all the cancer is removed. The advantage of the 'Raman biopsy' is that it provides direct biochemical information (vibrational fingerprint) in real time, it is not prone to subjective interpretations, and it monitors biological tissue without any external agents, in contrast to

VIRTUAL RAMAN HISTOPATHOLOGY IMAGE

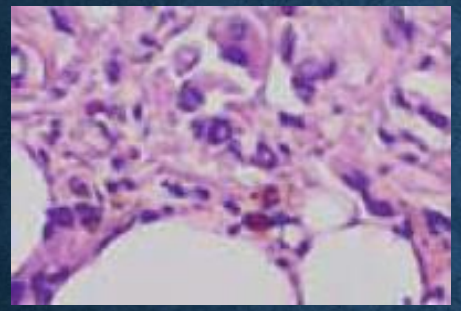

STANDARD H&E HISTOPATHOLOGY

RAMAN HISTOPATHOLOGY IMAGE

Abramczyk H et al., patent application

- **Fast histopathological analysis for clinical practice**
- **Label-free histopathological analysis (without any staining procedures)**
- **Real time diagnostics to access the safety margin during operation by** Raman-guided surgery
- **High spatial resolution (small cancer changes can be easy identified)**
- **Objective diagnosis (without human interpretation, Raman spectra)**
- **Discrimination of grades with high specificity and sensitivity (c.a. 90%)**
- **Monitoring of tumor tissue heterogenity**

RAMAN SPECTROSCOPY GUIDES IN VIVO BRAIN OPTICAL BIOPSIES

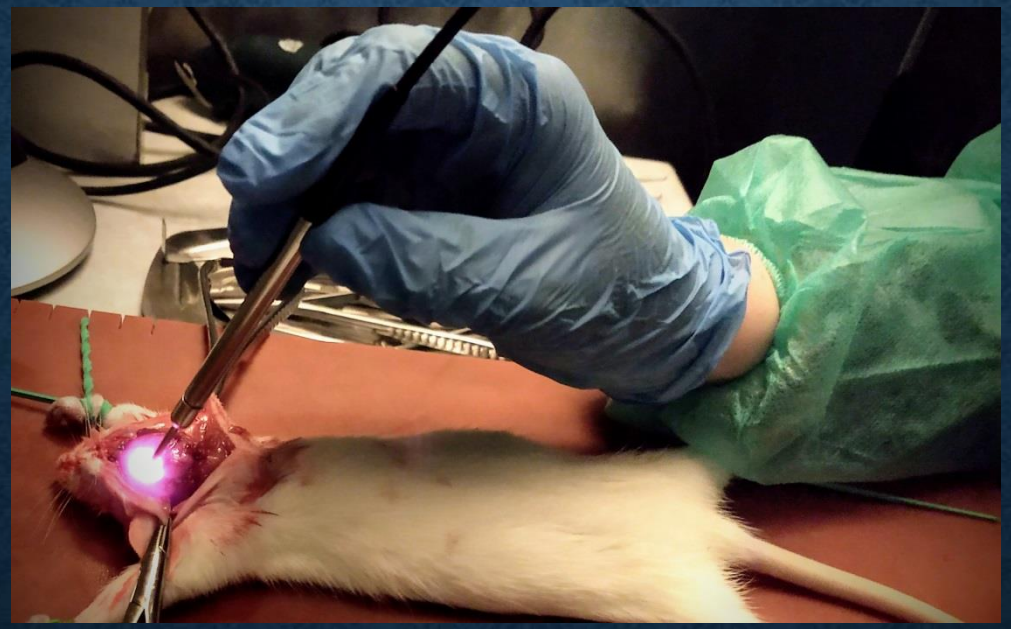

IN VIVO RAMAN OPTICAL BIOPSY ON RAT BRAIN IN LABORATORY OF LASER MOLECULAR SPECTROSCOPY

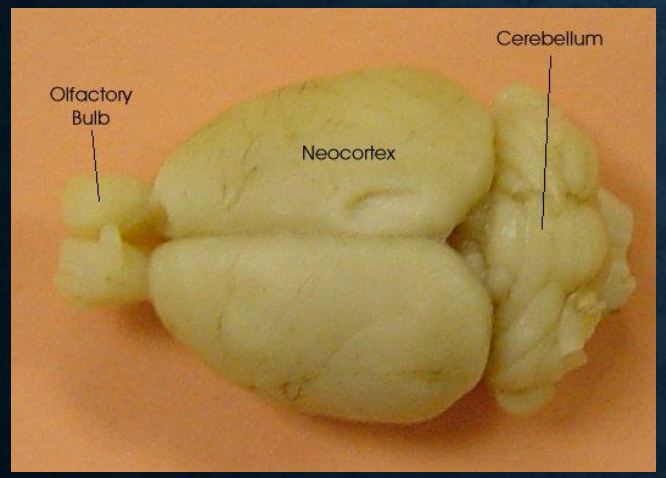

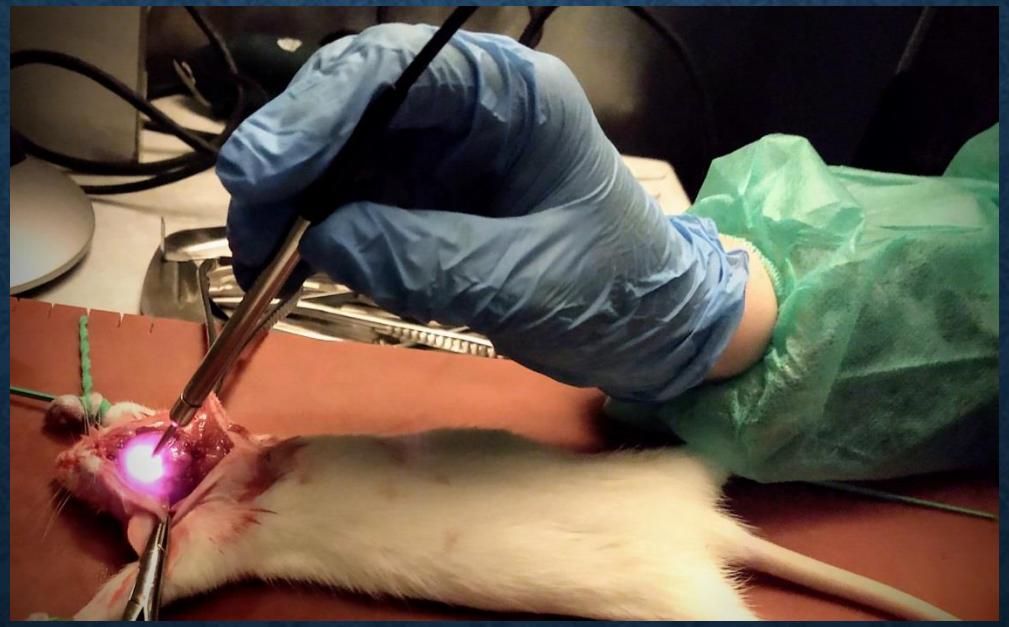

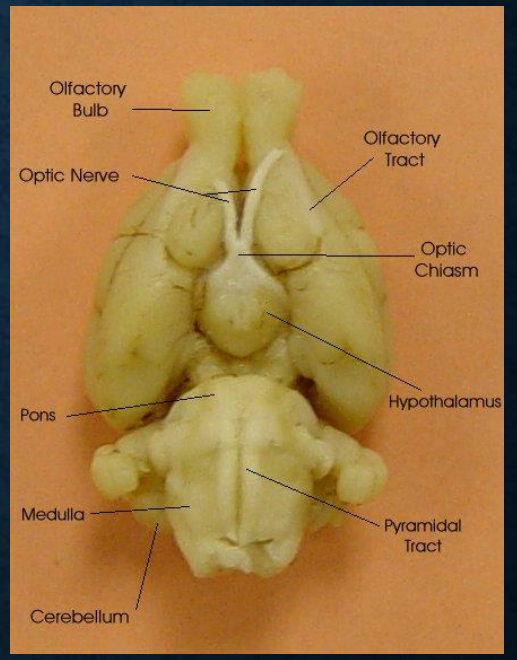

MOLECULAR SENSITIVITIES OF VARIOUS IMAGING MODALITIES

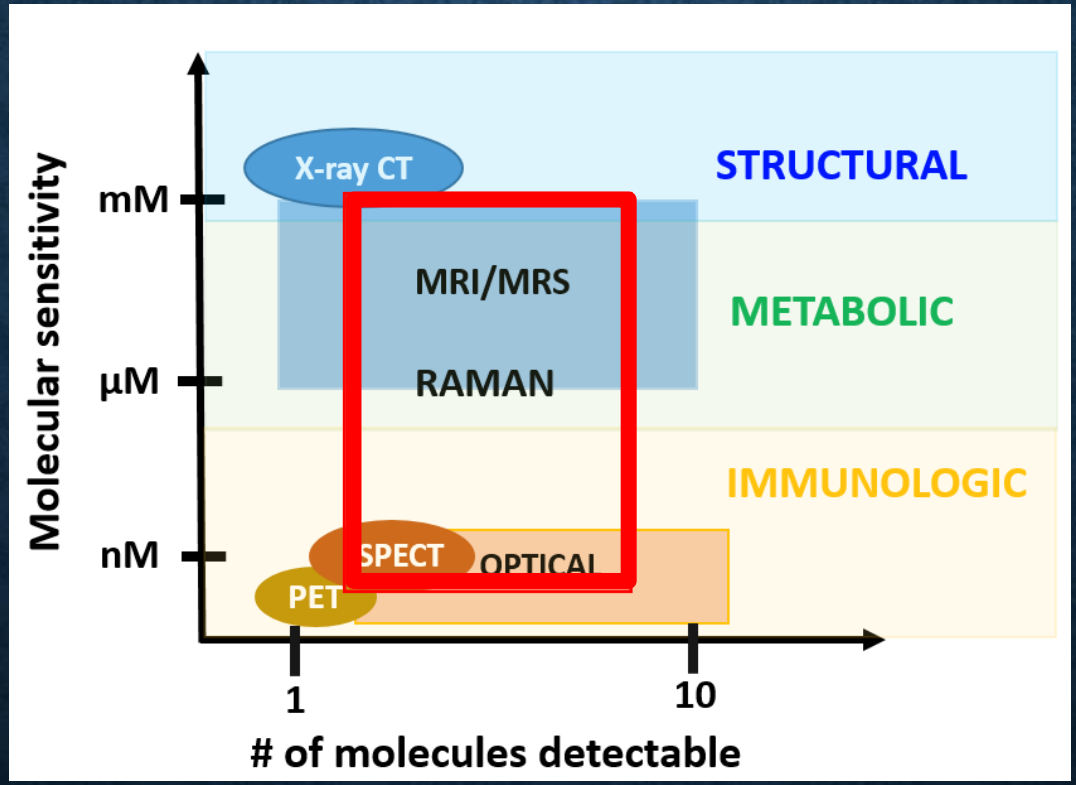

FUTURE DIRECTIONS OF CANCER RESEARCH
CANCER-OMICS

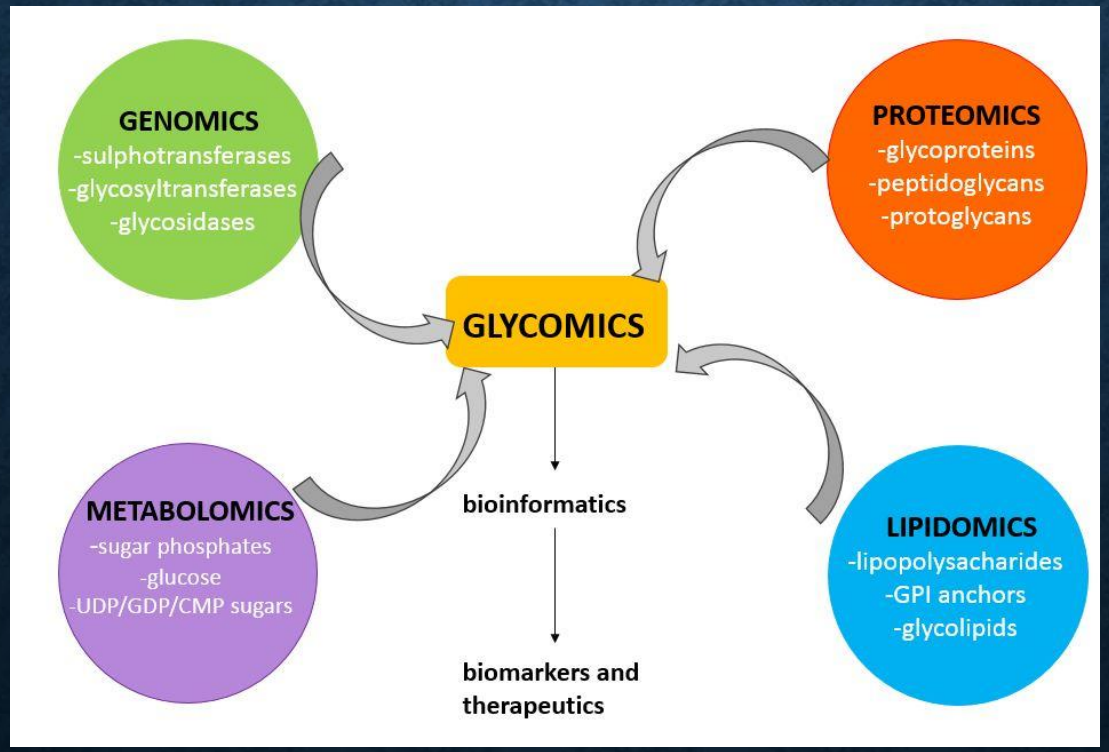

SINGLE CELL ANALYSIS: THE NEW FRONTIER IN ‘OMICS

- A combination of immunohistopathology and gene profile approaches are considered as gold standards to identify many cancer subtypes. Diagnostic approaches have limitations, such as, false positives, time delays, pain and trauma of patients, encouraging researchers to explore new non-invasive, reagent-free and less painful methodologies. Raman spectroscopy (RS), a vibrational spectroscopic technique, not only provides real time biochemical profile of tissues but also understanding of the disease as it progresses.

Concentration (molar)

mM | μM | nM | pM

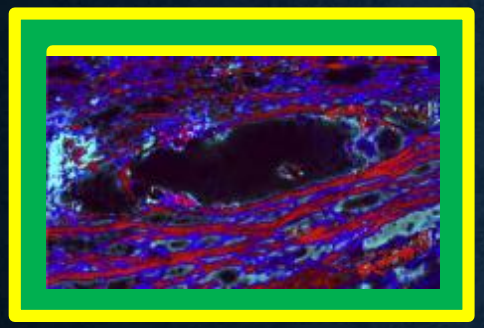

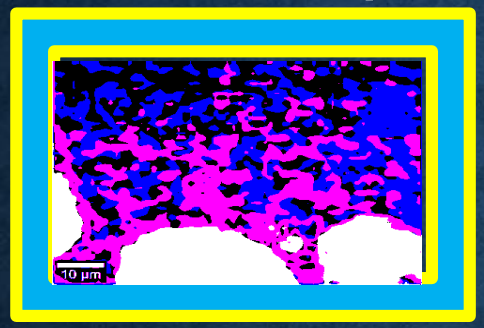

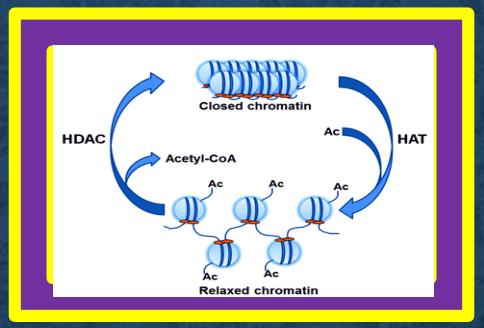

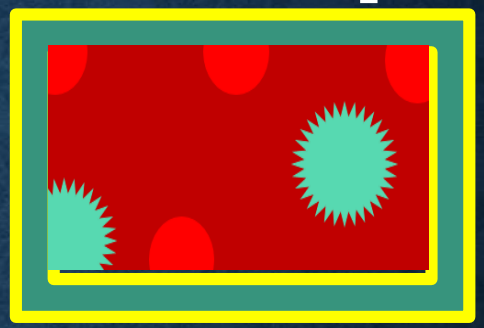

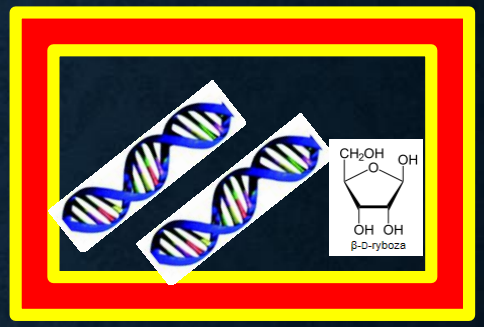

STRUCTURAL

- epithelium
- connective
- nerves
- muscle

OMICS

- lipids
- proteins
- carbohydrates
- minerals
- enzymes

EPIGENETIC

- DNA methylation
- histone methylation
- histone acetylation

IMMUNOLOGIC

- receptors
- growth factors
- cytokines
- hormones

GENETIC

- DNA
- mRNA

EASE OF DETECTABILITY → **POTENTIAL SPECIFICITY INCREASE**

Separately, cancer biology with genomics and proteomics protocols provides only a partial picture of cancer pathologies. Protocols of isolation of DNA, proteins, lipids or organelli from cells and tissues involve cel disruption to break open the cels and release the cellular structures. In Raman and IR imaging we do not need to disrupt cells to break open the cells and release the cellular structures to learn about their biochemical composition of lipid droplets, mitochondria, cytoplasm, nucleus, or membrane in living cells. Non-linear spectroscopy (pump-probe femtosecond spectroscopy, CARS imaging). Detectable molecular features in tissue can be categorized into four physiological bins: structural, metabolic, immunologic and genentic. The key factor limiting most imaging methods is signal-to-noise related to the concentration of the feature to be imaged. Fig.1 shows detectable molecular features in tissue (specificity) vs. concentration (sensitivity)

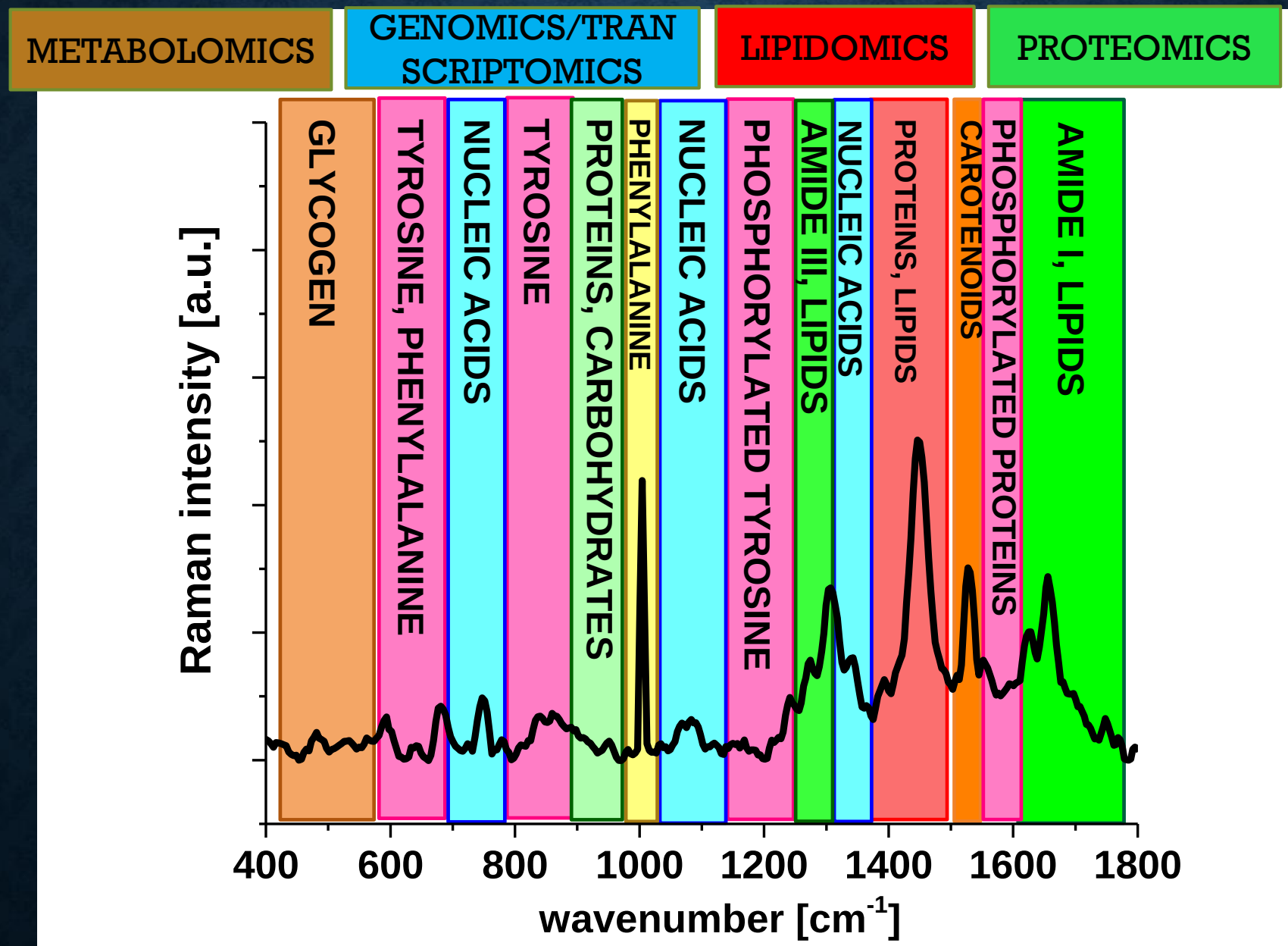
METABOLOMICS
GENOMICS/TRAN SCRIPTOMICS
LIPIDOMICS
PROTEOMICS
GLYCOGEN
TYROSINE, PHENYLALANINE
NUCLEIC ACIDS
TYROSINE
PROTEINS, CARBOHYDRATES
PHENYLALANINE
NUCLEIC ACIDS
PHOSPHORYLATED TYROSINE
AMIDE III, LIPIDS
NUCLEIC ACIDS
PROTEINS, LIPIDS
CAROTENOIDS
PHOSPHORYLATED PROTEINS
AMIDE I, LIPIDS
Raman intensity [a.u.]
400
600
800
1000
1200
1400
1600
1800
wavenumber [cm-1]

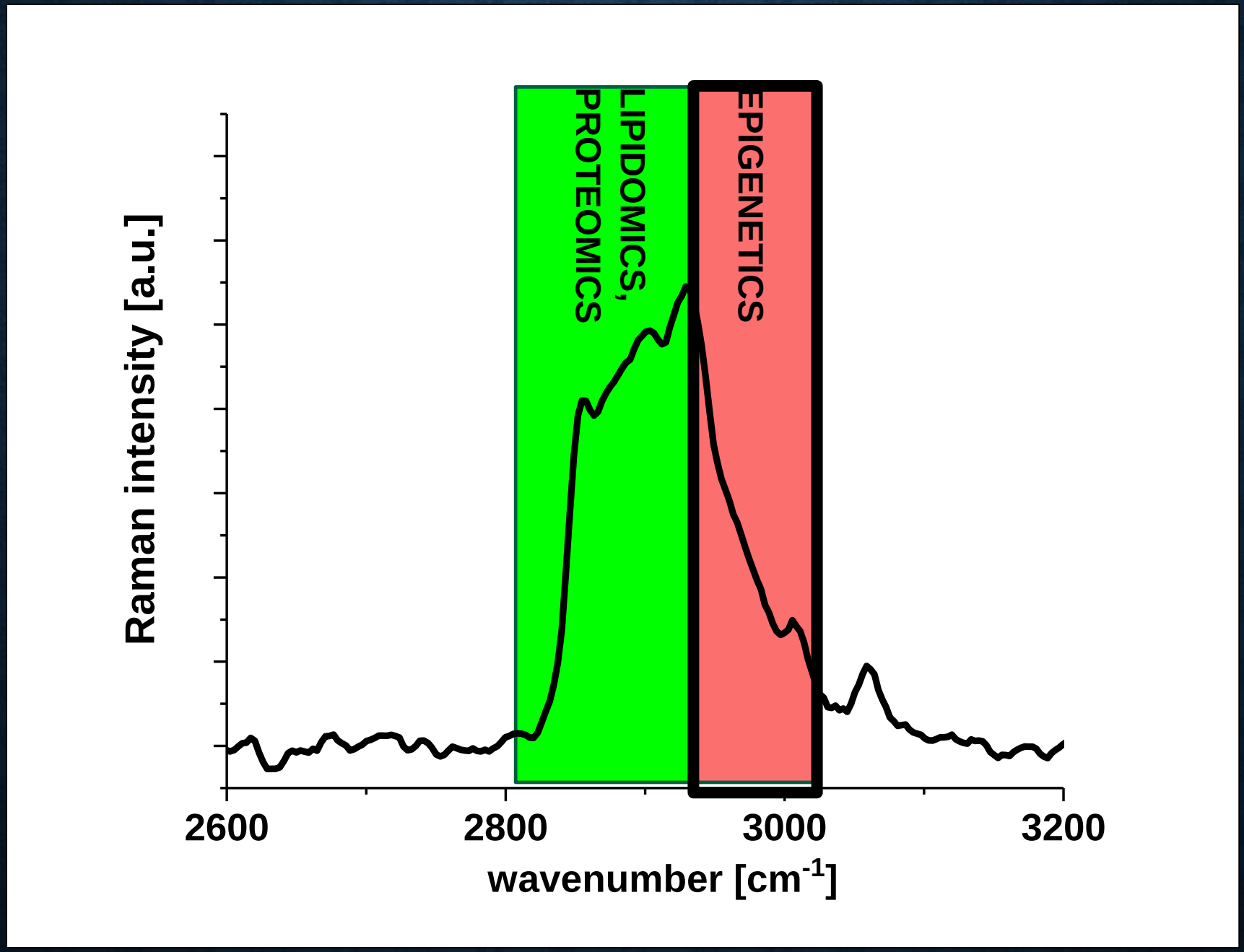
LIPIDOMICS,
PROTEOMICS
EPIGENETICS
Raman intensity [a.u.]
2600
2800
3000
3200
wavenumber [cm-1]

Conventional molecular biology imaging vs Raman imaging

Conventional techniques (e.g. SEM, IHC, H&E, and fluorescence imaging)	Raman spectroscopy-based diagnostics
Destructive	**Non-invasive and non-destructive**
Requires prior knowledge in order to target molecules	**Provides the full range of chemical information** in the spectrum
Laborious preparation procedures	**Minimal preparation** required can be directly applied to living cells and animals
Protocol optimization –often time consuming	Measurement condition is easy and quick to optimize
Fixation often required, not suitable for live cells	**Living cells** –can be analyzed without causing damage to the cells
Labelling required possibility of creating artefacts	**Label free**
Not suitable for heterogeneous samples conventional methods often required a large number of pure samples for characterization	Ca be performed on individual samples or get information *in situ*
High sensitivity but lower specificity	Lower sensitivity but higher specificity

RENISHAW

Conventional diagnostics methods vs Raman spectroscopy-based

Conventional techniques in histology, cytology and molecular biology (H&E, IHC, qPCR, mass spectroscopy)	**Raman spectroscopy-based diagnostics**
Destructive	**Non-invasive and non-destructive**
Requires prior knowledge in order to target molecules	**Provides the full range of chemical information** in the spectrum
Sample processing can take hours to days (e.g. DNA preparation, PCR and western blots runs)	**Minimal to no sample processing is required**
Protocol optimisation – often time consuming (e.g. western blots and PCR)	**Measurement condition is easy to optimise.** Rapid measurement can be enabled
Loss of spatial information (e.g. PCR and mass spectroscopy)	Retains spatial information **High spatial resolution** (sub-micrometre)
Labelling required (e.g. PCR and western blots) possibility of creating artefacts and costly (time, reagents and labour)	**Label free**

Conventional-omics molecular techniques vs Raman spectroscopy-based-omics

Conventional techniques (DNA microarray, sequencing, mass-spectroscopy, PCR, immunoprecipitation, western blotting)	**Raman spectroscopy and imaging**
Destructive (e.g. qPCR and mass spectroscopy)	**Non-invasive and non-destructive**
Requires prior knowledge in order to target molecules (e.g. IHC and qPCR)	**Provides the full range of chemical information** in the spectrum
Sample processing can take days to weeks (e.g. tissue sectioning and staining, microbiology cultures)	**Minimal to no sample processing** is required and therefore is faster and cheaper to perform -> quicker patient diagnosis and less cost to hospital
Protocol optimisation –often time consuming(e.g. IHC and qPCR)	**Measurement condition is easy and quick to optimise**
Loss of spatial information (e.g. qPCR and mass spectroscopy)	Retains spatial information **High spatial resolution** (sub-micrometre)
Fixation often required not suitable for live cells	**Living cells** –can be analysed without causing damage to the cells
Labelling required (e.g. IHC and qPCR) possibility of creating artefacts and costly (time, reagents and labour)	**Label free**

RENISHAW

CONFOCAL RAMAN MICROSCOPY

1.5 Confocal Raman Microscopy

Confocal microscopy requires a point source (usually a laser), which is focused onto the sample. The reflected light (Raman, fluorescence) is collected with the same objective and focused through a pinhole at the front of the detector (Fig. 3). This ensures that only light from the image focal plane can reach the detector, which greatly increases image contrast and with the proper selection of pinhole size, slightly increases resolution (max. gain in resolution: factor $\sqrt{2}$).

For Raman microscopy, the enhancement of image contrast and depth resolution is very important. An enhancement of the lateral resolution in confocal microscopy requires extremely small pinhole diameters and will therefore decrease the detection efficiency to a level usually unacceptable in most experiments (Fig. 4).

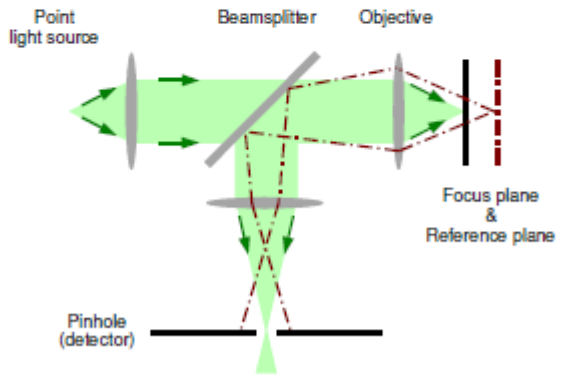

Fig. 3: Principal setup of a confocal microscope

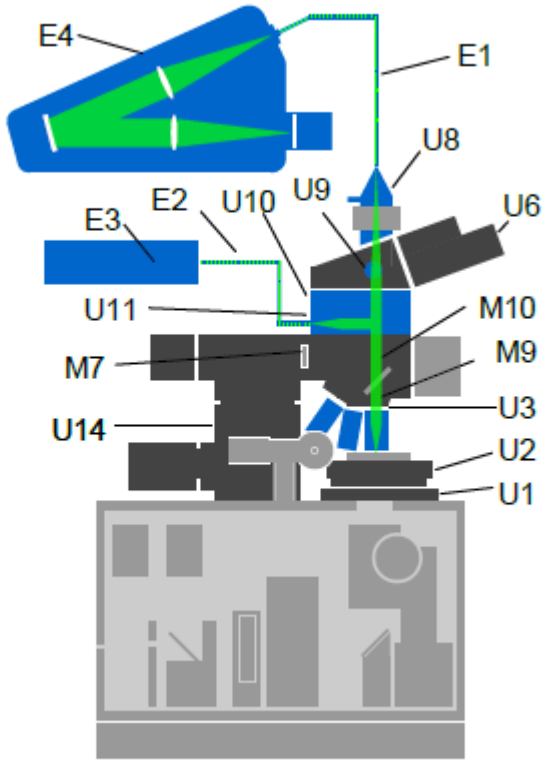

Fig. 8: Schematic illustration of the beam path for confocal Raman microscopy.

SNOM

Near field microscopy is far below the diffraction limit

3.1 SNOM AC in transmission configuration

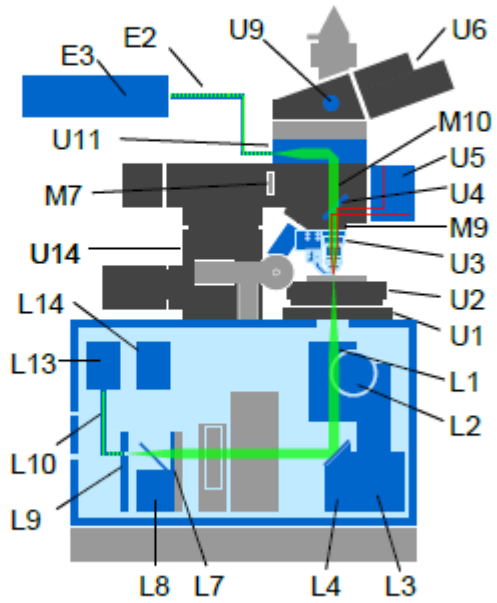

Fig. 5: Schematic illustration of the beam path for Scanning Near-field Optical Microscopy in AC transmission mode.

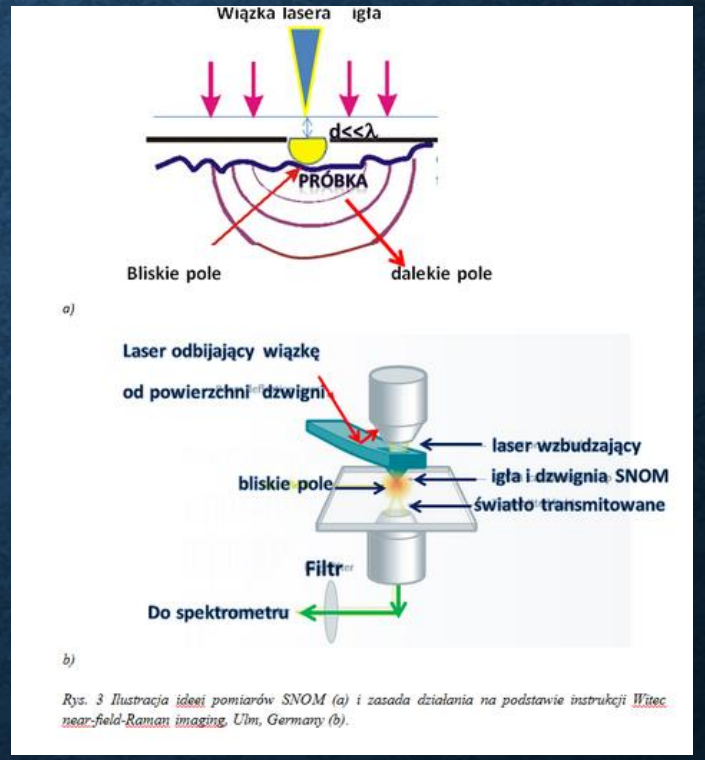

Rys. 3 Ilustracja idei pomiarów SNOM (a) i zasada działania na podstawie instrukcji Witec near-field-Raman imaging, Ulm, Germany (b).

SNOM IN AC MODE

WITec

AFM (ATOMIC FORCE MICROSCOPY)

AFM is not based on spatial resolution limited by diffraction . The spatial resolution depends on the tip size , and is far below the diffraction limit .

AFM is a very-high-resolution type of scanning probe microscopy (SPM), with demonstrated resolution on the order of fractions of a nanometer, more than 1000 times better than the optical diffraction limit.

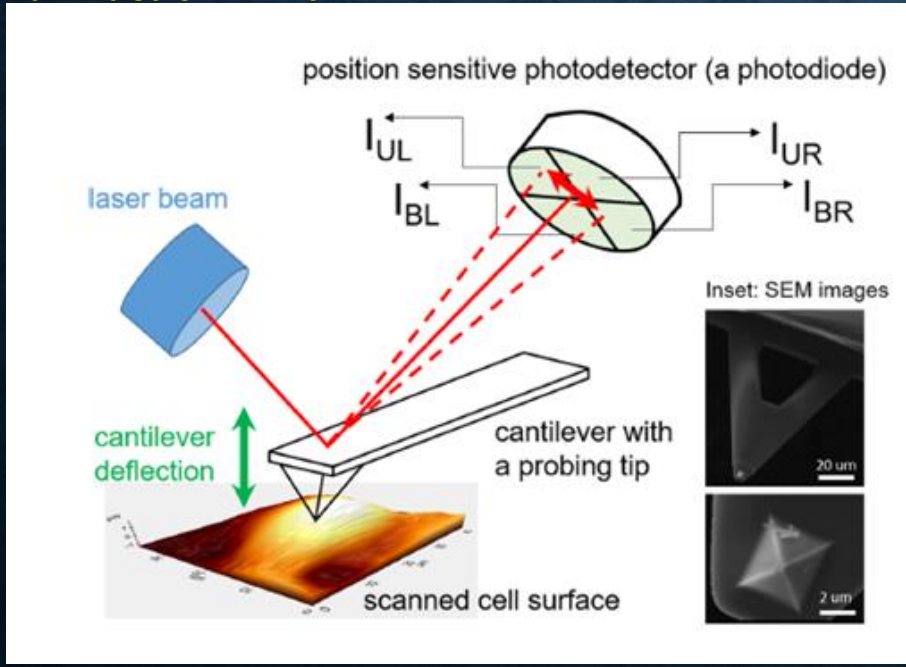

Light-lever detection based on laser and photodiode

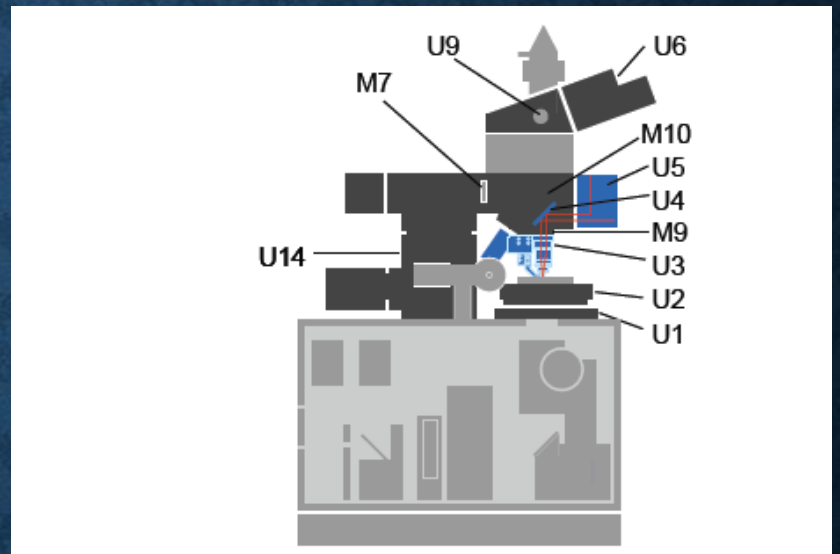

Fig. 5: Schematic illustration of the beam path for AFM AC Mode .

AFM IN AC MODE

WITec

U1 XY positioner

U2 Scan stage

U3 Objective turret with objectives including the inertial drive and the SNOM tip

U4 Dichroic mirror

U5 Beam deflection unit

U6 Binocular tube with ocular camera

U9 Pushrod

U14 Microscope Z stage with stepper motor

RESOLUTION OF DIFFERENT IMAGING METHODS

To optimize AFM for the investigation of dynamical biological systems, each component of AFM can be modified to improve the speed of AFM scanning. As a result, high-speed AFM (HS-AFM) achieved scanning speeds several orders of magnitude faster than that of conventional AFM, thus enabling monitoring of conformational dynamics of single proteins on substrates with a subsecond temporal resolution.

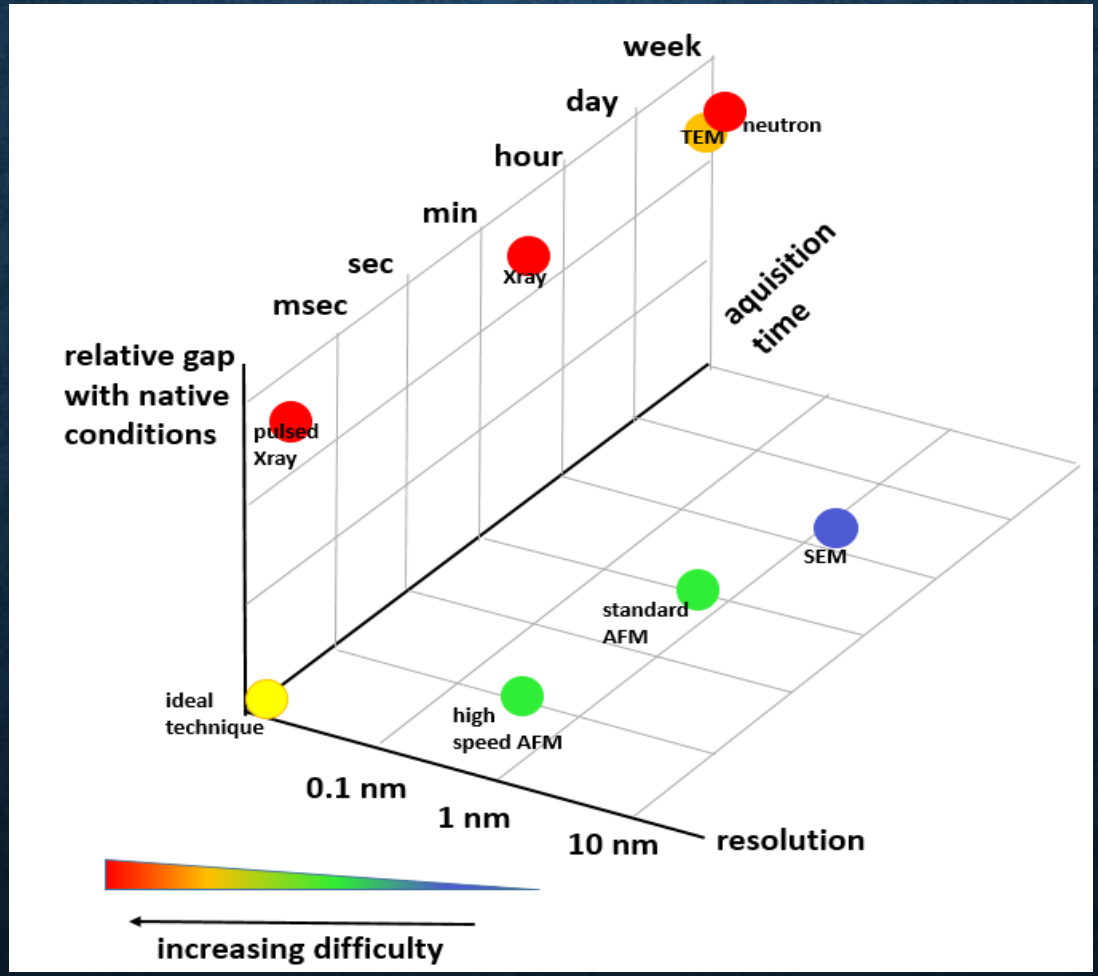

Thus, the successful observations of nanostructural dynamics in live neurons may open the possibility to vizualize the morphology of synapse plasticity at nanometer resolution in real time in the near future.

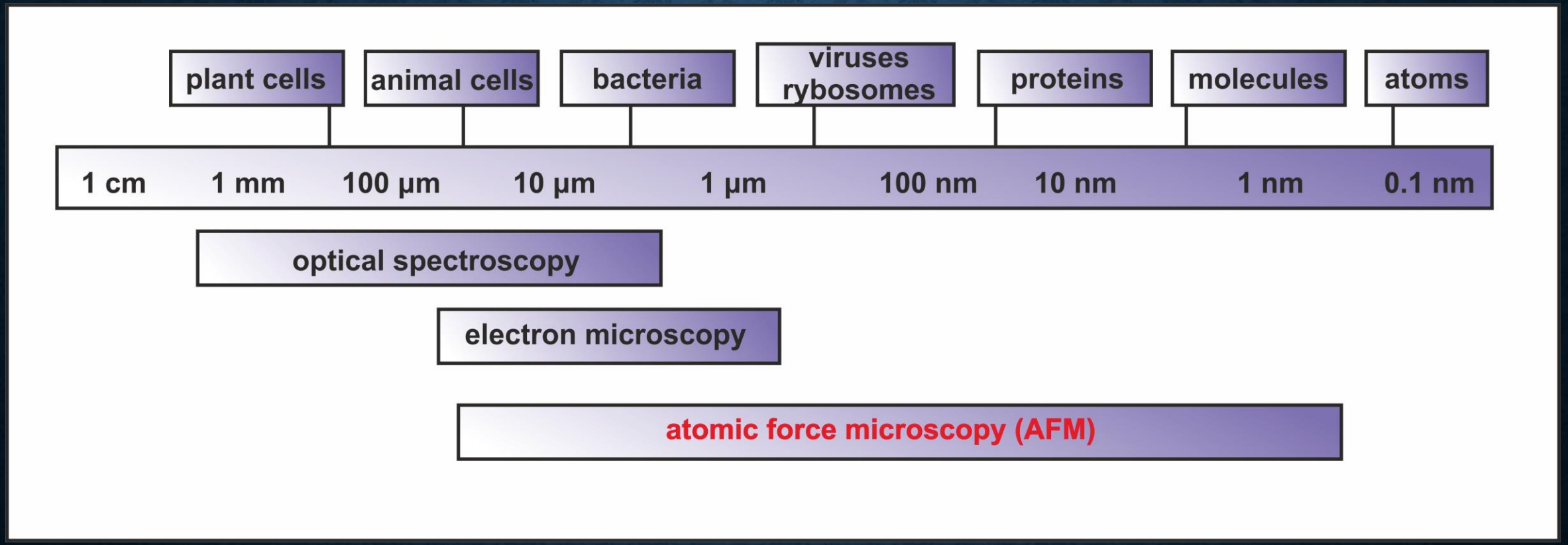

The AFM is useful for obtaining 3D topographic information of samples with lateral resolution (in the x/y plane) down to 0.3 nm and vertical resolution (in the z-axis) down to 0.1 nm [26]. These samples include clusters of atoms and molecules [27], individual macromolecules [28], and biological species (cells, DNA, proteins) [29, 30].

PHOTOACTIVATION OF BACTERIORHODOPSINE

- Fast imaging AFM na BR Mutant D96N
- w 10 mM TRIS, 150 mM KCl, pH 7.6
- AM AFM z A=1.0 nm
- 1 kl / s (64 px2)
- Eksperyment trwał 200 fps
- To samo miejsce (te same molekuły)

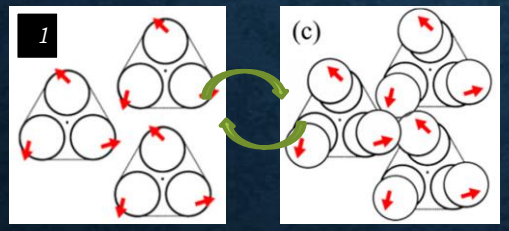

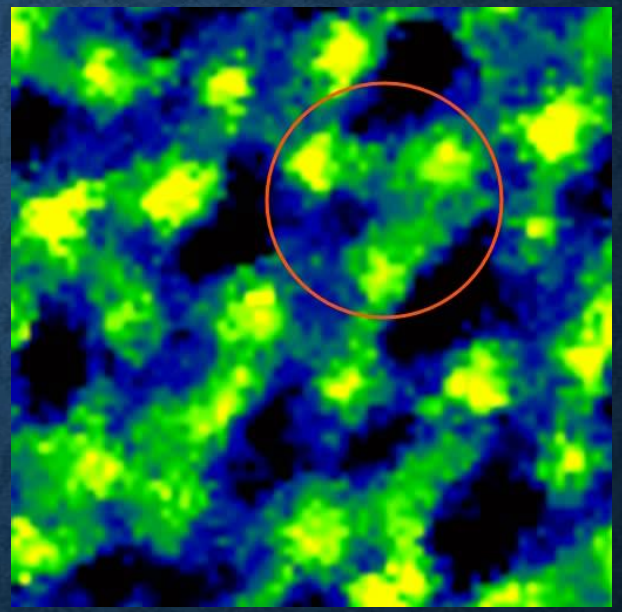

x,y-range=18x18nm^2, z=325pm

[1] *Ando T et al., Nanotechnology 23 (2012) 062001*

STIFFNESS

- Using these force curves (sometime called *indentation curves*), one can easily calculate the *stiffness*, which is defined as a derivative of force *F* with respect to penetration *z*
- (indentation), *dF/dz*.
-

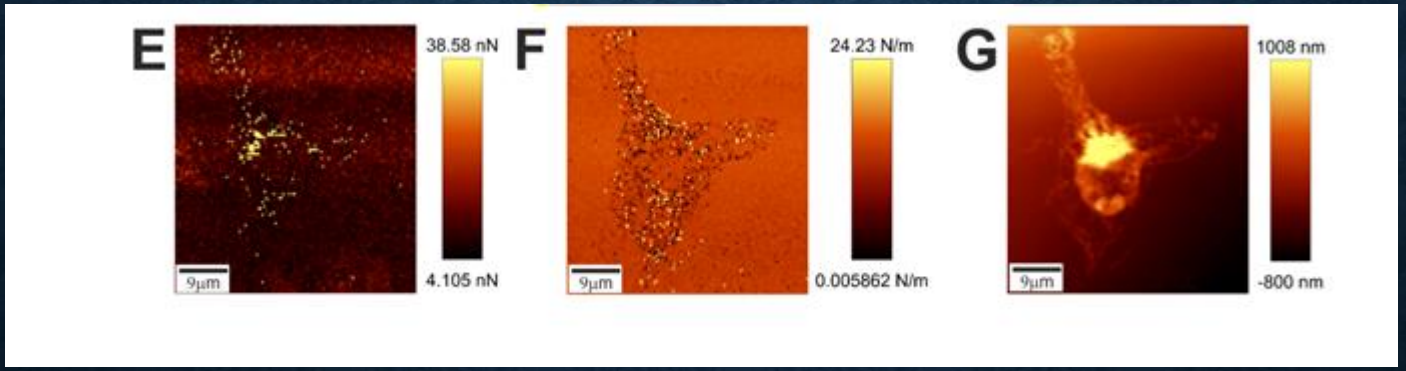

adhesion image (E), stiffness image (F) and topography image (G) of air-dried cell.

ADHESION

- **One more interesting feature of the retracting curve is the non-zero force required to disconnect the tip from the surface. This is the so-called *adhesion force*. It appears due to weak forces (such as van der Waals forces) acting between**

Int. J. Mol. Sci. **2015**, *16*

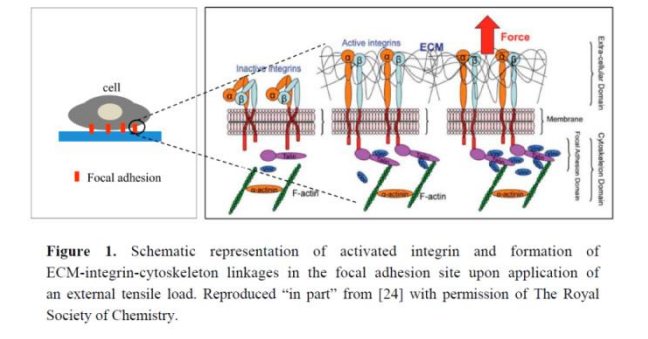

Figure 1. Schematic representation of activated integrin and formation of ECM-integrin-cytoskeleton linkages in the focal adhesion site upon application of an external tensile load. Reproduced "in part" from [24] with permission of The Royal Society of Chemistry.

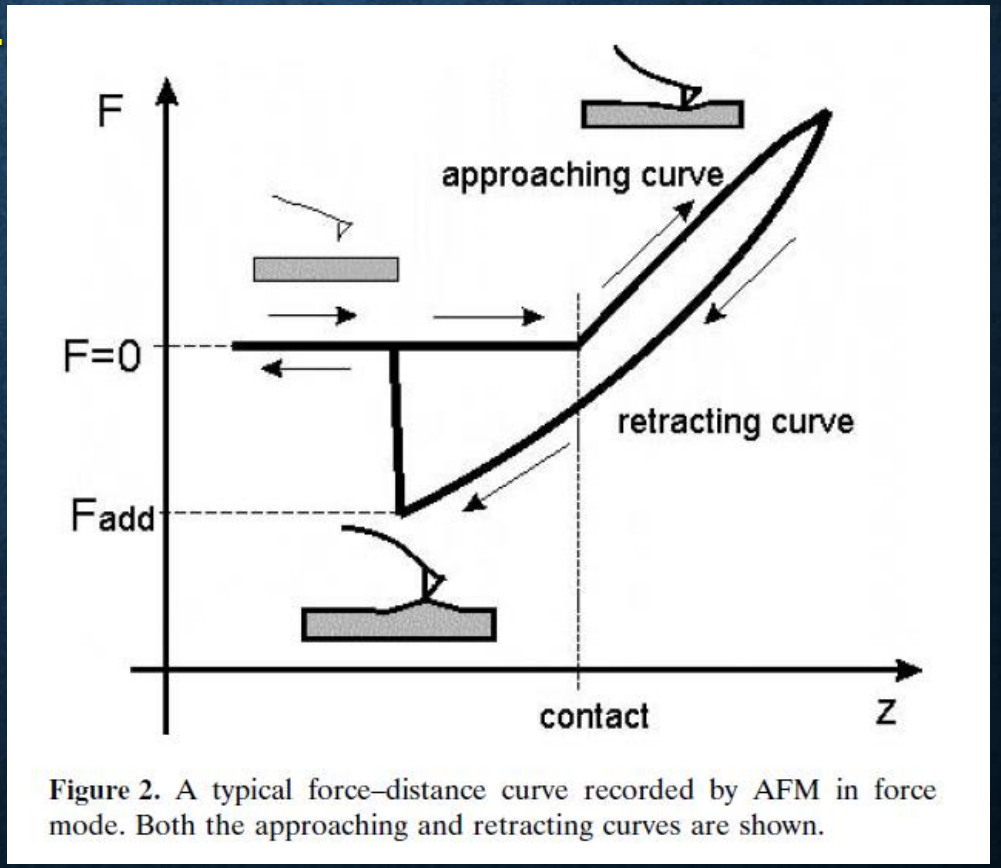

Figure 2. A typical force–distance curve recorded by AFM in force mode. Both the approaching and retracting curves are shown.

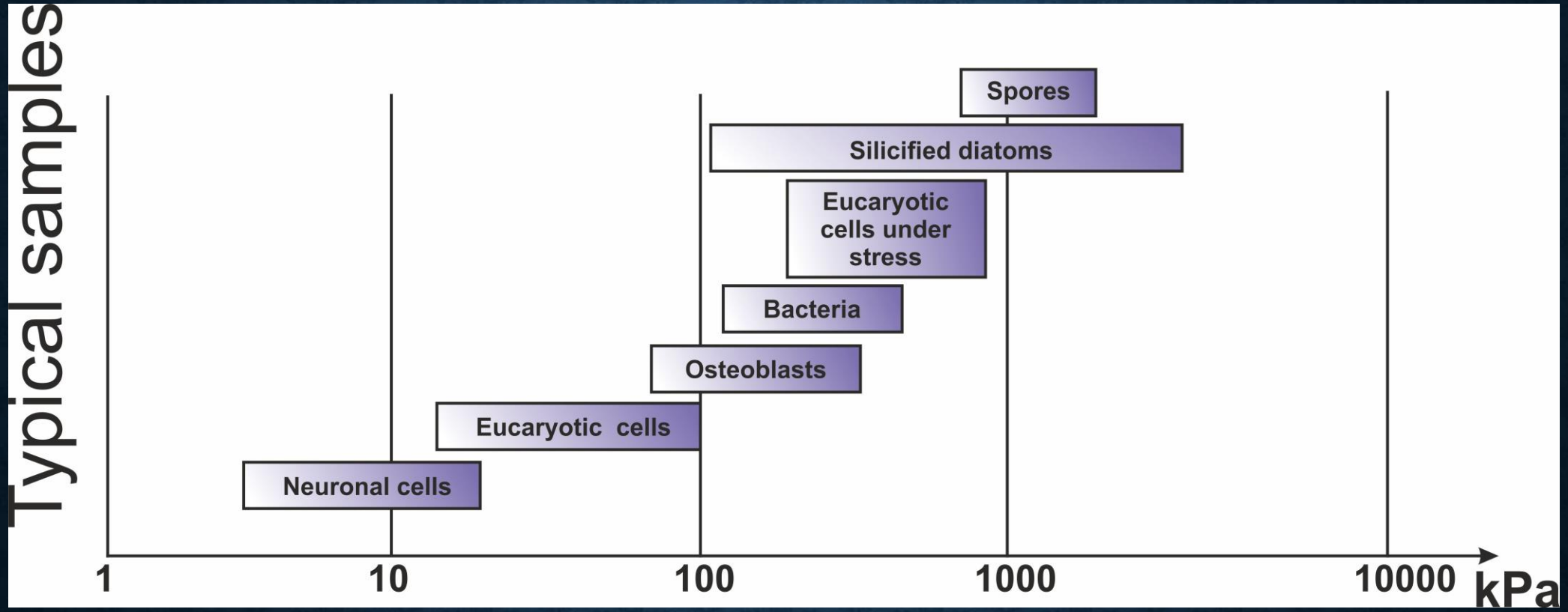

Figure 4. Range of Young's modulus values of various biological samples. Young's modulus is an indicator of a cell's response to stress (force). Depending on their type, eukaryotic cells can exhibit very different mechanical properties. Neurons are extremely soft (down to 1 kPa), whereas bone cells are as robust as bacteria.

AFM TOPOGRAPHY FOR OBTAINING SURFACE PROFILES

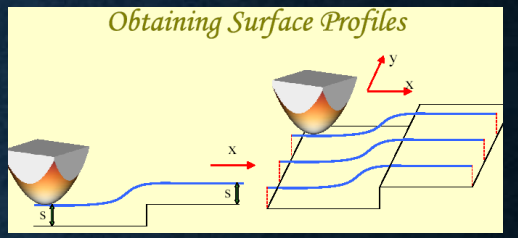

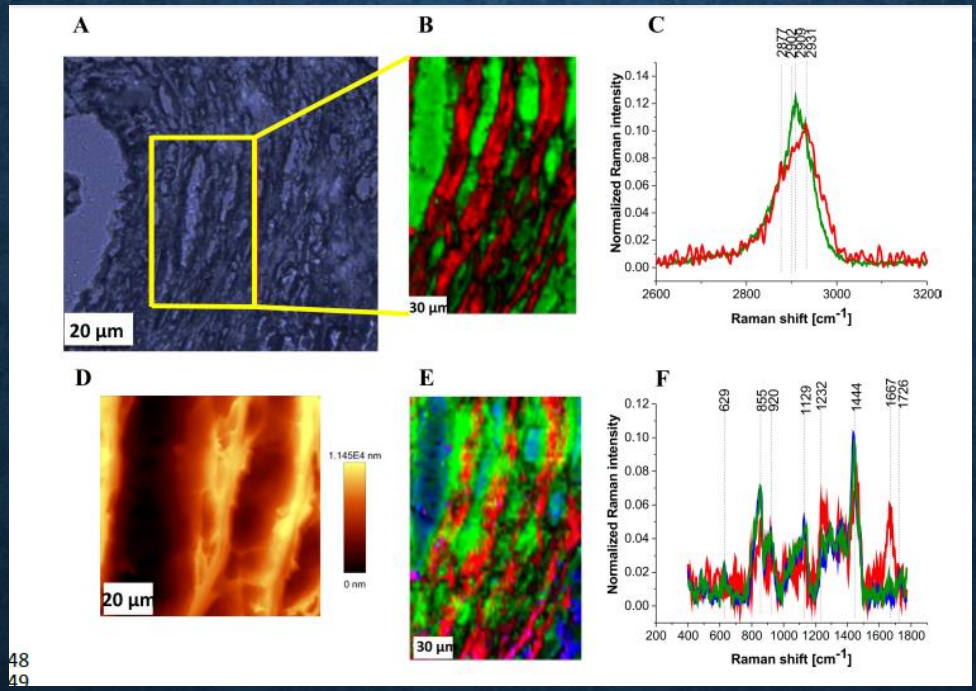

48
49

Fig. 6 Distribution of the glycans (green), lipids (blue) and protein (red) in the human breast tumor tissue, the white light microscopy image (A), Raman image (150 µm x 230 µm) obtained from the basis analysis (B) and Raman spectra (C) in the high frequency spectral region. AFM image (D), Raman image obtained from the basis analysis (E) and Raman spectra (F) in the fingerprint region of the tumor breast tissue (Patient P155, Infiltrating adenocarcinoma grade WHO according to Elston and Ellis modification G2), integration time for Raman images 0.5 s in the high frequency region and 1 s in the low frequency region, resolution step 0.5 µm, laser excitation power 10 mW. The line colors of the spectra correspond to the colors of the Raman maps.

ADVANTAGES OF NON-LINEAR OPTICS IN CANCER RESEARCH

NONLINEAR OPTICAL PUMP-PROBE MICROSCOPY IS A NEW AREA FOR HIGH RESOLUTION 3D IMAGING IN MODERN MICROSCOPY. THE IMAGING CONTRAST RELIES UPON THE CHARACTERISTIC SPECTROSCOPIC PROPERTIES OF SPECIFIC MOLECULES, FOR EXAMPLE THEIR SPECIFIC INTERNAL ENERGY LEVEL STRUCTURE.

NON-LINEAR OPTICS	LINEAR OPTICS
Stimulation and readout of the nonlinear interactions are achieved by at least two pulses of well-defined properties: a pimp and a probe pulse. This different to other nonlinear optical imaging methods like fluorescence and incoherent Raman microscopy	
Stimulated readout suppress incoherent processes such as spontaneous emission	Spontaneous emission
The combination of high excitation laser power and sensitive detection results in an efficient overall yield of the nonlinear interaction	
This enables images to be acquired quickly	Long time of acquisition
The short laser exposure time reduces the photo damage on the sample caused by the high powered laser	
Particular marker moleculs are not needed for sample preparation as they are in fluorescence imaging	
One of the key goals of current research is reducing the time it takes to acquire an image. This is often directly related to detection sensitivity. With a modern scanning microscope, acquisition times of up to 30 fps are possible for 512 by 512 pixel image	

NON-LINEAR OPTICS	LINEAR OPTICS
The application of femtosecond laser pulses instead of the widely used picosecond pulses in another innovative feature of the microscope. Due to the increased excitation bandwidth of shorter pulses, the femtosecond laser pulses are able to better excite isolated vibrational resonances	
Due to the higher peak power of the femtosecond laser pulses, photodamage on biological samples is an important issue. This was addressed by balancing the excitation power to the near-infrared Stokes pulses (40mW). At this level, possible photodamage is relatively smaller than that of visible pump pulses (10mW). Images are also collected with high-sensitivity and high-speed. The exposure time to the laser of one sample pixel, the pixel dwell time, is still below 4 ms.	

NONLINEAR OPTICAL PHENOMENA

$$P_i = \chi_{ij}^{(1)} E + \chi_{ijk}^{(2)} E_j E_k + \chi_{ijkl}^{(3)} E_j E_k E_l$$

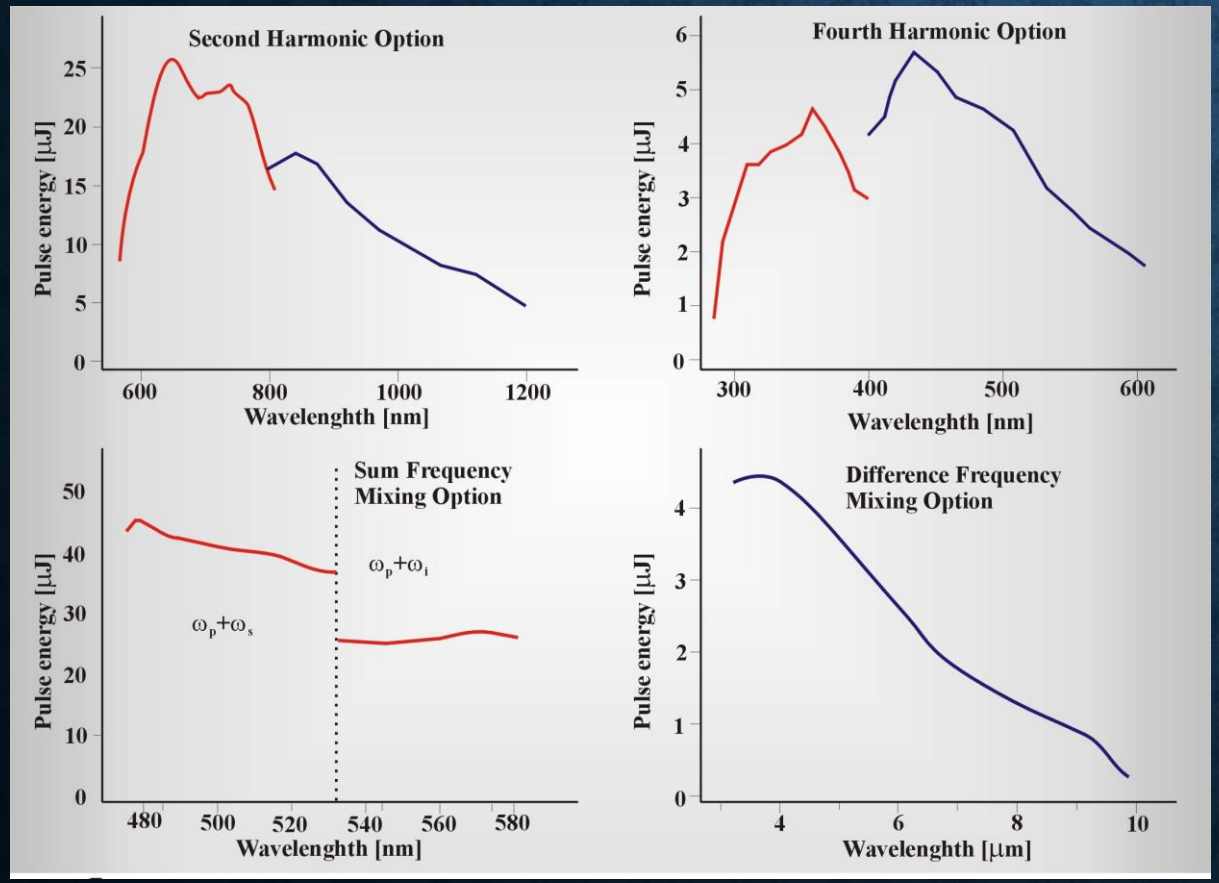

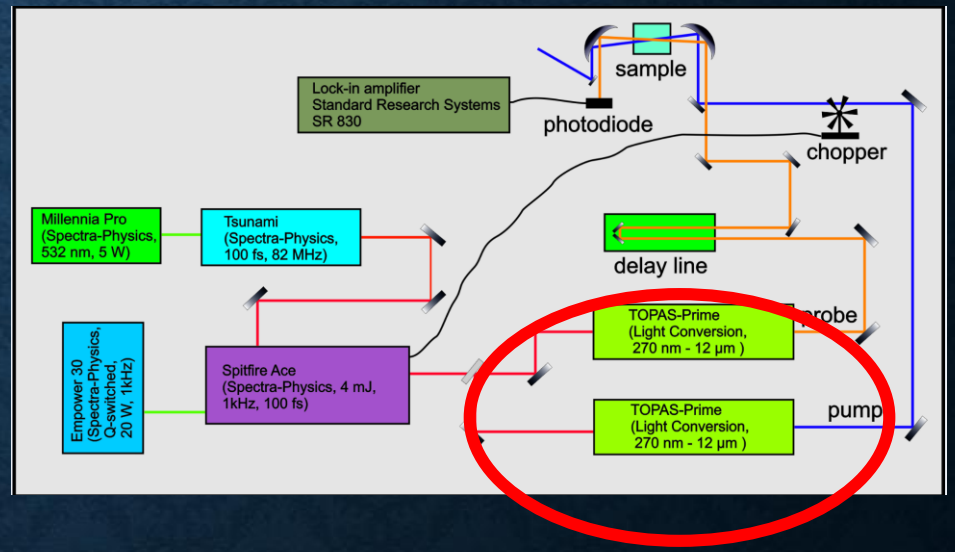

METHODS OF GENERATION OF ULTRASHORT PULSES-MODELOCKING

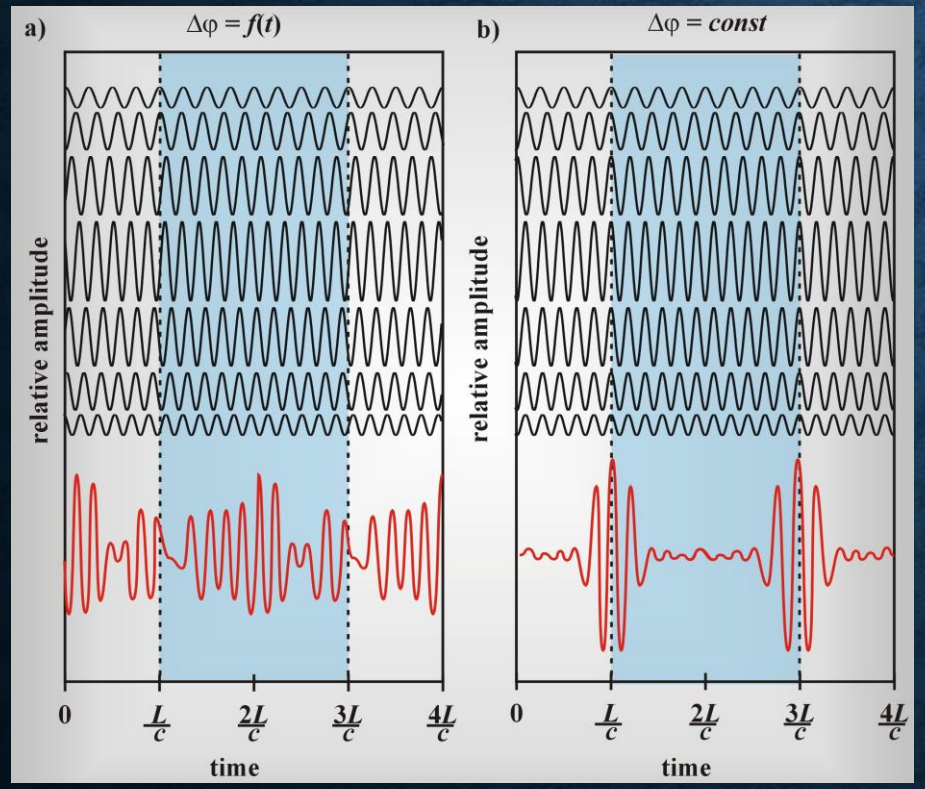

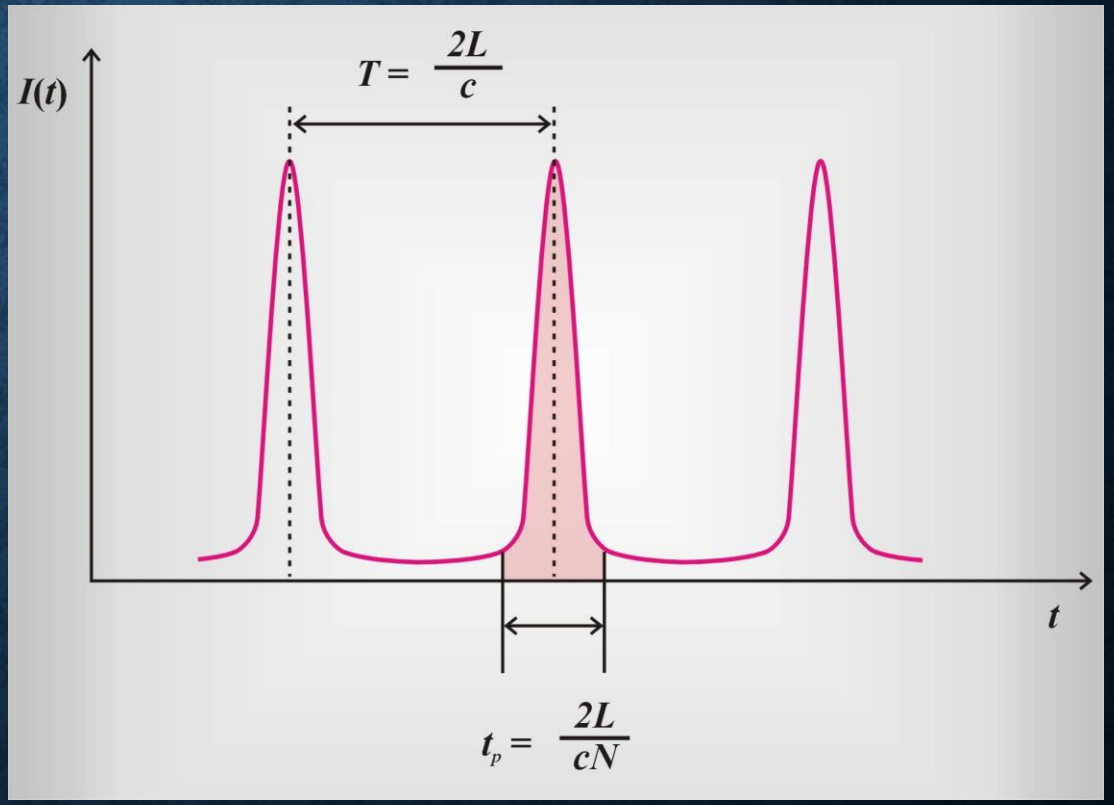

METHODS OF MODELOCKING

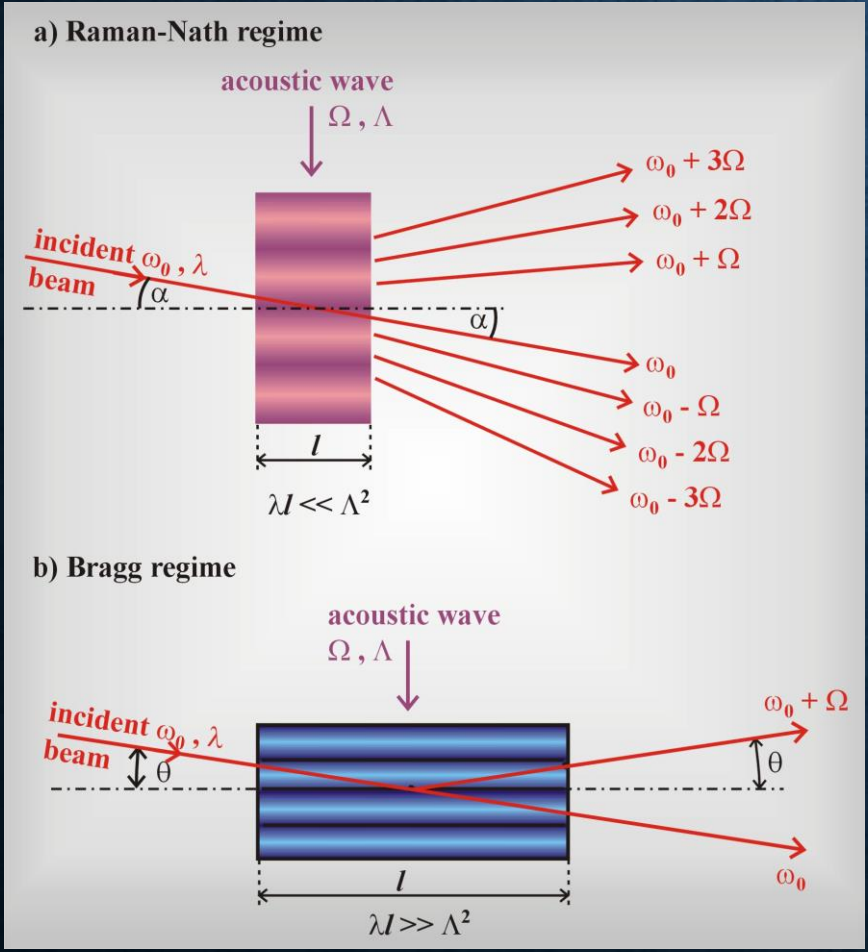

a) Acusto-optical devices
b) electro-optical devices
c) Saturable absorbers
d) Kerr-lens modelocking
e) Saturable Bragg reflectors

METHODS OF GENERATION OF ULTRASHORT PULSES-Q-SWITCHING

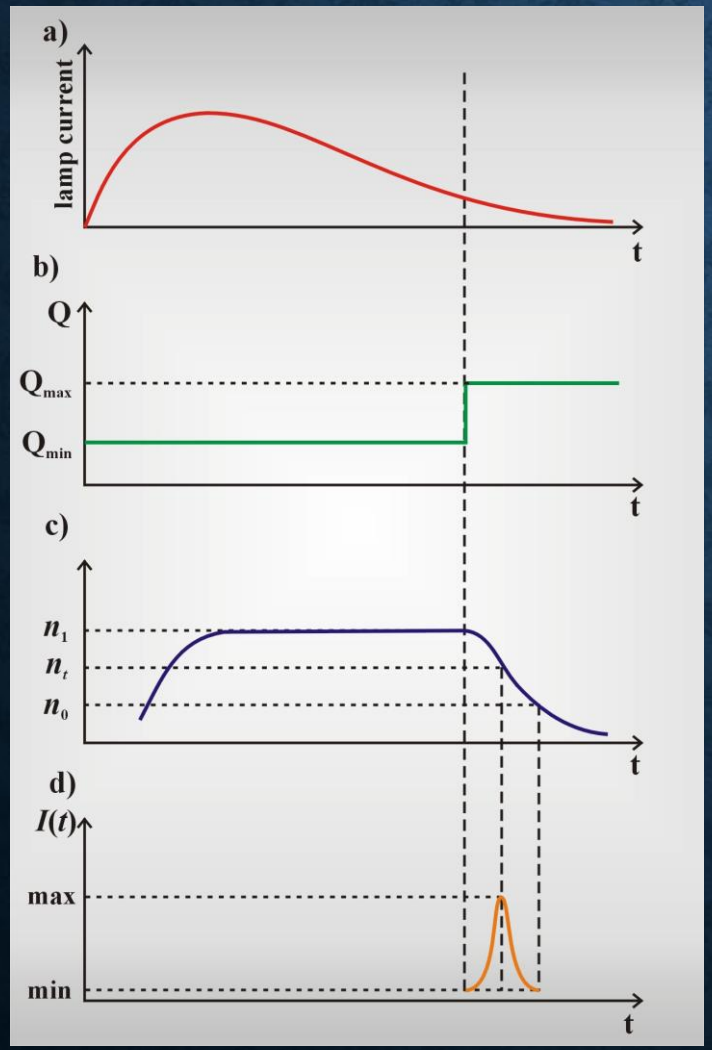

Mechanism of generation of a Q-switched pulse, a) pumping, b) Q-switching, c) Energy storage , d) pulse generation

CHIRPED PULSE AMPLIFICATION (CPA)

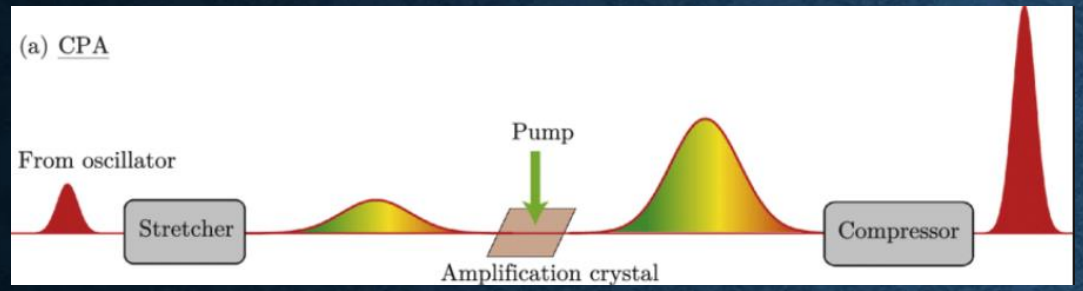

CPA for lasers was introduced by Donna Strickland and Gérard Mourou at the University of Rochester in the mid-1980s, work for which they received the Nobel Prize in Physics in 2018

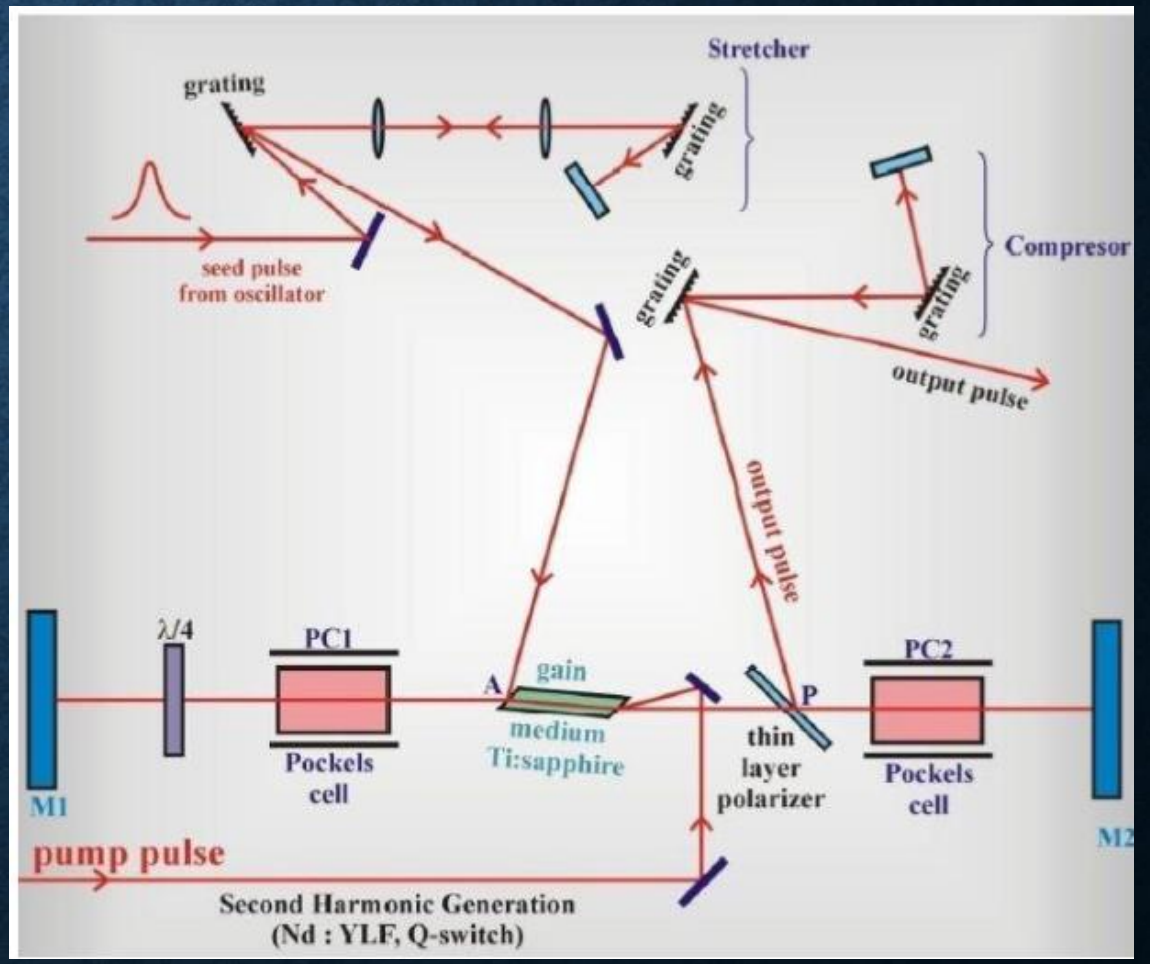

Apart from these state-of-the-art research systems, a number of commercial manufacturers sell Ti: sapphire - based CPAs with peak powers of 10 to 100 gigawatts.

CPA is the current state-of-the-art technique used by all of the highest-power lasers (greater than about 100 TW

SECOND-ORDER NONLINEAR PHENOMENA

$$P_i = \chi_{ij}^{(1)} E + \chi_{ijk}^{(2)} E_j E_k + \chi_{ijkl}^{(3)} E_j E_k E_l$$

SECOND HARMONIC GENERATION (SHG)

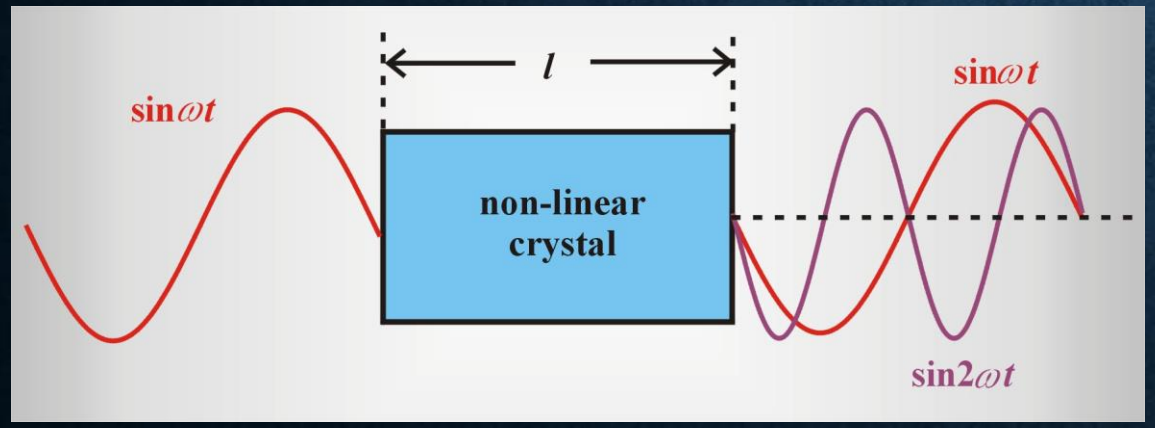

THIRD-ORDER NONLINEAR PHENOMENA

$$P_i = \chi_{ij}^{(1)} E + \chi_{ijk}^{(2)} E_j E_k + \chi_{ijkl}^{(3)} E_j E_k E_l$$

STIMULATED RAMAN SCATTERING

PUMP - PROBE TRANSIENT ABSORPTION SPECTROSCOPY

STIMULATED RAMAN SCATTERING

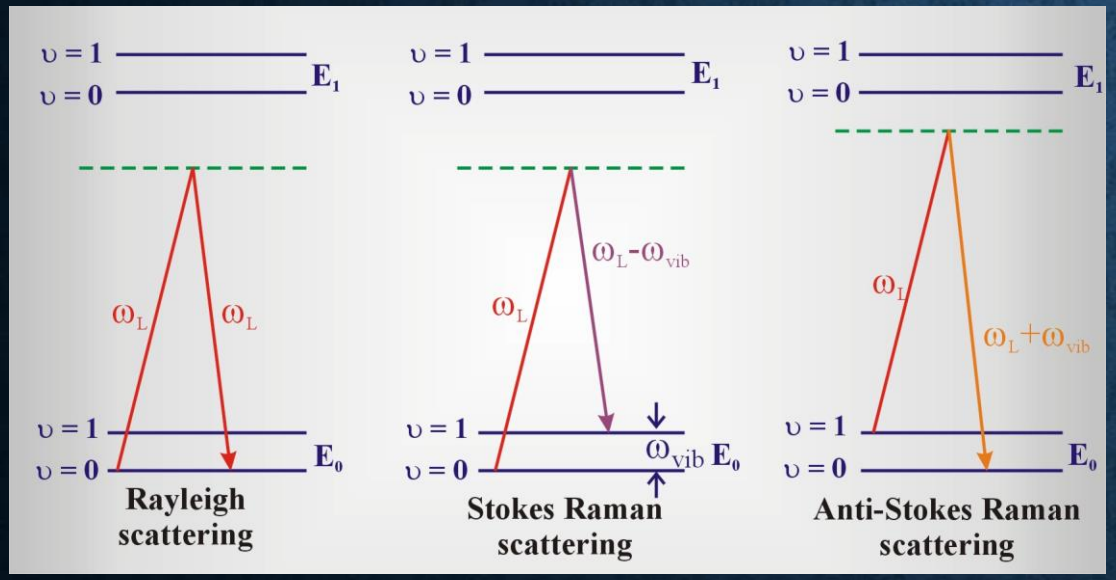

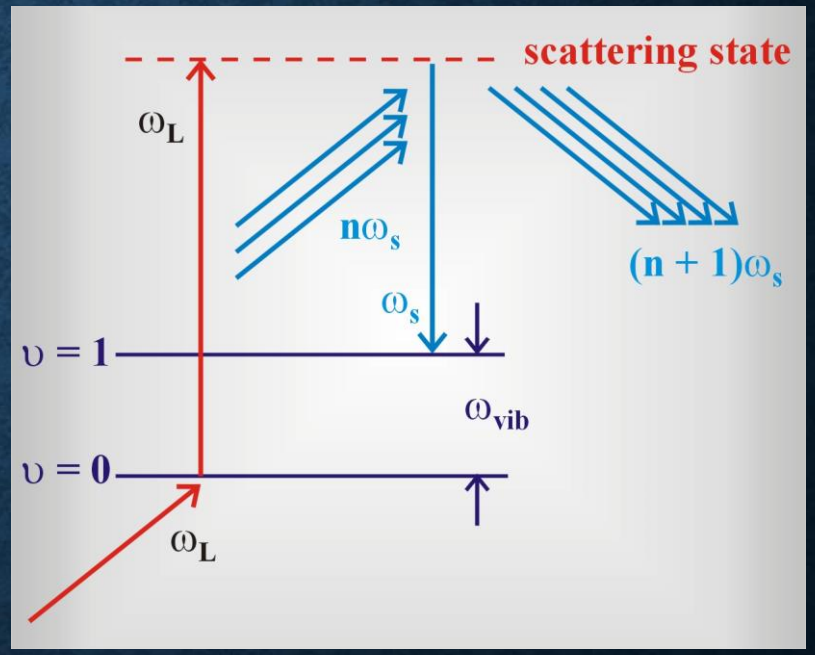

THIRD-ORDER NONLINEAR PHENOMENA

$$P_i = \chi_{ij}^{(1)} E + \chi_{ijk}^{(2)} E_j E_k + \chi_{ijkl}^{(3)} E_j E_k E_l$$

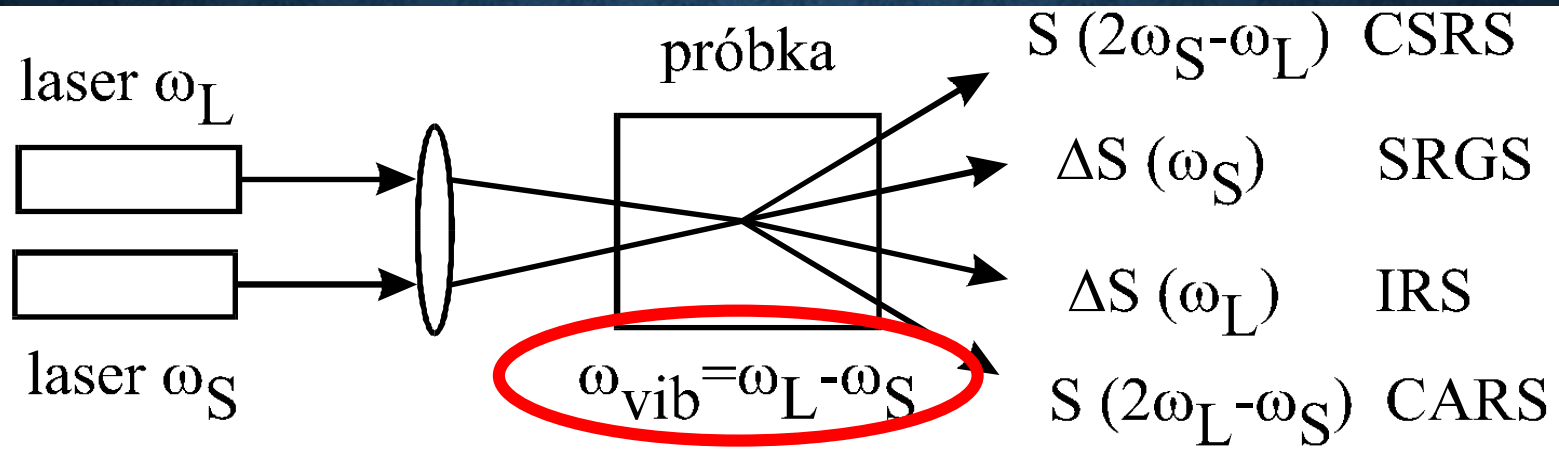

Rys. 6.19. Schematyczny diagram najczęściej stosowanych technik nieliniowego wymuszonego rozpraszania Ramana

CARS

DIRECTION OF PROPAGATION OF THE STIMULATED ANTI-STOKES RAMAN SCATTERING

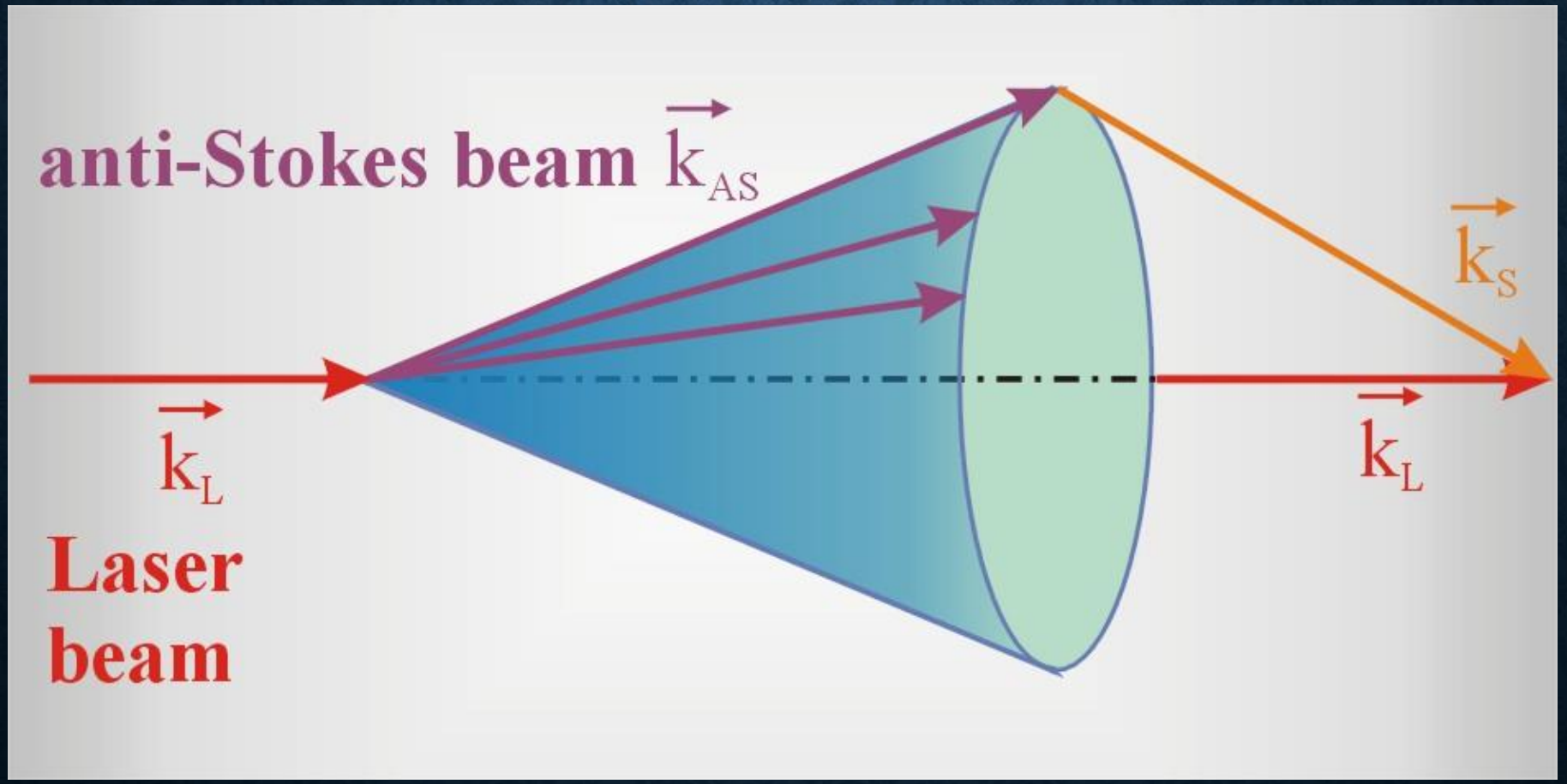

COHERENT RAMAN MICROSCOPY

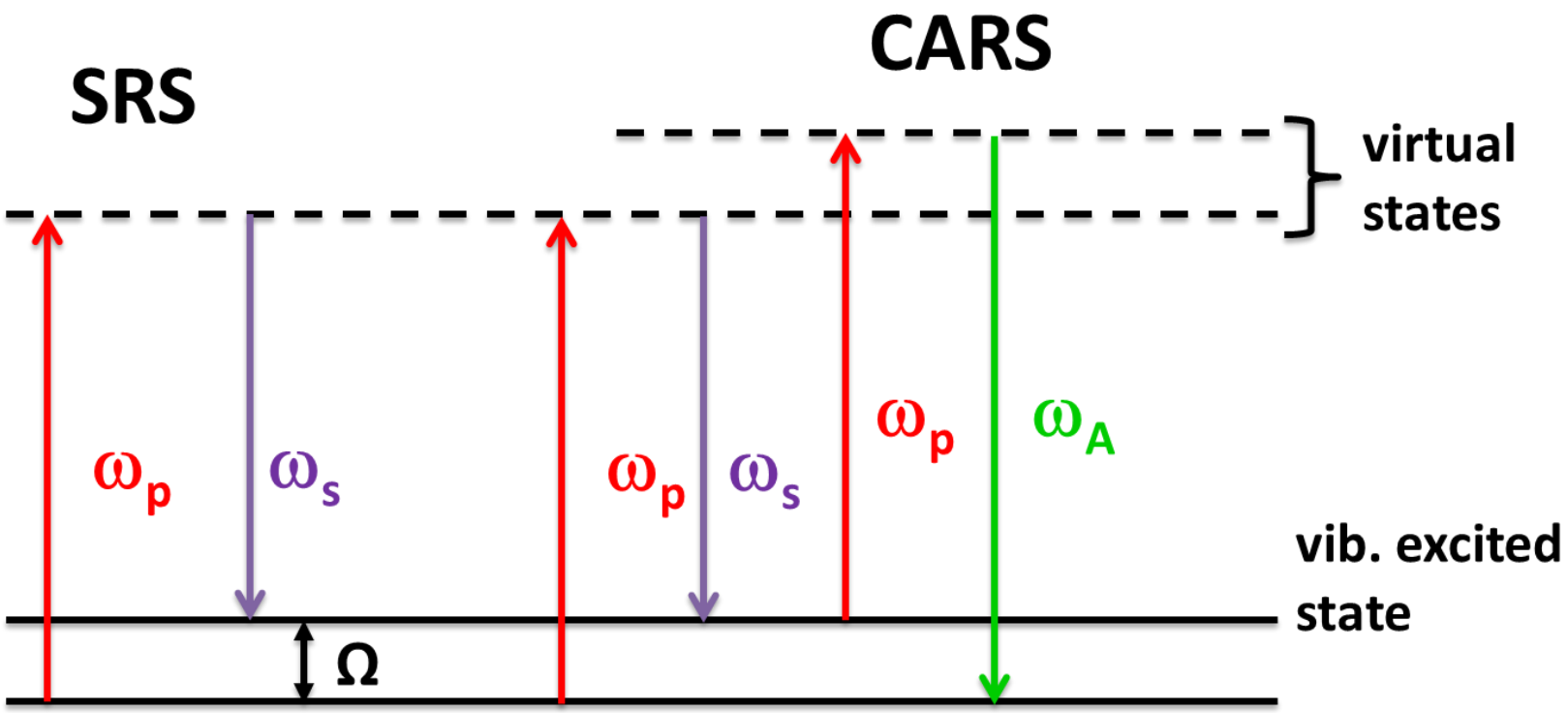

Nonlinear optical pump-probe microscopy is a new field for 3D high resolution imaging in modern microscopy

TRANSIENT ABSORPTION MICROSCOPY

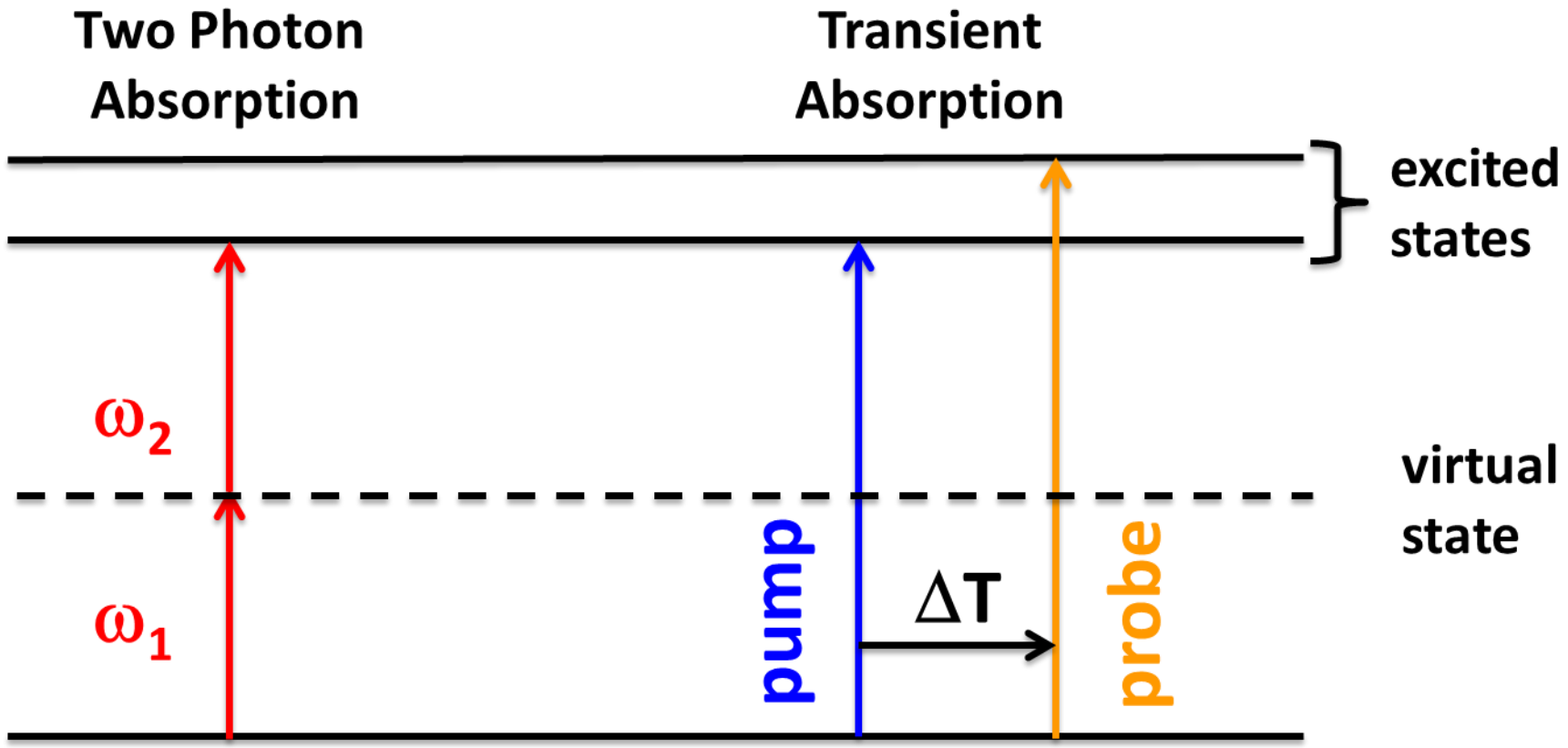

Examples for nonlinear absorption processes

Pump-probe measurements

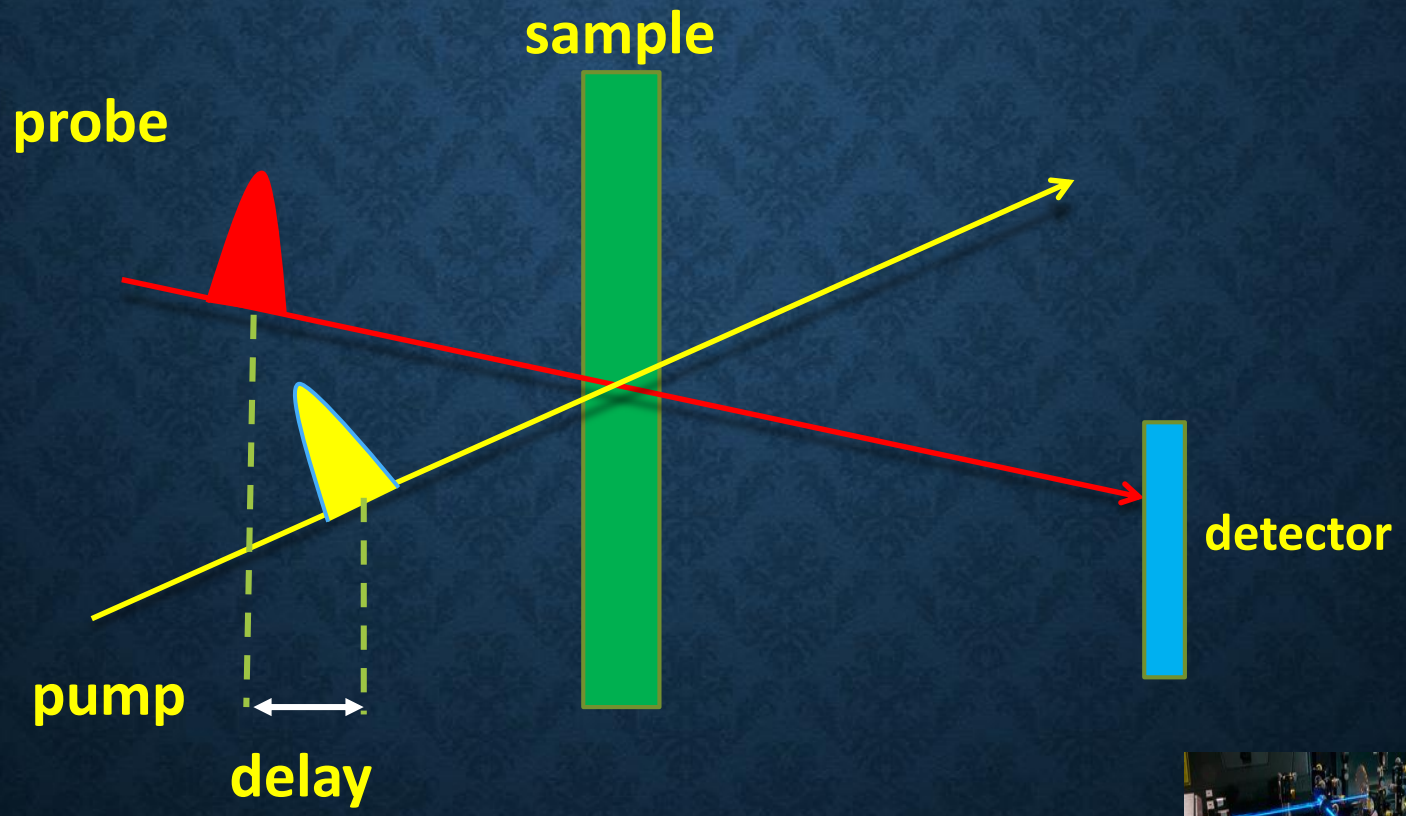

NONLINEAR OPTICAL PUMP-PROBE MICROSCOPY IS A NEW AREA FOR HIGH RESOLUTION 3D IMAGING IN MODERN MICROSCOPY. THE IMAGING CONTRAST RELIES UPON THE CHARACTERISTIC SPECTROSCOPIC PROPERTIES OF SPECIFIC MOLECULES, FOR EXAMPLE THEIR SPECIFIC INTERNAL ENERGY LEVEL STRUCTURE.

PUMP - PROBE TRANSIENT ABSORPTION SPECTROSCOPY

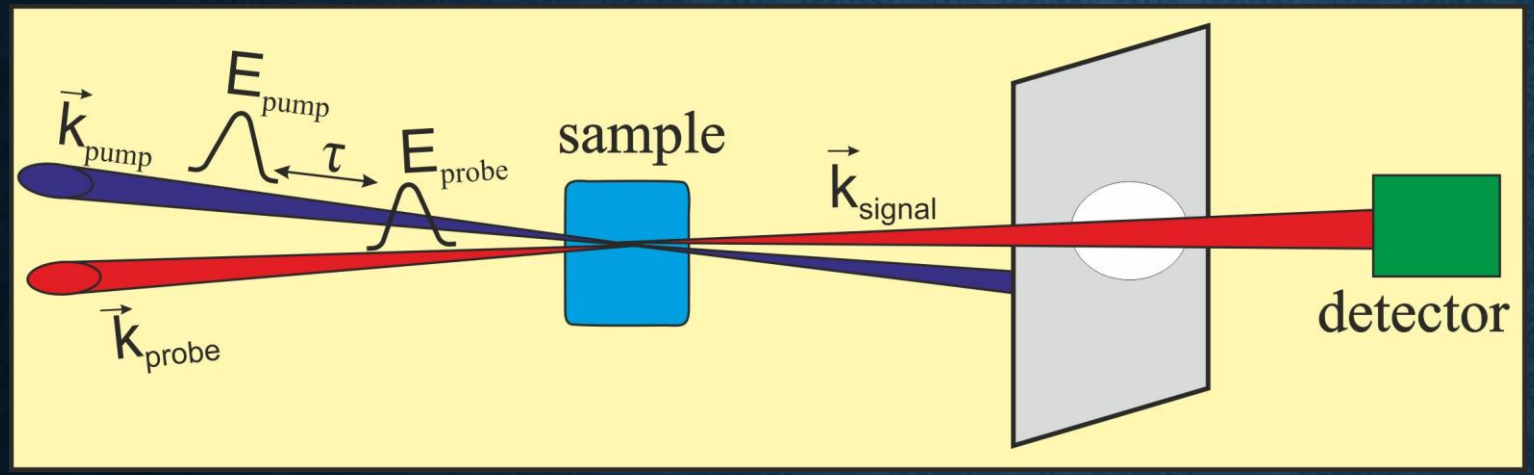

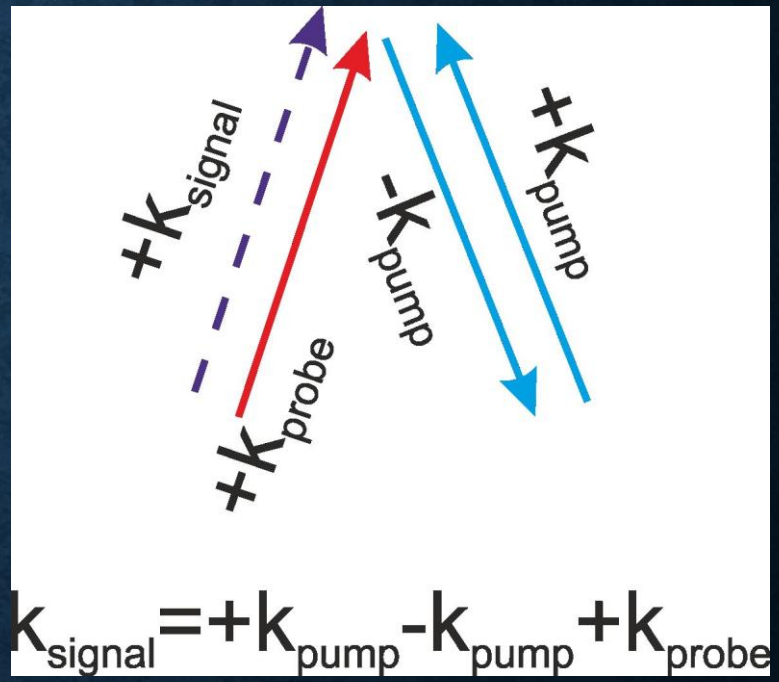

$$\Delta I(\tau)=2\omega_{sig}lIm[E_{pr}P^{(3)}(\tau)]$$

The pump-probe or transient absorption experiment is perhaps the most widely used third-order nonlinear experiment. It can be used to follow many types of time-dependent relaxation processes and chemical dynamics, and is most commonly used to follow population relaxation, chemical kinetics, or wavepacket dynamics and quantum beats.

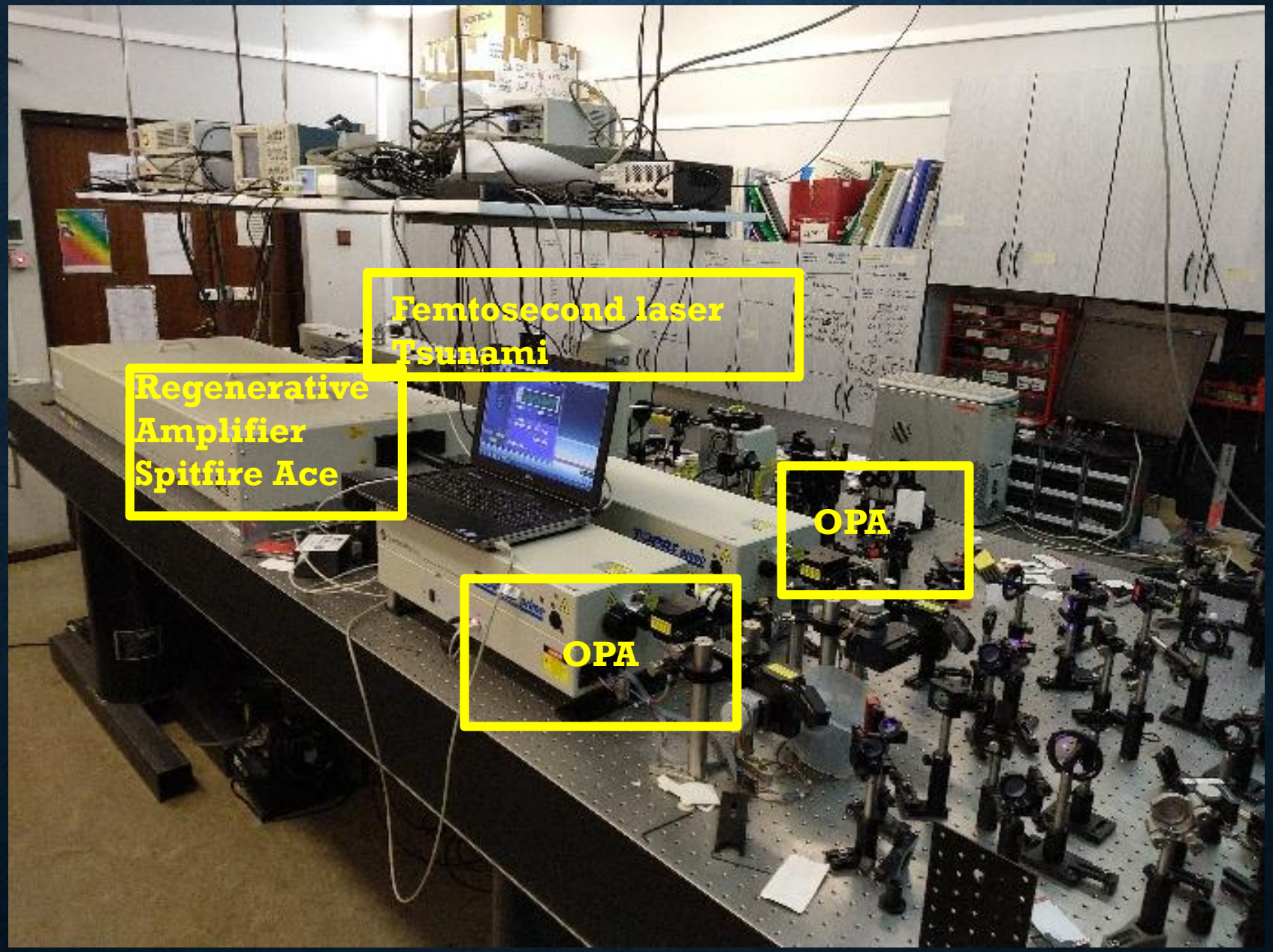
Femtosecond laser
Tsunami
Regenerative
Amplifier
Spitfire Ace
OPA
OPA

THE ROLE OF RETINOIDS IN CELLULAR SIGNAL TRANSDUCTION

- **To understand the role of retinoids in** cellular signal transduction in many vital processes in living organisms we must find proper tools for sensing retinoids in vivo to monitor retinoid distribution in cells and tissues, and temporal dynamics.

My presentation is not intended to be fully comprehensive or to upstage original discoveries, but rather to provide an overview of the recent progress from the perspective of my own laboratory's research.

RETINOIDS

ester

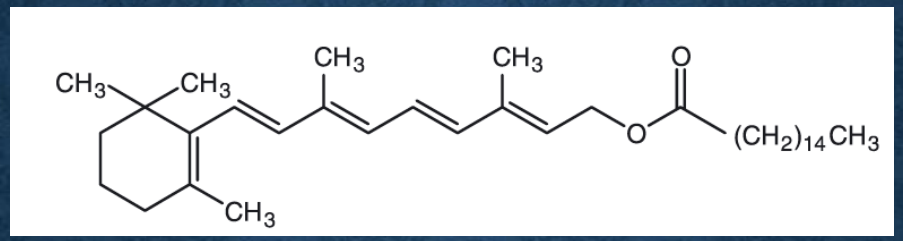

Retinyl palmitate

aldehyde

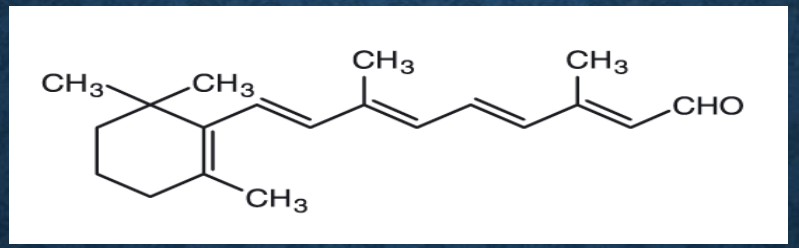

All-trans retinal

alcohol

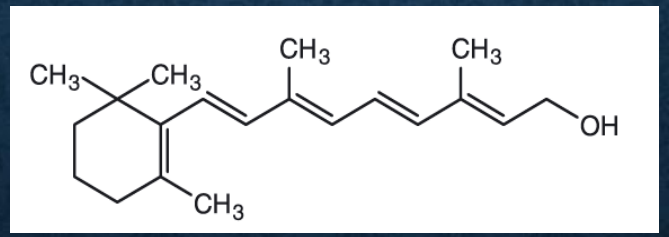

Retinol

The basic structure of the hydrophobic *retinoid* molecule consists of a cyclic end group, a *polyene* side chain and a polar end group

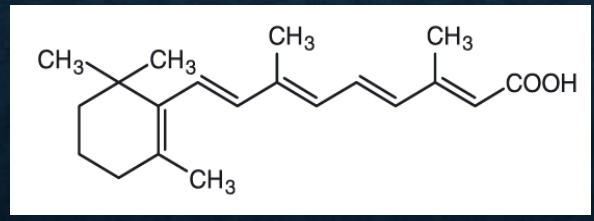

Retinoic acid

RETINOIDS METABOLISM IN VERTEBRATES

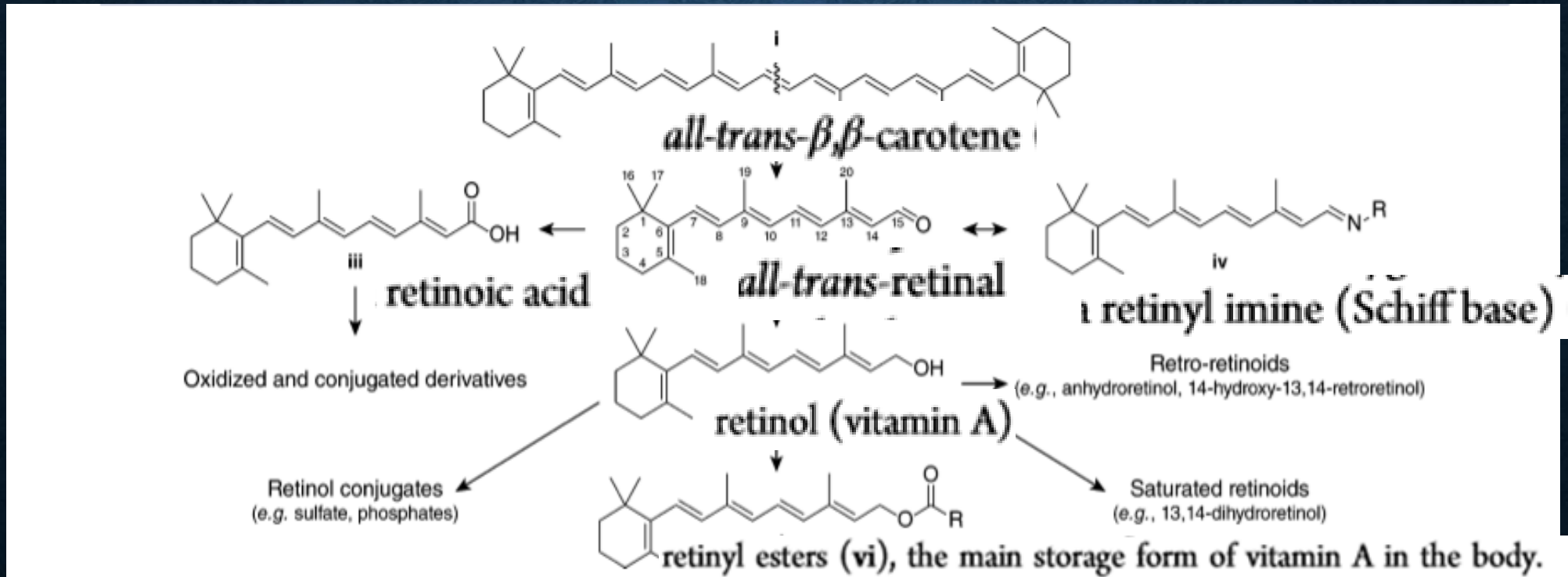

Figure 5. Retinoid metabolism in vertebrates. Dietary *all-trans*-β,β-carotene (i), obtained primarily from plants, is oxidatively cleaved in a symmetric manner by β-carotene monooxygenase I (BCMO I), yielding two molecules of *all-trans*-retinal (ii). Retinal can reversibly combine with an amino group to form a retinyl imine (Schiff base) (iv). Retinal is also subject to oxidation and reduction to form retinoic acid (iii) and retinol (vitamin A) v, respectively, the latter in a physiologically reversible manner. Retinoic acid can be converted into several conjugated and/or oxidized derivatives, some of which exert biological effects. Retinol also can be converted into several derivatives including retro-retinoids, saturated retinols, and phosphate conjugates. Retinol is also reversibly esterified to produce retinyl esters (vi), the main storage form of vitamin A in the body.

VITAMIN A ABSORPTION, METABOLISM, AND DELIVERY TO THE EYE

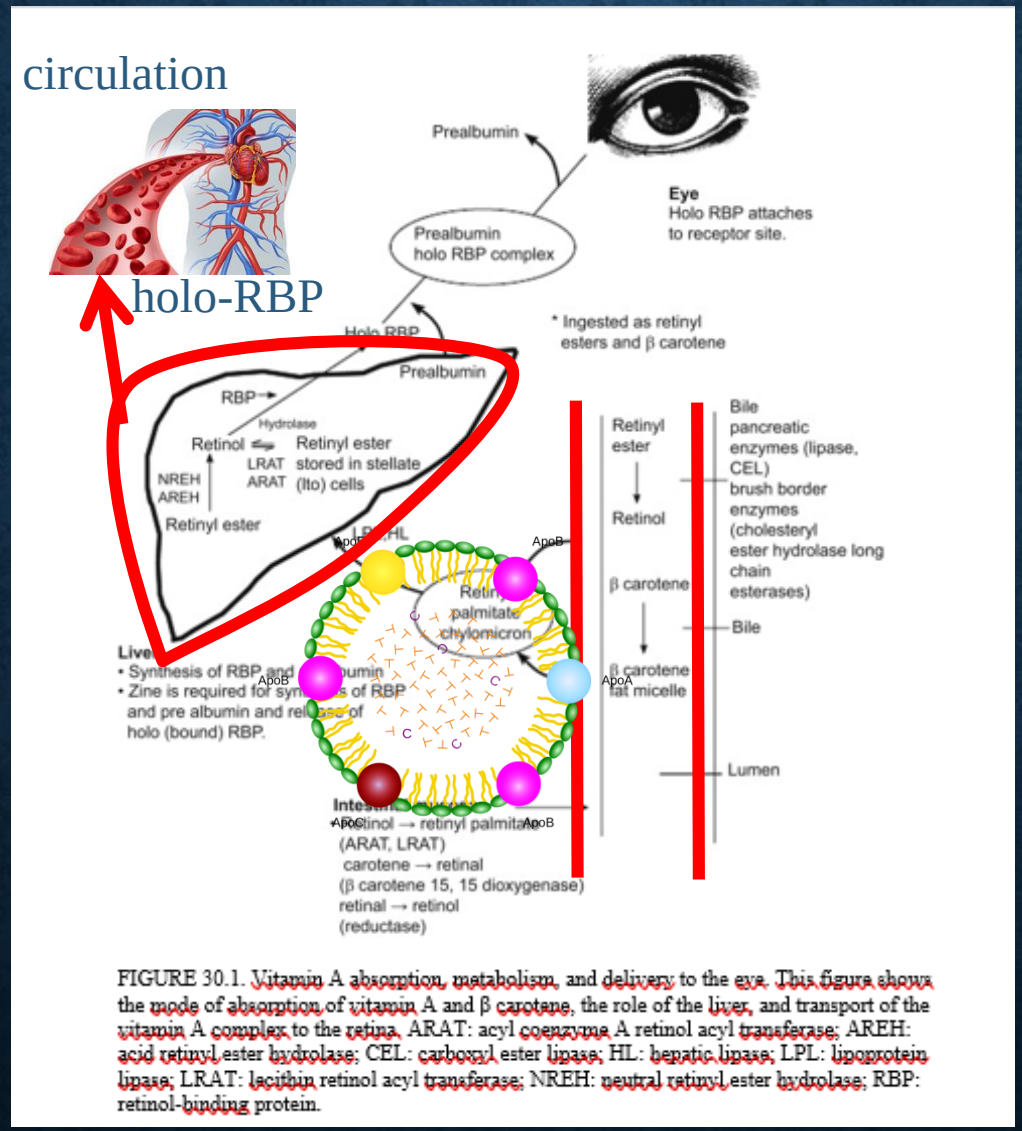

FIGURE 30.1. Vitamin A absorption, metabolism, and delivery to the eye. This figure shows the mode of absorption of vitamin A and β carotene, the role of the liver, and transport of the vitamin A complex to the retina. ARAT: acyl coenzyme A retinol acyl transferase; AREH: acid retinyl ester hydrolase; CEL: carboxyl ester lipase; HL: hepatic lipase; LPL: lipoprotein lipase; LRAT: lecithin retinol acyl transferase; NREH: neutral retinyl ester hydrolase; RBP: retinol-binding protein.

The liver accumulates vitamin A as retinyl ester when vitamin A intake exceeds the body's requirements. Under vitamin A–adequate conditions, most of the released retinol is transferred from **hepatocytes to hepatic stellate** cells, where retinol is bound to CRBP2 and reesterified by LRAT and then stored as retinyl esters within cytoplasmic lipid droplets.[33] Storage also serves as a detoxification mechanism, removing excess "free" retinol. When peripheral tissues require retinol, these **stored esters are hydrolyzed and retinol is mobilized back to hepatocytes.** Hepatocytes are also the major site of synthesis of RBP. **The newly released retinol combines with apo-RBP** to form the holo-RBP complex, which is released from the liver into the circulation.

Cellular retinoid-binding proteins (CRBP)

Chylomicrons transport dietary lipids and esters from the intestines to other locations in the body.

Hepatic stellate cells
Hepatic stellate cells reside between the hepatocytes and small blood vessels in the liver. They are characterised by the presence of lipid droplets and thin protrusions extending around the blood vessels. Their activation in damaged liver leads to secretion of collagen and formation of scar tissue, leading to chronic fibrosis or cirrhosis.

LRAT

LECITHIN RETINOL ACYLTRANSFERASE

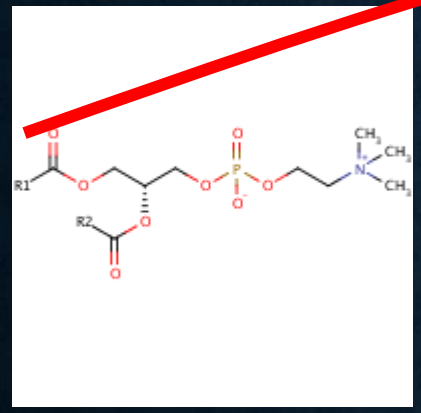

a 1,2-diacyl-*sn*-glycero-3-phosphocholine

+

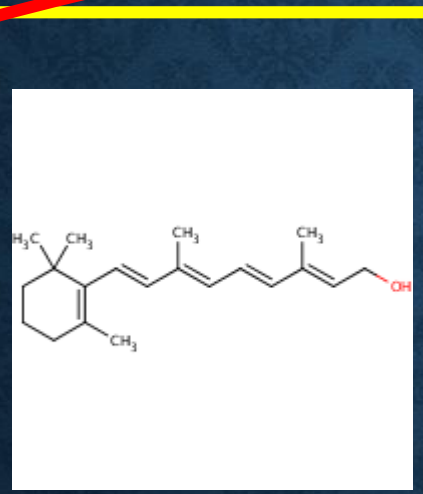

all-trans-retinol

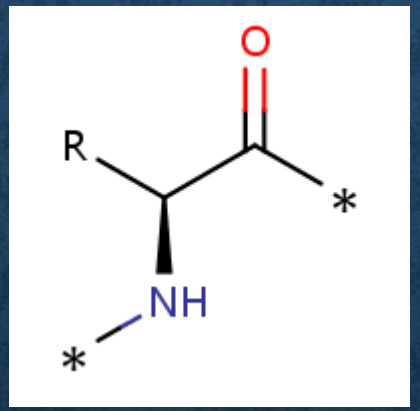

an L-α amino acid residue

=

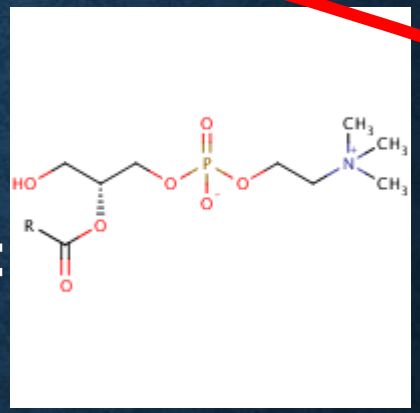

a 2-acyl-*sn*-glycero-3-phosphocholine

+

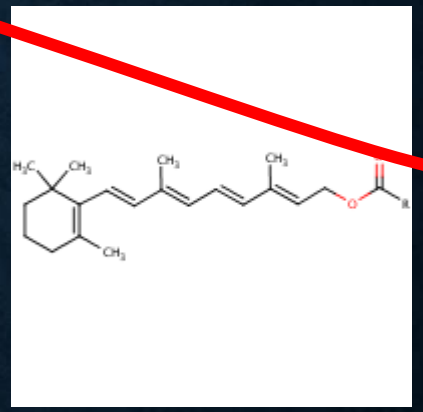

an all-trans-retinyl ester

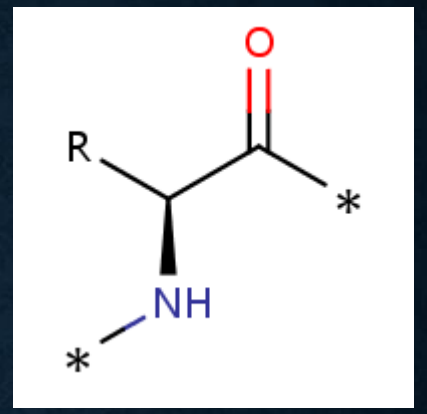

+

all-trans-retinol--[retinol-binding protein RBP]

LRAT transfers the acyl group from the sn-1 position of phosphatidylcholine to all-trans retinol, producing all-trans retinyl esters. Retinyl esters are storage forms of vitamin A.

EPIGENETIC MODIFICATIONS IN BRAIN TUMOR PATHOGENESIS

- There is an increasing evidence that retinoic acid and retinoic acid receptors (RAR) play important role in inducing epigenetic changes, and regulate epigenetic changes in carcinogenesis.
- Subcell Biochem. 2014; 70: 129–149.

Is Glioblastoma an Epigenetic Malignancy?

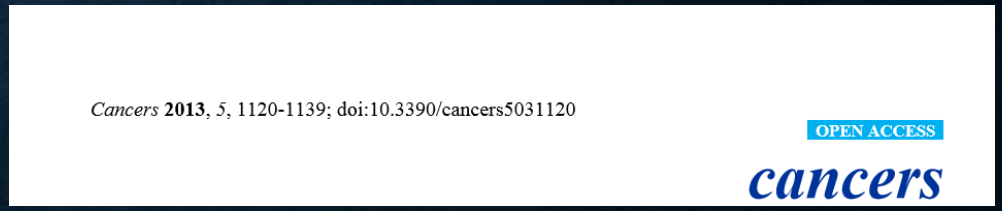

HISTONE -MODIFYING GENES AND EPIGENETIC ALTERATIONS IN MEDULLOBLASTOMA

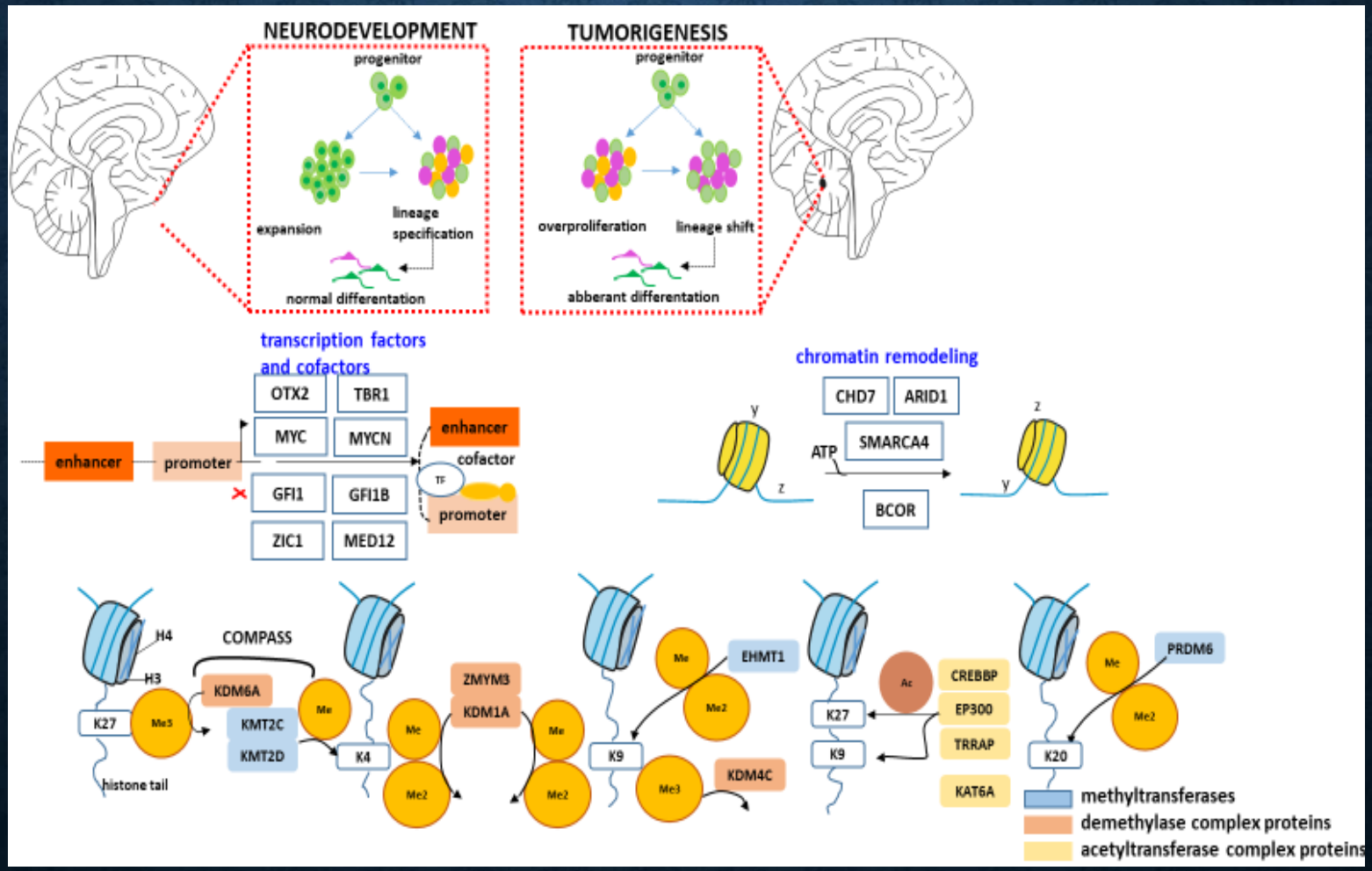

CELLULAR SIGNAL TRANSDUCTION

- **Vitamin A plays an important role in cellular signal transduction in many vital processes. Proton gradient triggers the synthesis ATP. There are two types of generation of proton gradient.**
-
- **the light-activated mechanism in vision processes (rhodopsin family)**
-
- **the electron transport chain forms a proton gradient across the inner mitochondrial membrane, which drives the synthesis of ATP via chemiosmosis.**
-

The light-activated mechanism of proton gradient

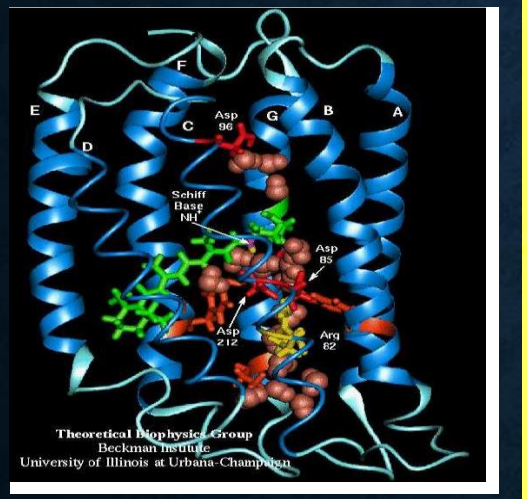

Light activation *triggers* trans to cis isomerization of a bound retinal

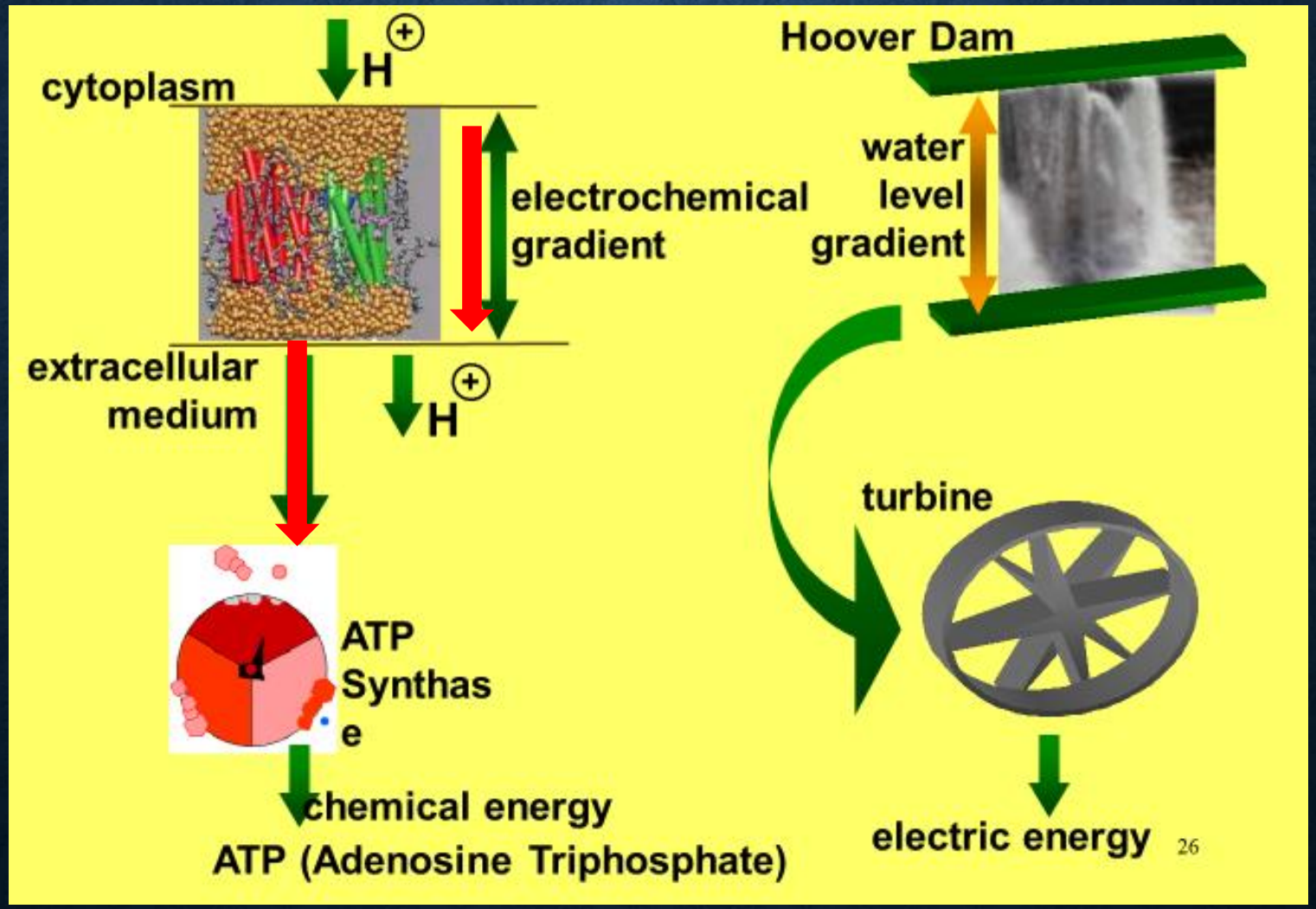

It acts as a proton pump; that is, it captures light energy and uses it to move protons across the membrane out of the cell. The resulting proton gradient across the membrane triggers ATP synthesis used for metabolism and phosphorylation by *ATP* synthase

THE ELECTRON TRANSPORT CHAIN FORMS A PROTON GRADIENT ACROSS THE INNER MITOCHONDRIAL MEMBRANE, WHICH DRIVES THE SYNTHESIS OF ATP VIA CHEMIOSMOSIS.

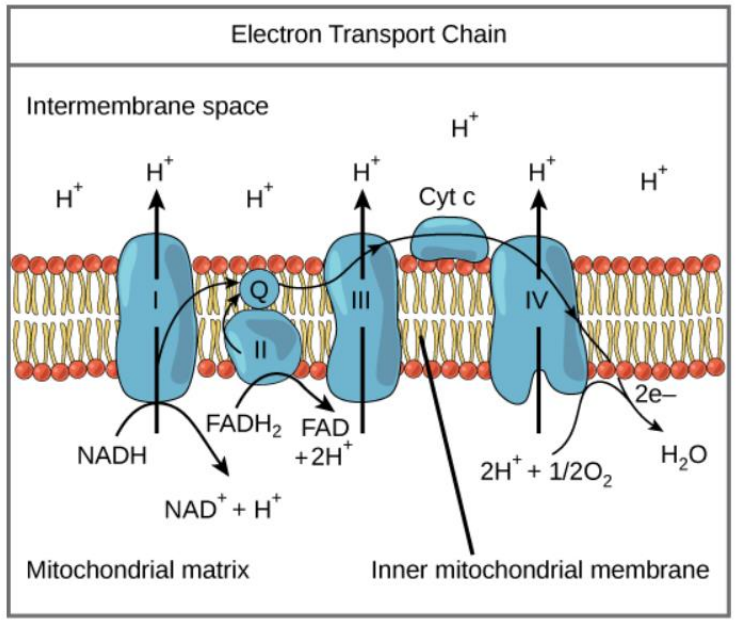

Image modified from "Oxidative phosphorylation: Figure 1", by OpenStax College, Biology (CC BY 3.0).

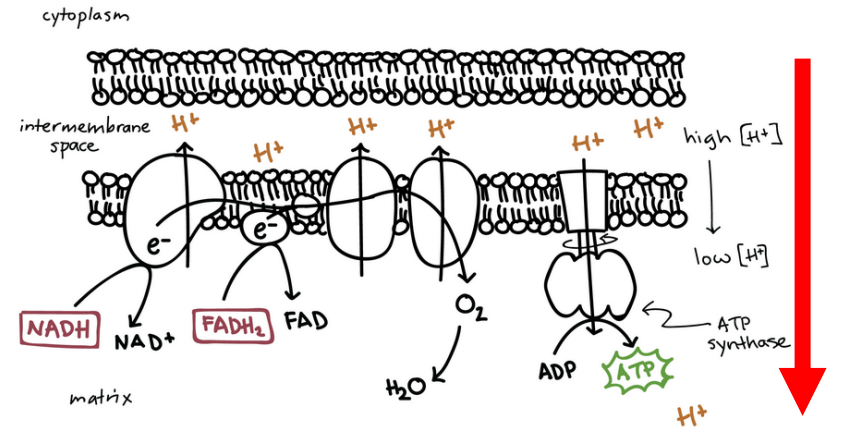

The **electron transport chain** is a series of proteins and organic molecules found in the inner membrane of the mitochondria. Electrons are passed from one member of the transport chain to another in a series of redox reactions. Energy released in these reactions is captured as a proton gradient, which is then used to make ATP in a process called **chemiosmosis**. Together, the electron transport chain and chemiosmosis make up **oxidative phosphorylation**. The key steps of this process, shown in simplified form in the

RETINOIDS BOUND TO PROTEINS

„ FREE” RETINOIDS

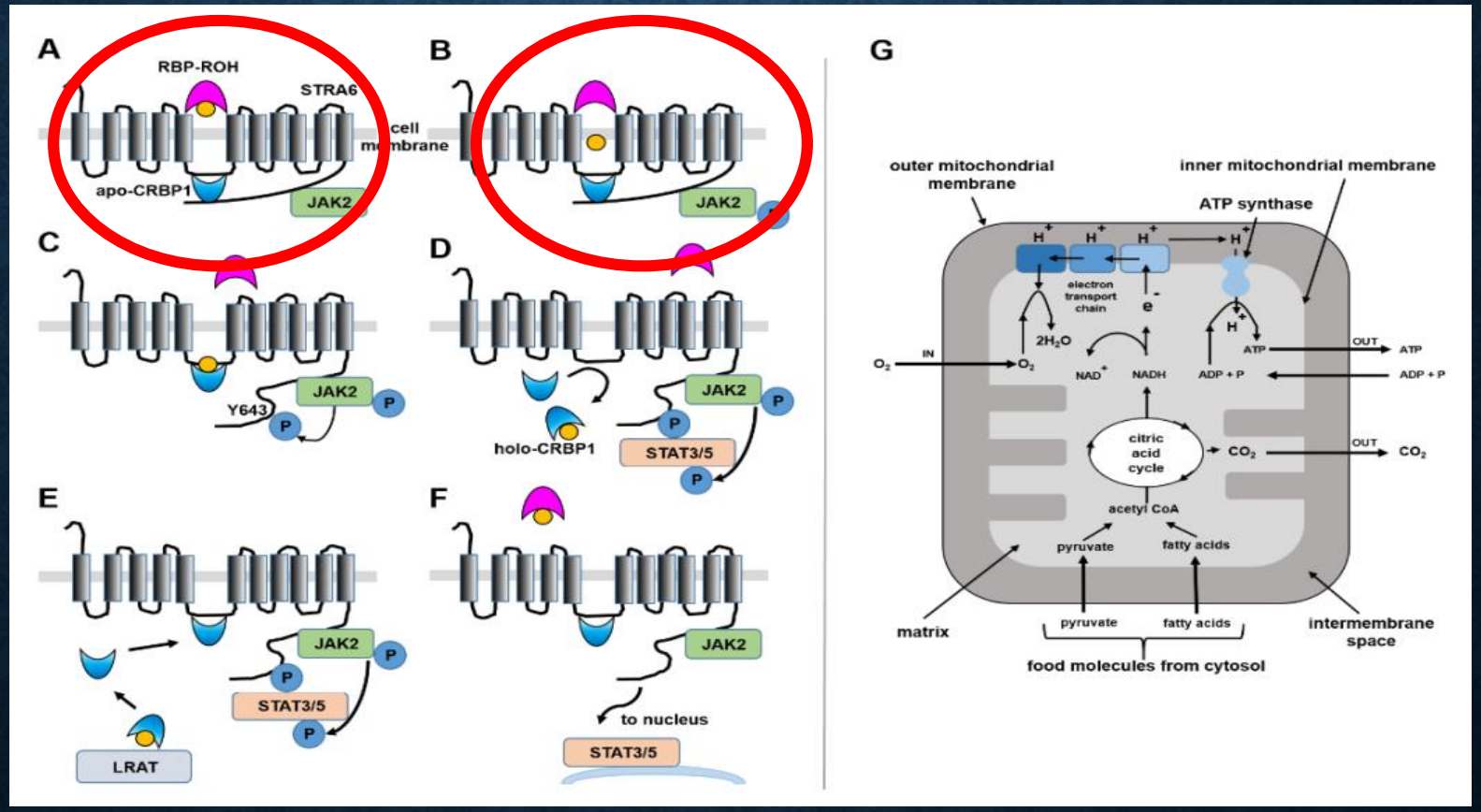

RETINOIDS BOUND TO PROTEINS

1. H. ABRAMCZYK, *FEMTOSECOND PRIMARY EVENTS IN BACTERIORHODOPSIN. REVISION OF COMMONLY ACCEPTED INTERPRETATION OF ELECTRONIC SPECTRA OF TRANSIENT INTERMEDIATES*, J. CHEM.PHYS. 120 11120 (2004)

1. A. TERENTIS, L.UJI, H. ABRAMCZYK, G. H. ATKINSON, *PRIMARY EVENTS IN BACTERIORHODOPSIN PHOTOCYCLE: TORSIONAL VIBRATIONAL DEPHASING IN THE FIRST EXCITED ELECTRONIC STATE*, CHEM. PHYS. 313(2005) 51-62

bacteriorhodopsine

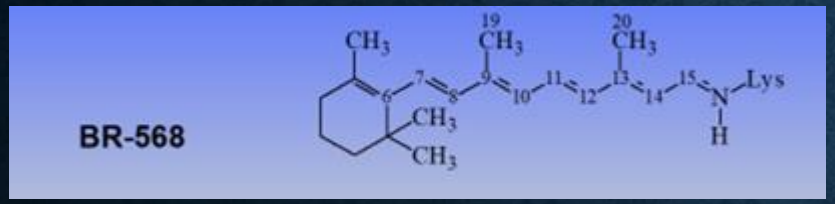

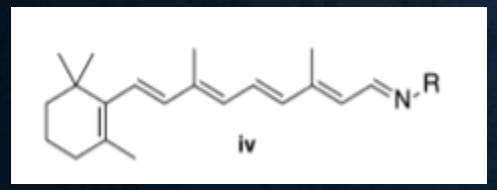

Retinyl imine (Schiff base)

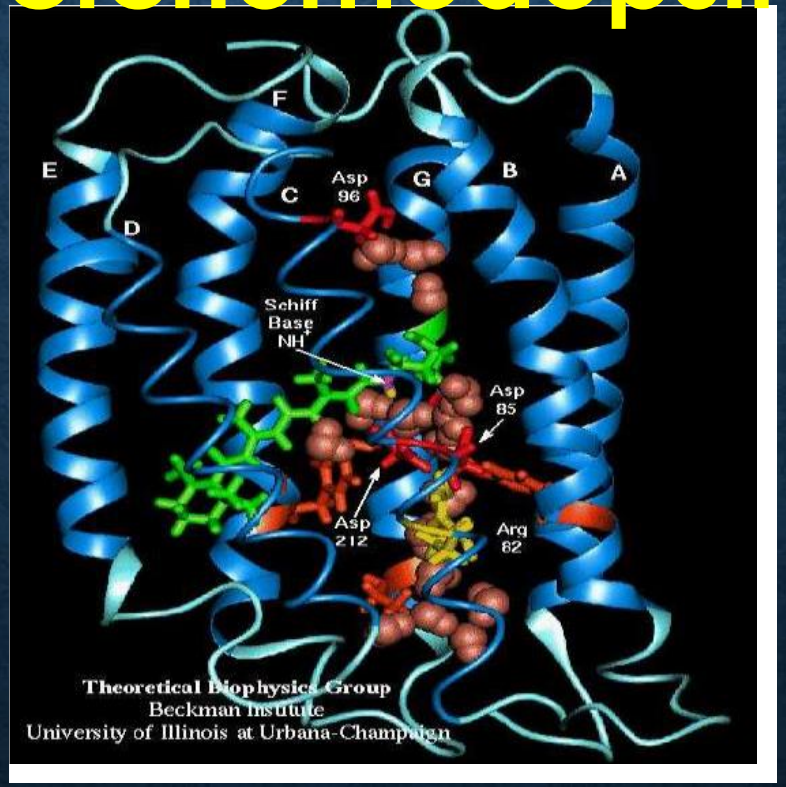

BR contains a polyene chromophore, retinal, which is covalently bound to the Lys^{216} residue of the protein by a protonated Schiff base linkage

RETINOIDS BOUND TO PROTEINS

hv

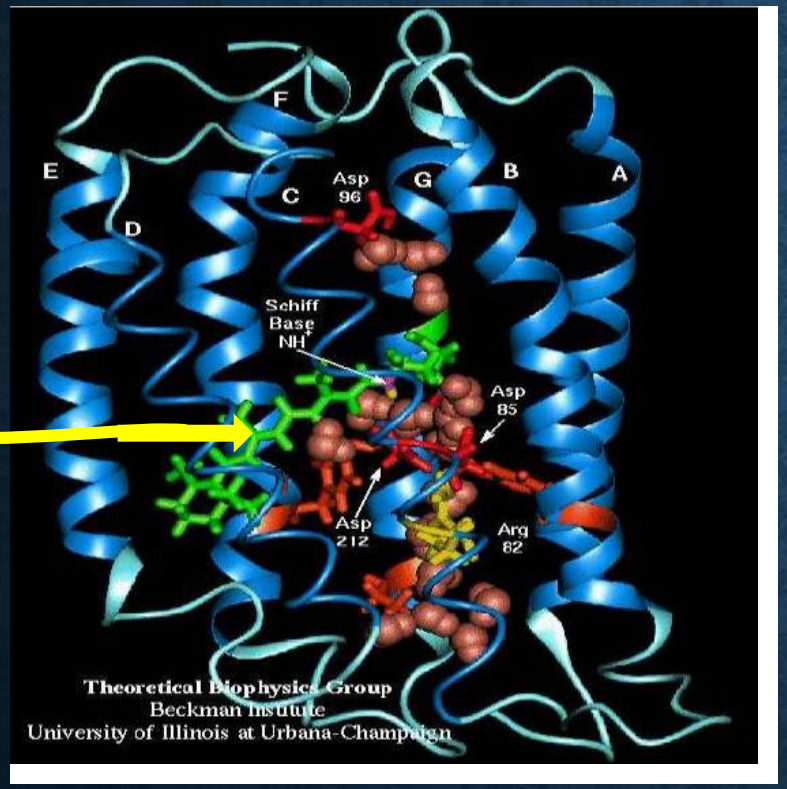

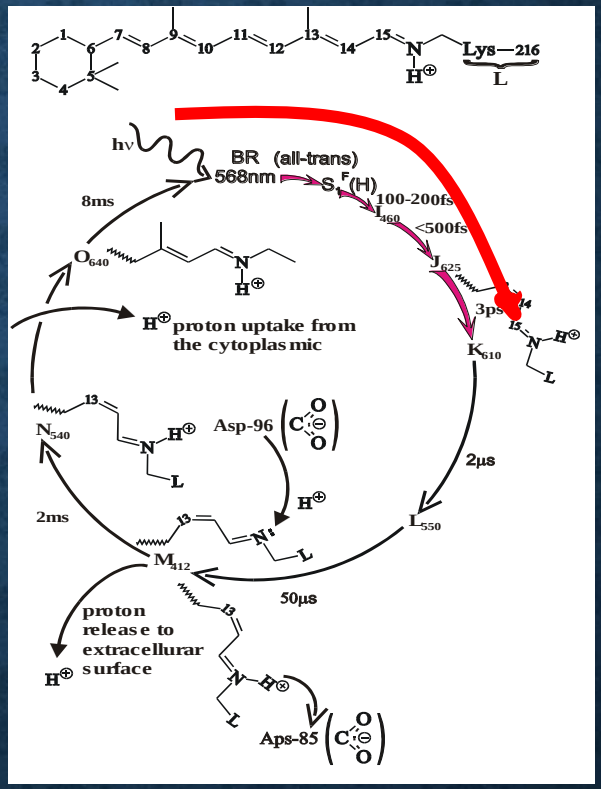

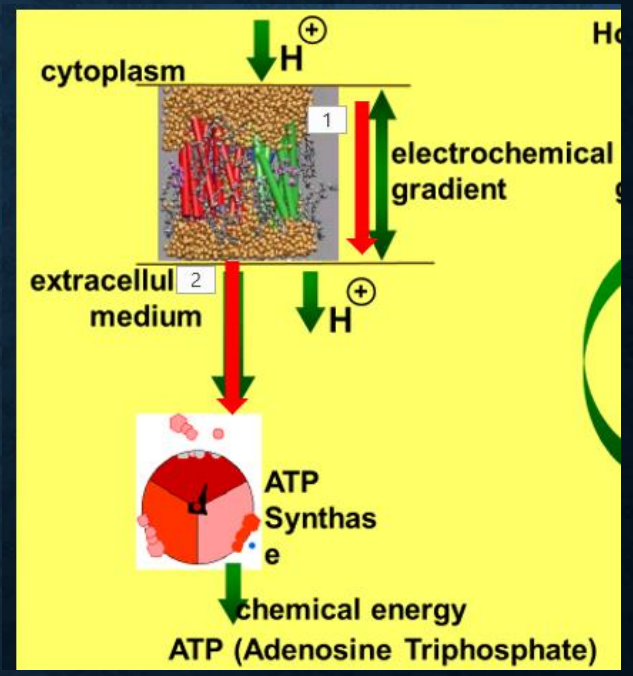

The absorption of a photon from the visible range (568 nm) initiates in bacteriorhodopsin a cyclic sequence of reactions that is completed on the milisecond time scale (Scheme 1) leading to the proton moving from the cytoplasmic side to the extracellular surface and generation of an electrochemical potential that is used by a bacterium to maintain its metabolism. As one can see from the Scheme 1 the observed time constants of BR photocycle span about 11 decades. The photocycle can be divided into two distinct parts. The first one comprises very fast molecular processes occurring on femto- and picosecond time scale upon BR-568 (all-trans) excitation up to the formation of the K intermediate that has the 13-cis configuration. The second part of the photocycle is much slower.

BROADBAND CARS (BCARS) MICROSCOPY VS SINGLE FREQUENCY CARS MICROSCOPY

- In order to probe a full BCARS spectrum, typically a broadband Stokes beam is employed . The broadband supercontinuum can be generated inside a photonic crystal fiber . Often a charge-coupled device (CCD) detector is used, where vertical binning generates a linear array of non-negative integers, i.e., signal intensities per wavenumber. A single spectrum is collected in each image point and sample scanning can be performed to acquire a spectral map.

- Although the collection of BCARS images is faster than spontaneous Raman spectral images, the read out is more challenging due to the contribution of the non-resonant background. This non-resonant component is non-frequency dependent and entirely real, while the resonant component that contains the chemical information can be divided into a real and imaginary part. The imaginary part is directly comparable to spontaneous Raman signals . Both display a linear dependence on molecular concentration : $I\{\chi\}= \quad A \quad \Gamma\, \Omega-(\omega- \omega)+ \Gamma$ eq. 6 $I \propto \quad A \quad \Gamma\, \Omega-\omega+ \Gamma$ N is here the number of scatterers, A, Ω, Γ amplitude, frequency, and line width of the vibrational mode. In order to obtain the imaginary part of χ from raw BCARS spectra, the convolution of the resonant and non-resonant components has to be overcome. $I\{\chi\}$ can be extracted if the spectral phase is known, which can be achieved with a modified Kramers-Kronig relation. However, this analysis is technically only applicable to data covering an infinite frequency range. In order to extrapolate the data, one method can be the use of a Fourier transformation, replacing the negative time domain with a frequency dependent non-resonant response, and transforming back to the frequency domain

TIME RESOLVED CARS

FREQUENCY DOMAIN

UNIVERSITY OF ARIZONA
DEPARTMENT OF CHEMISTRY
85 721 TUSCON, AZ, USA

- H. Abramczyk, Femtosecond primary events in bacteriorhodopsin. Revision of commonly accepted interpretation of electronic spectra of transient intermediates, J. Chem. Phys. 120 11120 (2004)
-
- A. Terentis, L. Uji, H. Abramczyk, G. H. Atkinson, Primary events in Bacteriorhodopsin photocycle: torsional vibrational dephasing in the first excited electronic state, Chem. Phys. 313(2005) 51-62

PICOSECOND CARS

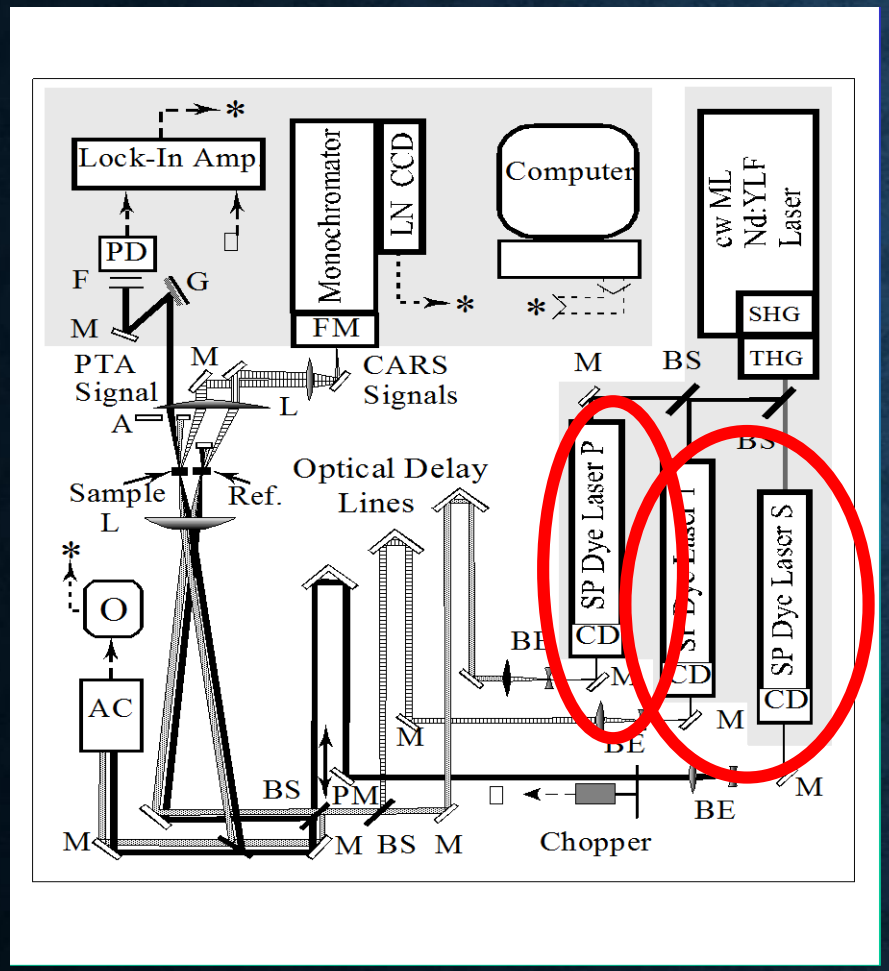

PUMP

PROBE

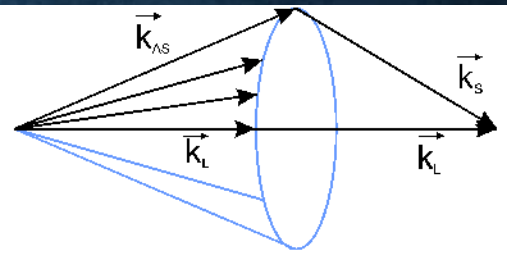

Fig. 4.5. Directions of propagation of the stimulated anti-Stokes scattering

Why the phase matching condition, $\Delta\mathbf{k} = 0$, that is always met for the stimulated Stokes scattering, it is not automatically complied with the stimulated anti-Stokes scattering? It results from the fact that the phase of vibrating molecules is defined by the more intense Stokes scattering.

To sum up, intense light of the frequency ω_L can cause intense stimulated Raman scattering: Stokes $\omega_S = \omega_L - \omega_{wib}$ and anti-Stokes $\omega_{AS} = \omega_L + \omega_{wib}$. As a result of photon interaction with matter, the energy exchange via optical phonons (or vibrations) takes place leading to the formation in a medium the third-order polarisation, $P^{(3)} \propto \chi^{(3)}_{ijkl} E_j E_k E_l$, that consists of the components changing with the frequency $\omega_{wib} = \omega_L - \omega_S$, $\omega_S = \omega_L - \omega_{wib}$ and $\omega_{AS} = \omega_L + \omega_{wib}$. The polarisation components generate new waves of the frequencies ω_S and ω_{AS} known as the stimulated Stokes and anti-Stokes Raman scattering. The phase matching condition is met in all directions for the Stokes radiation $(\Delta\mathbf{k} = 0)$, so the scattered light is emitted in all directions. The anti-Stokes stimulated scattering is observed in directions, $\mathbf{k}_{AS}$, for which the phase matching condition $2\mathbf{k}_L - \mathbf{k}_S = \mathbf{k}_{AS}$ is met.

Briefly, lightpulses from a narrowband (<4 cm1, FWHM) dye laser operated at 663 nm (l1) and a broadband (700 cm1)dye laser operated in the 700–750 nm region (ls) are phase-matched in a flowing BR (native or modified-retinal pigment) sample, generating CARS signals spanning an approximately 700 cm1 spectral region (λas). In order to cover the entire 750–1750 cm1spectral range of interest, either λ1is tuned a few nanometers or λ s is adjusted by using a different laser-dye solution.

CARS: theory

- **Intensity of the CARS signal:**

$$I_{as}(\omega_{as}) \mu |\chi^{(3)}(\omega_{as},\omega_1,\omega_s)|^2 . I_1^2 . I_s(\omega_s) . G^2$$

- **Normalized CARS spectrum fitting function (2-species mixture):**

$$\frac{I_{as}^{Sample}}{I_{as}^{Reference}} = \mu^2 \left| 1 + (1 - \eta) \sum_{j=1}^{N_A} \frac{A_j \, e^{i\Theta_j}}{\Delta_j - i} + \eta \sum_{k=1}^{N_B} \frac{A_k \, e^{i\Theta_k}}{\Delta_k - i} \right|^2$$

$$\Delta_j = (\Omega_j - (\omega_1 - \omega_s)) / \Gamma_j$$

- **Background-free (Lorentzian lineshapes) spectral intensity:**

$$I_{raman} = \sum_{j=1}^{N} \frac{A_j^2}{(\Omega_j - (\omega_1 - \omega_s))^2 + \Gamma_j^2}$$

Ω = Band Origin
A = Amplitude
Γ = Bandwidth
Θ = Vibrational phase
η = relative conc. ($0 \leq \eta \leq 1$)
μ = Scaling factor
N = Number of vibrations
$\chi^{(3)}$ = third-order susceptibility

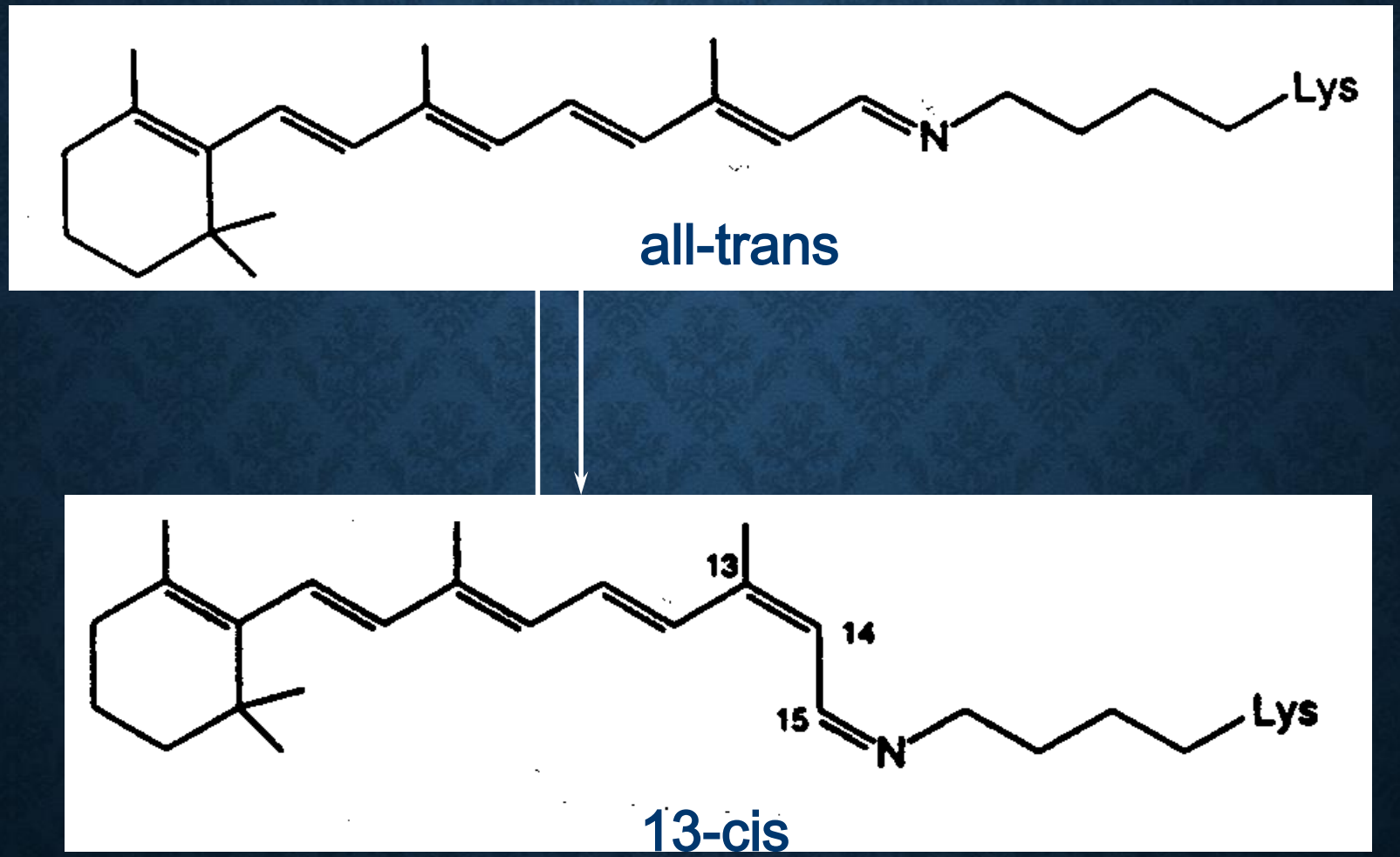

Light activation *triggers* trans to cis isomerization of a bound retinal

Native BR-568 and unlocked analogs BR 6.11 and 6.9

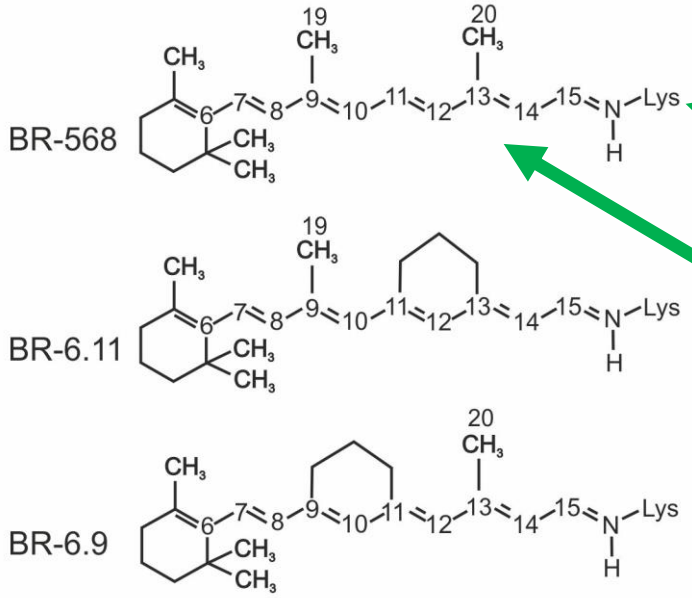

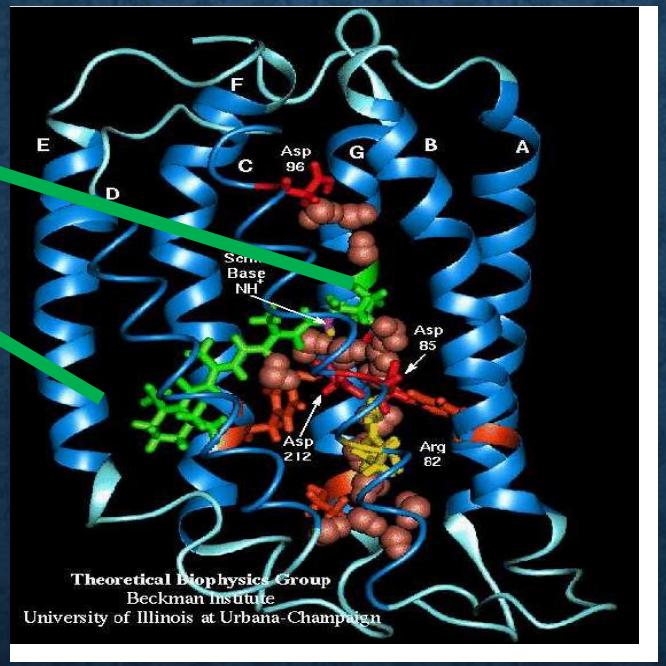

Locked analogs BR 5.12 and BR 5.13

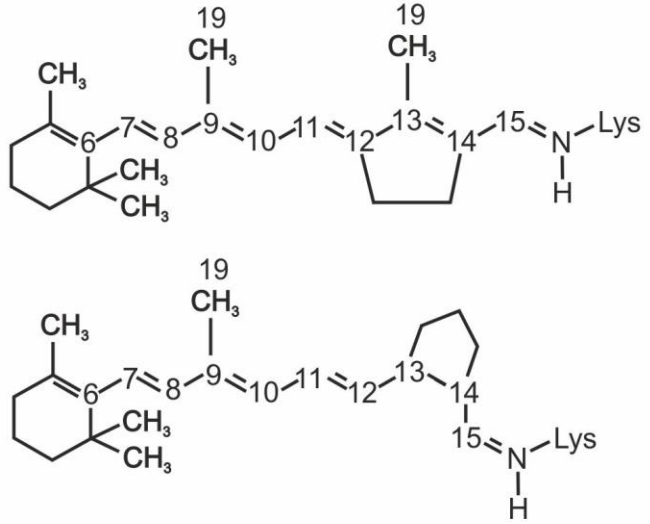

Andrew C. Terentis, Laszlo Ujj, Halina Abramczyk, George H. Atkinson*
Chemical Physics 313 (2005) 51–6

NATIVE BR-568 AND UNLOCKED ANALOGS BR 6.11 AND 6.9

The artificial BR pigments examined here contain a retinal with six-membered carbon ring incorporated into the retinal backbone that remains the 13C=C14 bond free to isomerize

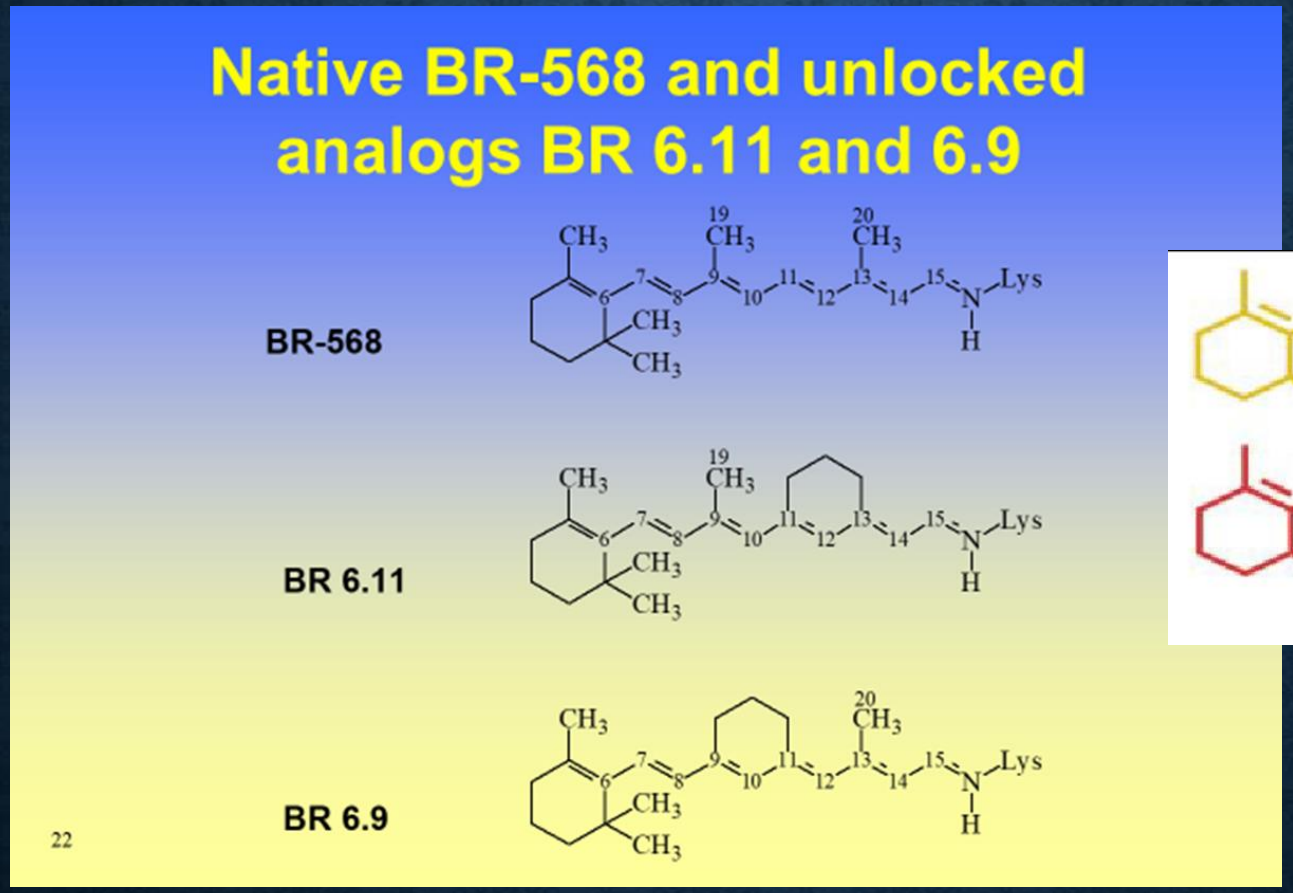

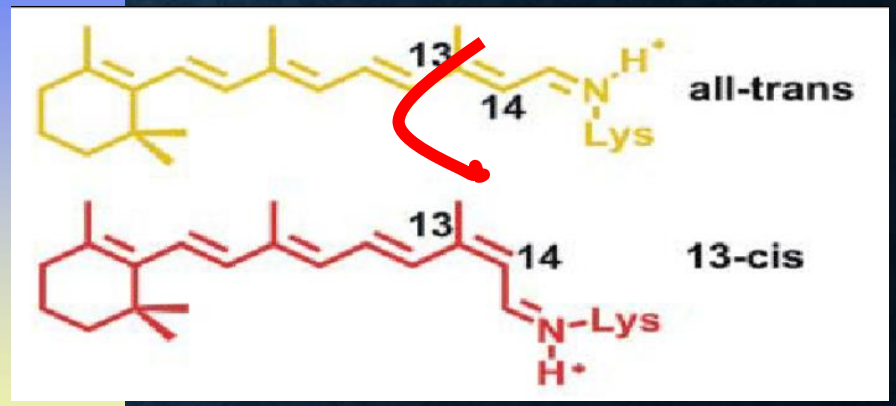

Primary events in the bacteriorhodopsin photocycle:Torsional vibrational dephasing in the first excited electronic stateAndrew C. Terentis, Laszlo Ujj, Halina Abramczyk, George H. Atkinson* Chemical Physics 313 (2005) 51–6

Locked analogs BR 5.12 and BR 5.13

BR 5.12

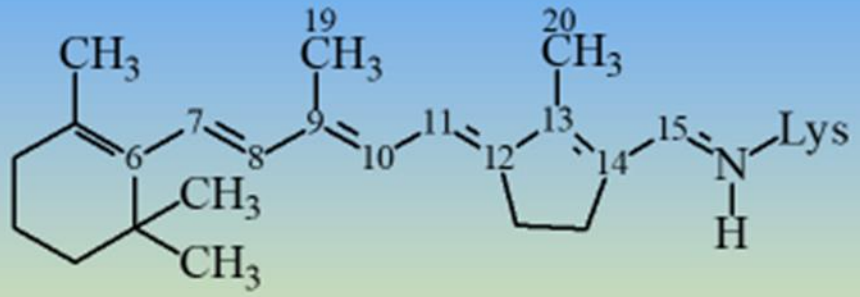

BR 5.13

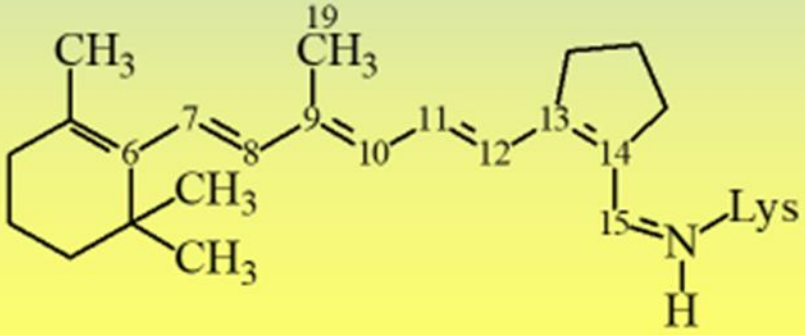

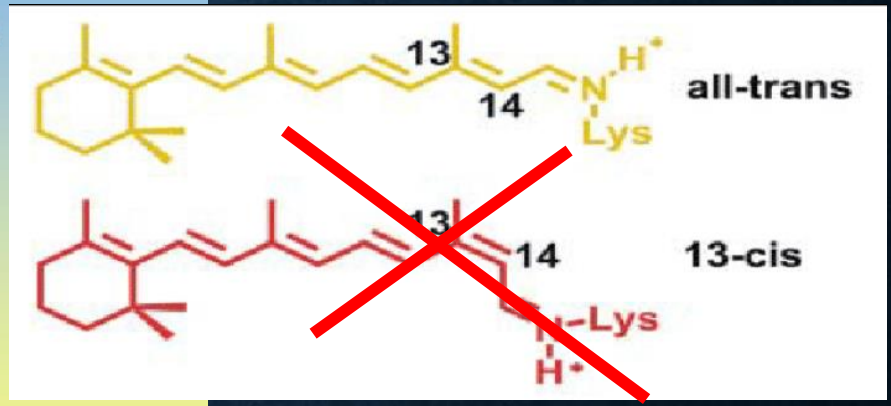

28

For BR5.12, the C13=C14 retinal bond is locked in the trans configuration by a rigid, five-membered carbon ring

NATIVE BR-568 AND UNLOCKED ANALOGS BR 6.11 AND 6.9

The artificial BR pigments examined here contain a retinal with six-membered carbon ring incorporated into the retinal backbone that remains the 13C=C14 bond free to isomerize

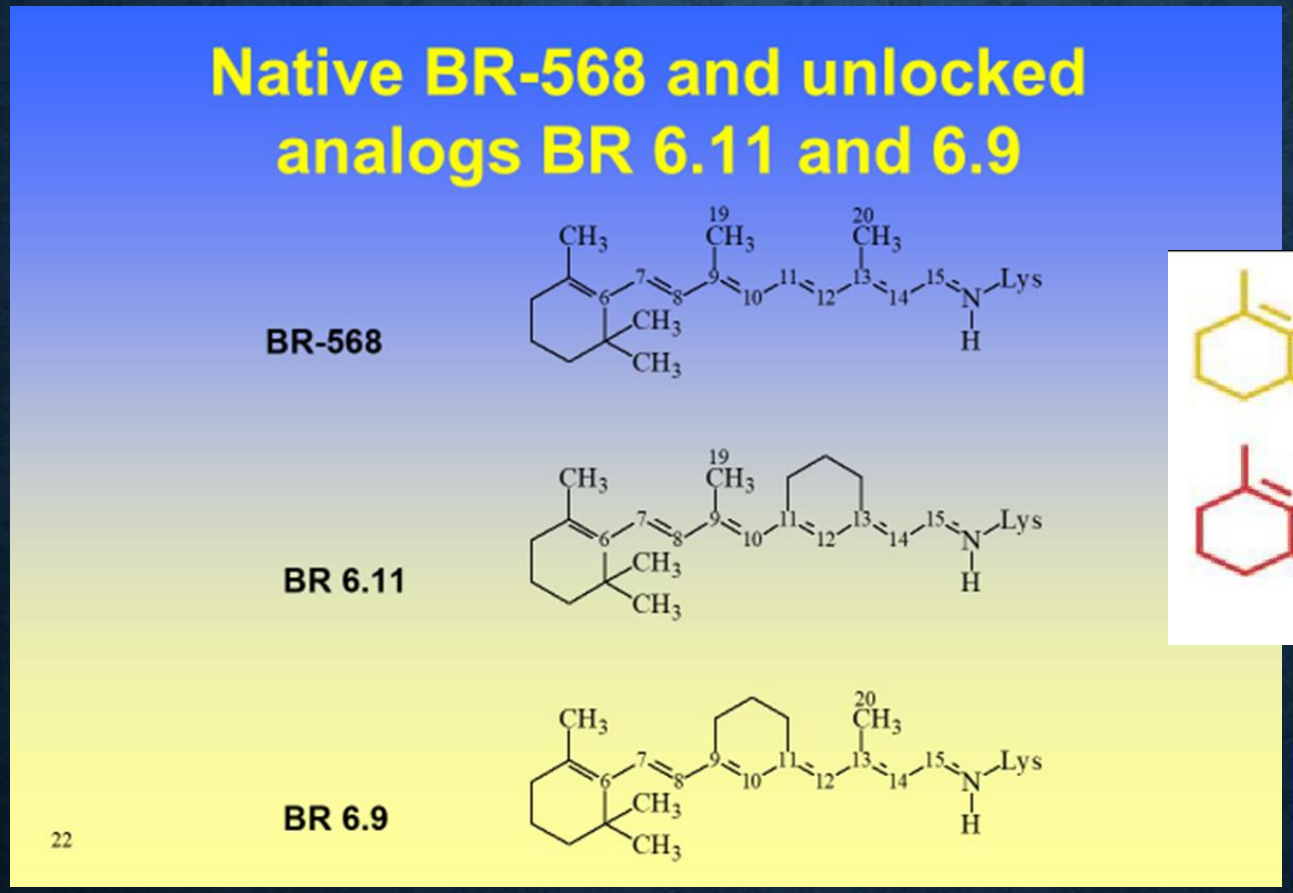

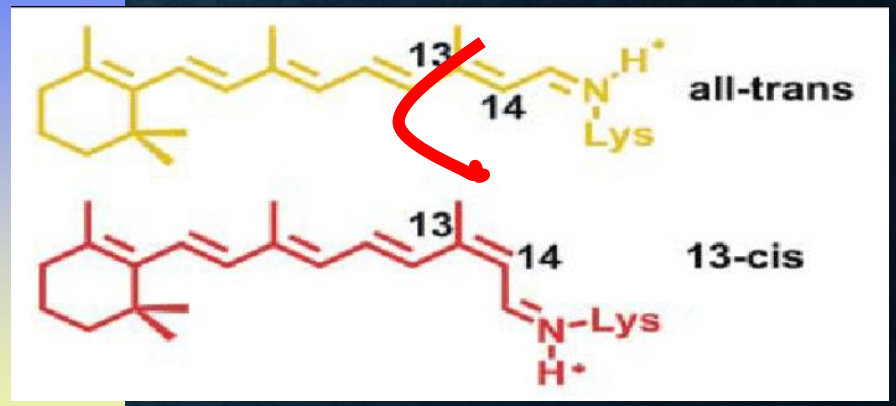

Primary events in the bacteriorhodopsin photocycle:Torsional vibrational dephasing in the first excited electronic stateAndrew C. Terentis, Laszlo Ujj, Halina Abramczyk, George H. Atkinson* Chemical Physics 313 (2005) 51–6

NATIVE BR-568 AND UNLOCKED ANALOGS BR 6.11 AND 6.9

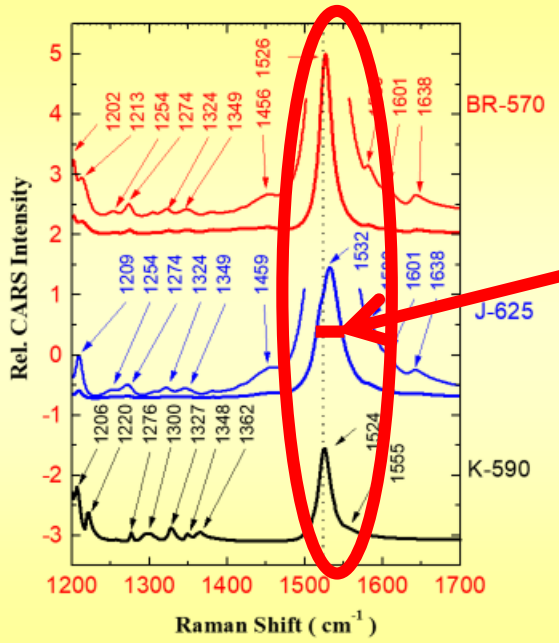

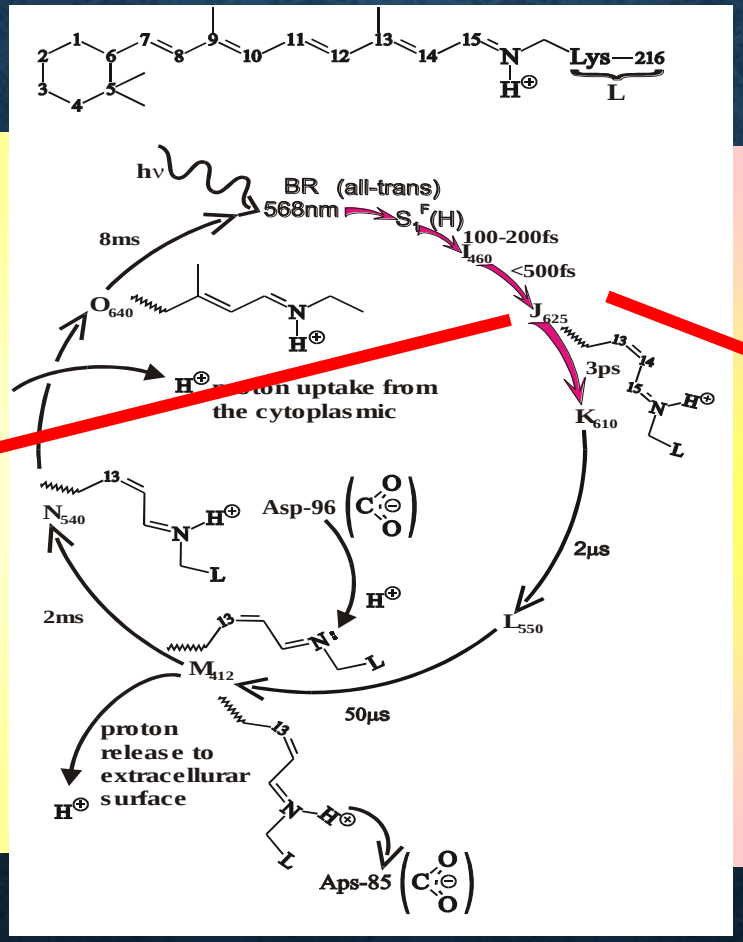

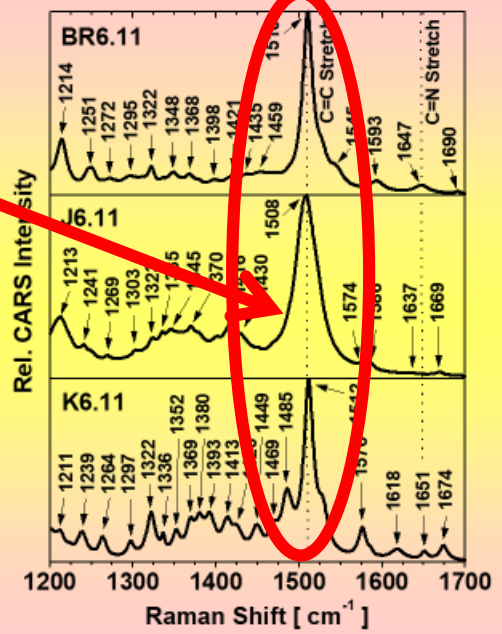

vibrational spectra of BR-570 (top), J-625 (center, derived from the 0-ps PTR/CARS data),and K-590 (bottom, derived from the 200-ps PTR/CARS data) in the1200–1700 cm1region

Locked analogs BR 5.12 and BR 5.13

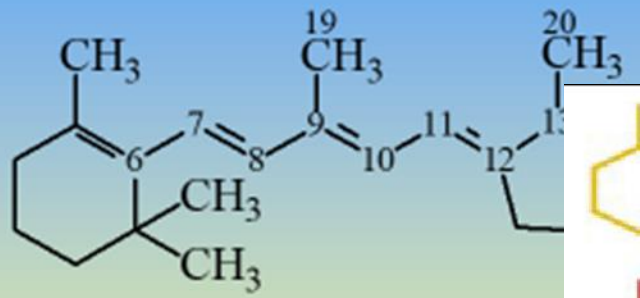

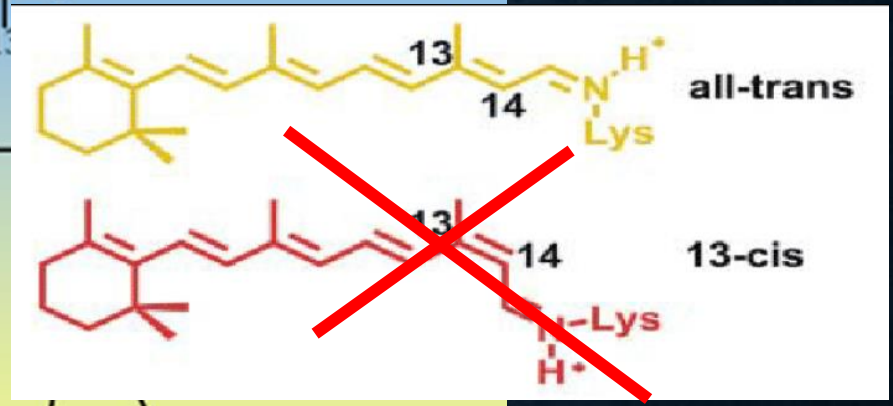

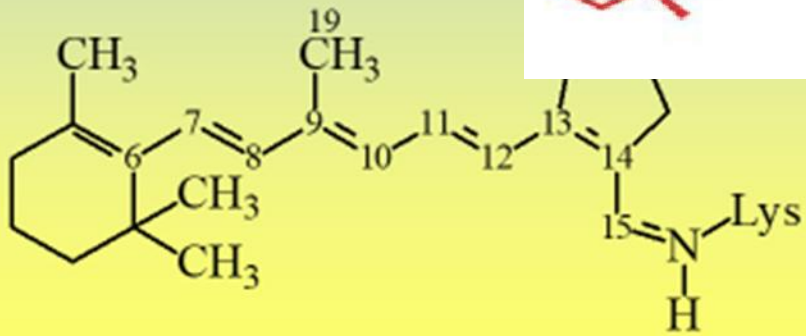

28

Andrew C. Terentis, Laszlo Ujj, Halina Abramczyk, George H. Atkinson* Chemical Physics 313 (2005) 51–6

For BR5.12, the C13=C14 retinal bond is locked in the trans configuration by a rigid, five-membered carbon ring

Locked analogs BR 5.12 and BR 5.13

BR 5.12

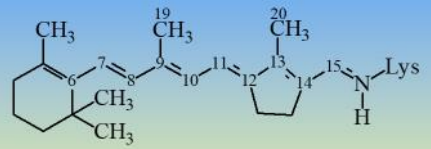

BR 5.13

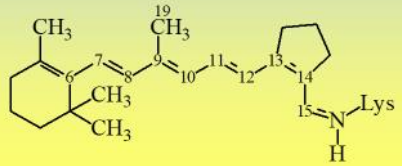

28

Andrew C. Terentis, Laszlo Ujj, Halina Abramczyk, George H. Atkinson*
Chemical Physics 313 (2005) 51–6

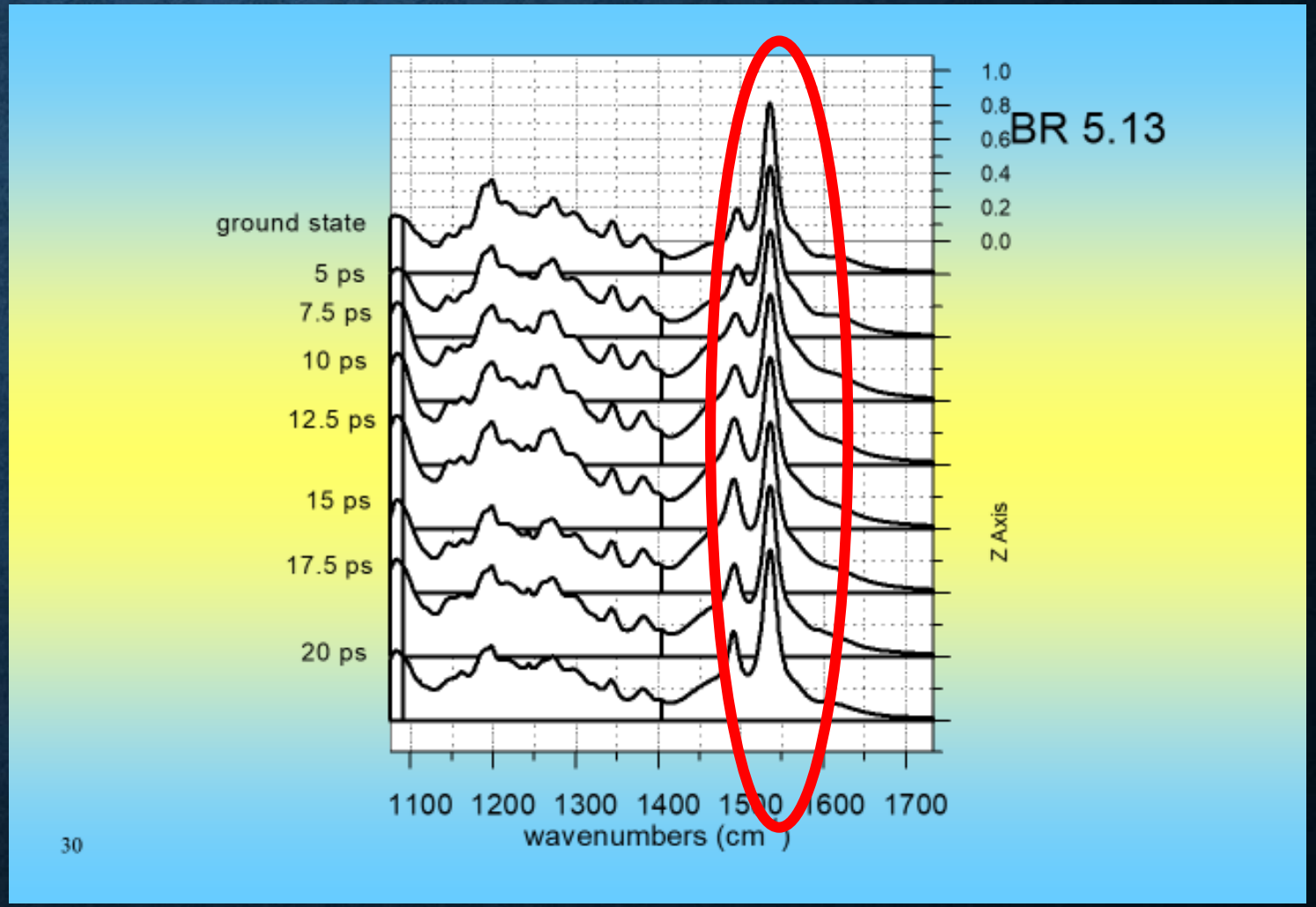

30

WHAT INFORMATION ABOUT VIBRATIONAL DYNAMICS IS CONTAINED IN THE CARS BAND SHAPE ?

1 Maxwell equation

$$\nabla^2 E + \frac{1}{c^2}\frac{\partial^2 (E(\vec{r},t))}{\partial t^2} = -\frac{4\pi}{c^2}\frac{\partial^2 P}{\partial t^2}$$

2 $$\langle \vec{P}(\vec{r},t) \rangle = T_r\left(\vec{P}(\vec{r},t)\right)\rho(t)$$

density operator

3

$$\frac{\partial \rho}{\partial t} = -\frac{i}{\hbar}[H(t),\rho] \rightarrow \rho(t) = \rho_0 \exp(-iHt)$$

$$H(t) = H_0$$

$$\rho = \rho^0 + \rho^{(1)} + \rho^{(2)} + \rho^{(3)} + \ldots$$

$$P^3; S^{(3)}(t); \chi^{(3)}(\omega)$$

4 Time domain response

$$S_{CARS} \sim \left| S^{(3)}(t_3, t_2, t_1) \right|^2$$

5

four time correlation functions

$$S^{(3)}(t) \Rightarrow \langle V(t_1)V(t_2)V(t_3)V(0)\rangle$$

$\Downarrow$ factorization of the Green functions

$\langle V(t)V(0)\rangle$ two time correlation functions

where

$$V = -\mu E \Rightarrow \begin{cases} \dfrac{\partial \mu}{\partial Q} \cdot Q \\ \dfrac{\partial \alpha}{\partial Q} \cdot Q \end{cases}$$

6 frequency domain response

$$S_{CARS} \sim \chi^{(3)}\left|(-\omega_s, \omega_1, \omega_2, \omega_3)\right|^2$$

$\Downarrow$ factorization

$$I(\omega_s)\cdot I(\omega_1)\cdot I(\omega_2)$$

$$\frac{1}{(\omega-\omega_1)^2+\Gamma_1}$$

vibrational correlation function

$$\left\langle \frac{\partial\alpha(0)}{\partial Q}\cdot\frac{\partial\alpha(t)}{\partial Q}\right\rangle \langle Q(0)Q(t)\rangle$$

7 $$Q = Q_0 e^{-i(\omega_0+\Delta\omega(t))t}$$

$\Downarrow$

8 $$Q = Q_0\left\langle e^{-i(\Delta\omega(t))t}\right\rangle e^{-i\omega_0 t}$$

$\Downarrow$ cumulant expansion

$$e^{-i\int_0^t\langle\Delta\omega(0)\Delta\omega(t')\rangle dt'}$$

$\Downarrow$

$$\Gamma = \frac{1}{2\pi c T_2} \Leftarrow T_2^{-1} = \left(T_2^{-1}\right)^* + \gamma^{-1}$$

life time

band width — vibrational dephasing — pure dephasing

NATIVE BR-568 AND UNLOCKED ANALOGS BR 6.11 AND 6.9

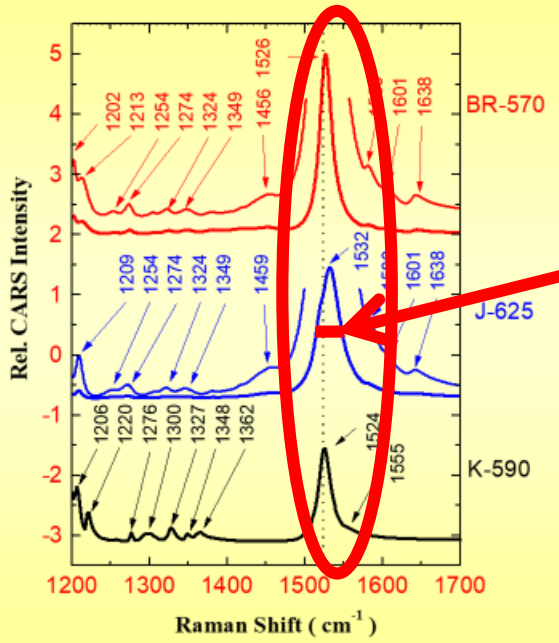

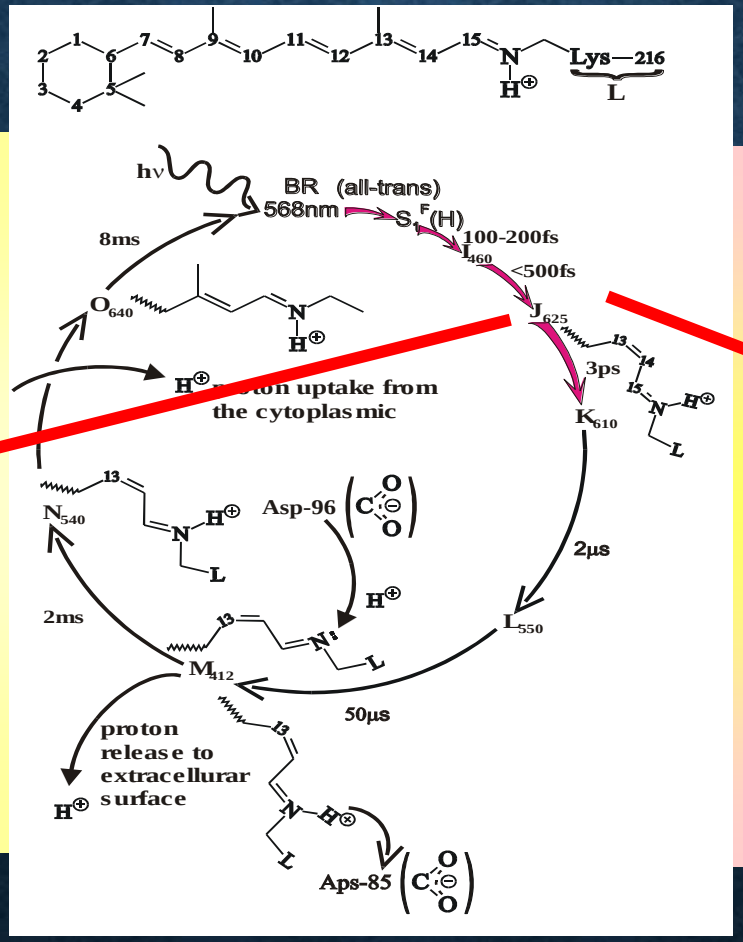

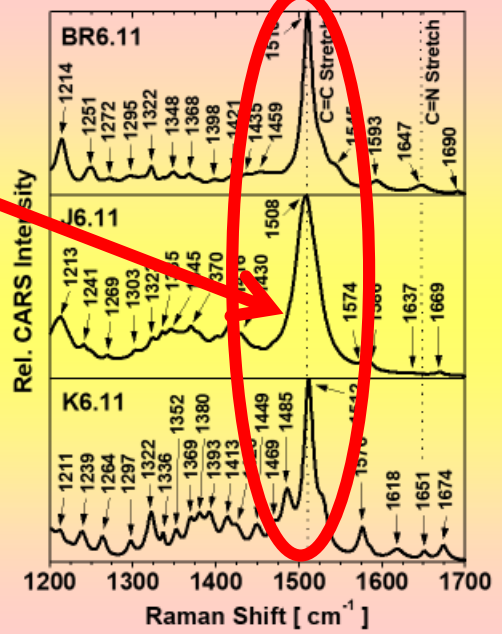

vibrational spectra of BR-570 (top), J-625 (center, derived from the 0-ps PTR/CARS data),and K-590 (bottom, derived from the 200-ps PTR/CARS data) in the1200–1700 cm1region

Locked analogs BR 5.12 and BR 5.13

BR 5.12

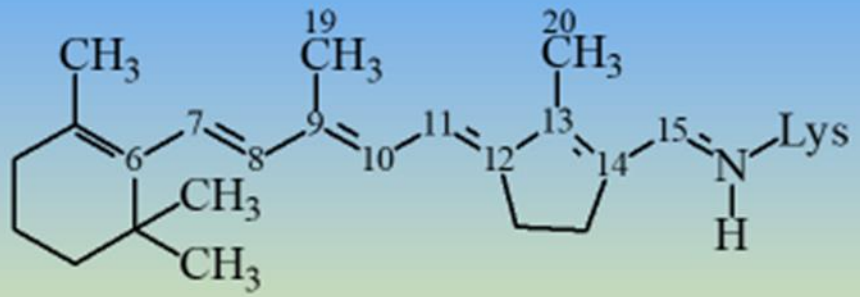

BR 5.13

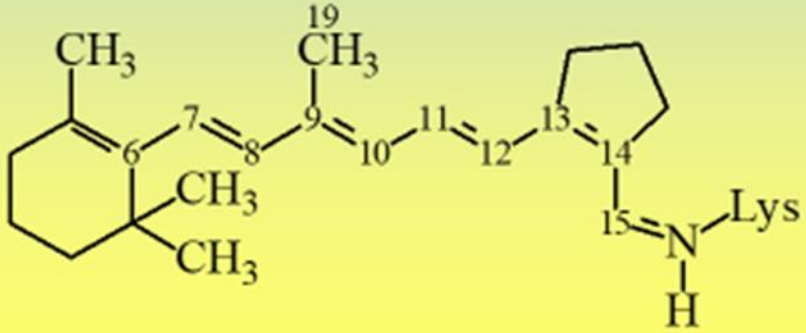

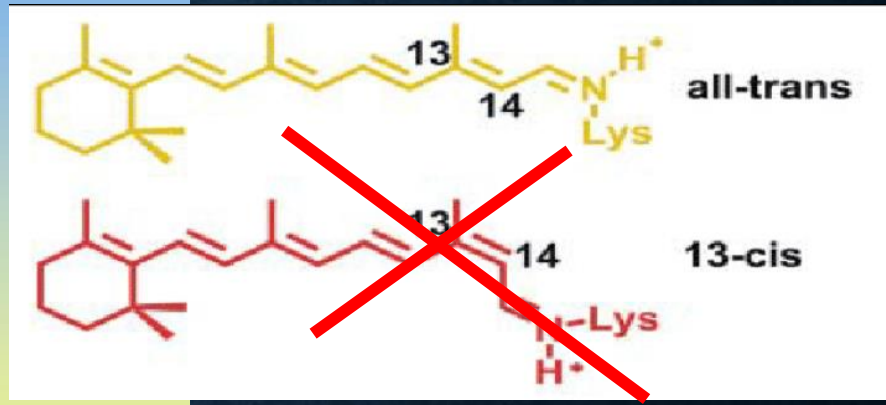

28

For BR5.12, the C13=C14 retinal bond is locked in the trans configuration by a rigid, five-membered carbon ring

Locked analogs BR 5.12 and BR 5.13

BR 5.12

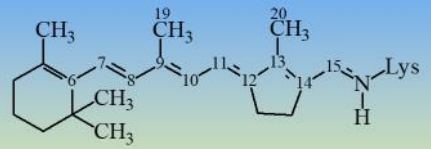

BR 5.13

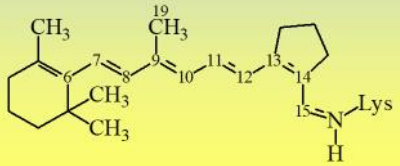

28

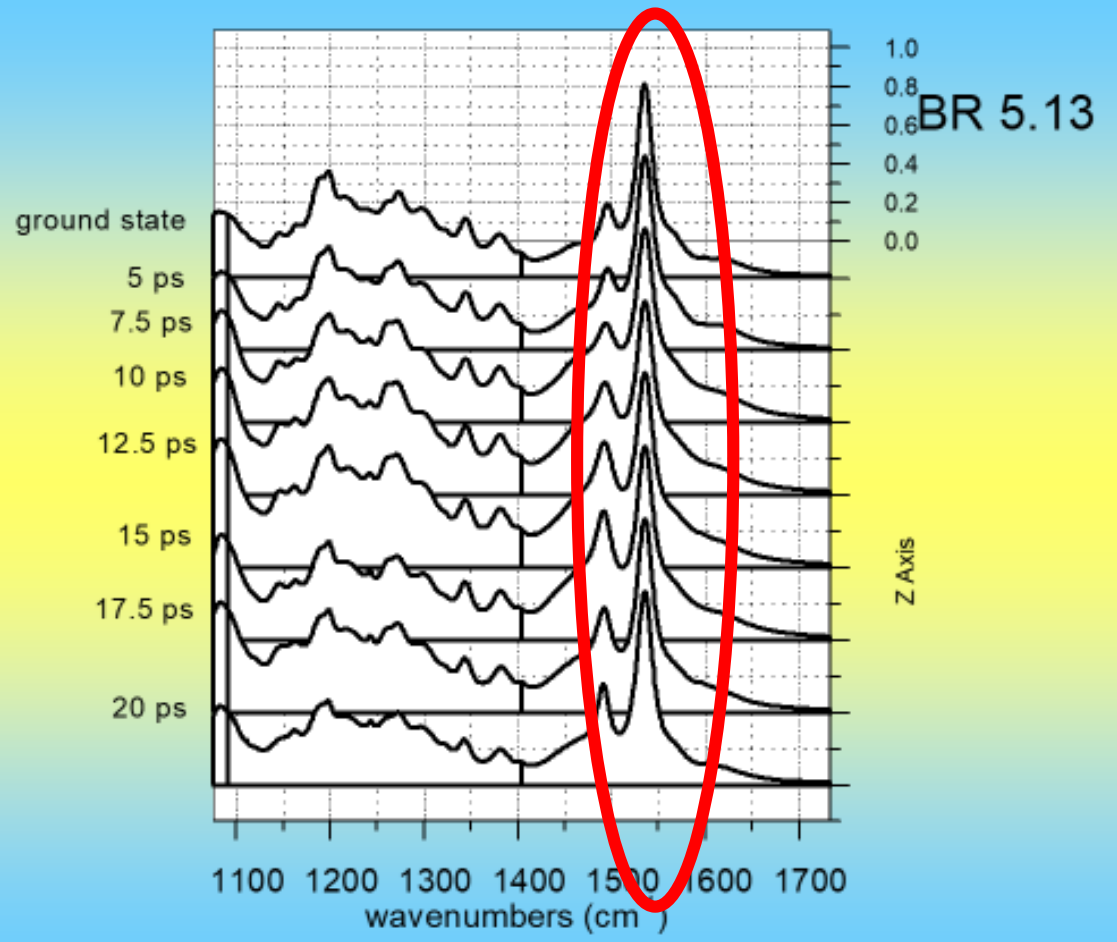

30

ELECTRONIC DYNAMICS OF BACTERIORHODOPSINE AND ITS MODIFIED ANALOGS

Excited state absorption

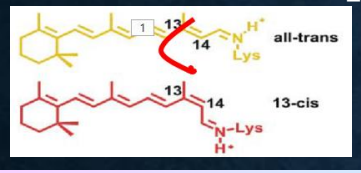

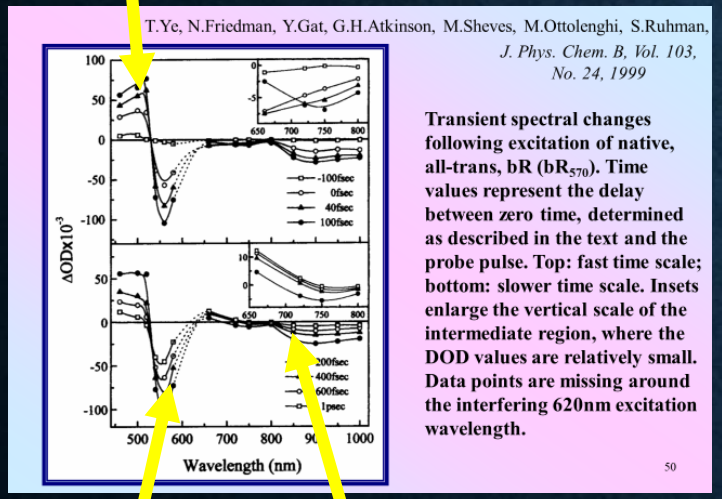

Stimulated emission

Ground state bleaching

Unanswered questions

- why the femtosecond spectra of native BR-568 and locked analogs are identical ?
- why the stimulated emission spectrum does not overlap with the spontaneous fluorescence?

53

Excited state absorption

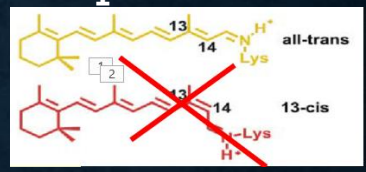

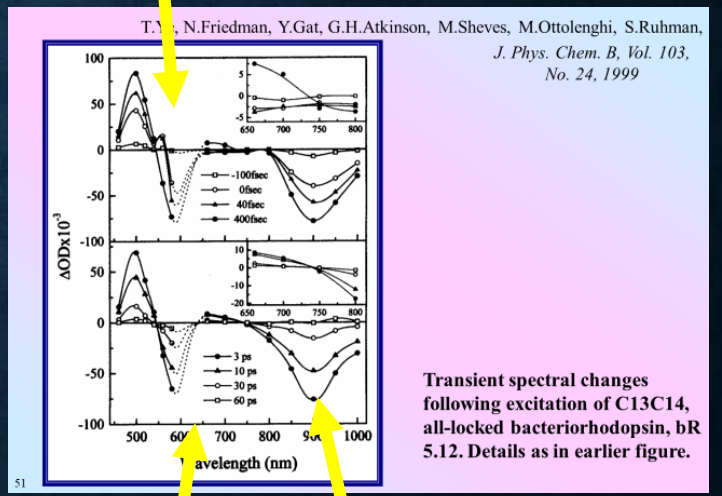

Ground state bleaching

Stimulated emission

The results demonstrated that the initial ultrafast spectral changes observed in native BR are virtually identical to those recorded for the modified analogs including a rise of the absorption/emission bands (460/860 nm) in less than 30 fs

LINEAR AND NONLINEAR RESPONSES VIBRATIONAL COUPLING THEORETICAL MODEL

$$I(\omega) = (2\pi)^{-1}\left[1 - \exp\left(-\frac{\hbar\omega}{kT}\right)\right]\int_{-\infty}^{+\infty} dt e^{i\omega t}\left\langle M_{01}^{+}(0) M_{10}(t)\right\rangle$$

$$S_{HB}(\omega_1\omega_2\tau) = \left(\frac{1}{\hbar}\right)^3 2\omega_2 \int_0^\infty 2\omega_2 \int_0^\infty dt_1 \int_0^\infty dt_3 \left[e^{i(\omega_2 t_3 + i\omega_1 t_1)\chi(t_3+t_1)}[R_1^H(t_3,\tau,t_1) + R_4^H(t_3,\tau,t_1)]\right] +$$

$$e^{(i\omega_2 t_3 - i\omega_1 t_1)\chi(t_3-t_1)}[R_2^H(t_3,\tau,t_1) + R_3^H(t_3,\tau,t_1)]$$

55

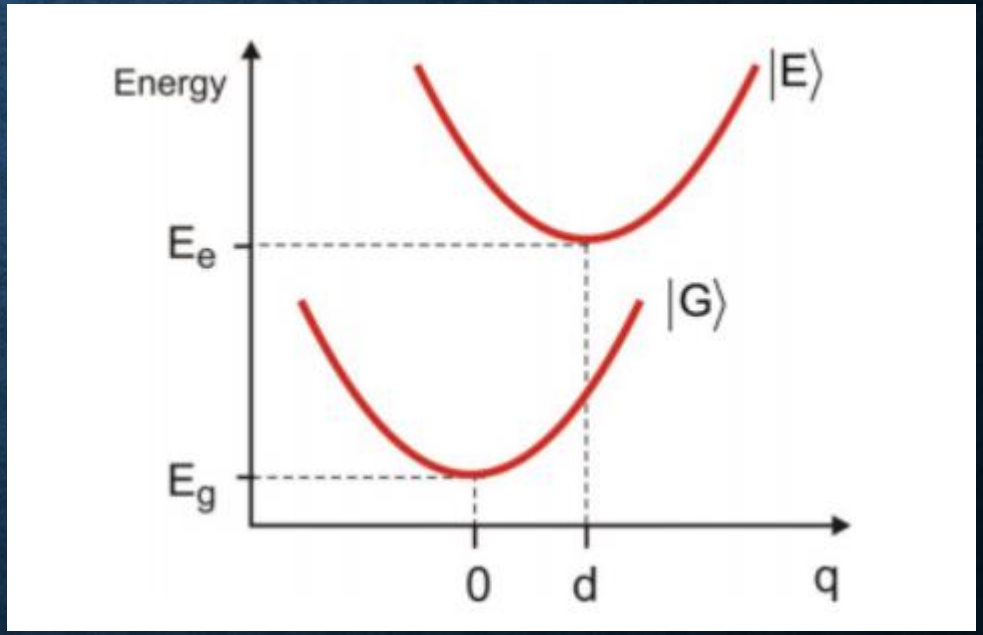

Shaul Mukamel Principles of Nonlinear Optical Spectroscopy

Molecular excited states have geometries that are different from the ground state configuration as a result of varying electron configuration. This parametric dependence of electronic energy on nuclear configuration results in a variation of the electronic energy gap between states as one stretches bond vibrations of the molecule. We are interested in describing how this effect influences the electronic absorption spectrum, and thereby gain insight into how one experimentally determines the coupling of between electronic and nuclear degrees of freedom. We consider electronic transitions between bound potential energy surfaces for a ground and excited state as we displace a nuclear coordinate q. The simplified model consists of two harmonic oscillators potentials whose 0-0 energy splitting is $E_e - E_g$ and which depends on q. We will calculate the absorption spectrum in the interaction picture using the time-correlation function for the dipole operator.

HOLE BURNING PROFILES

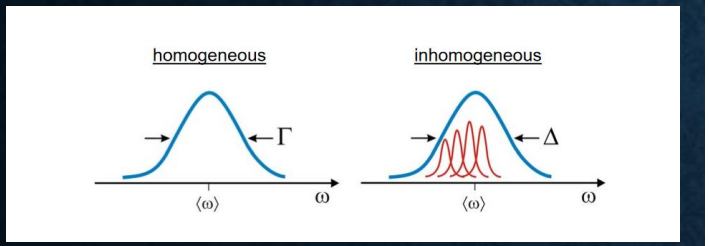

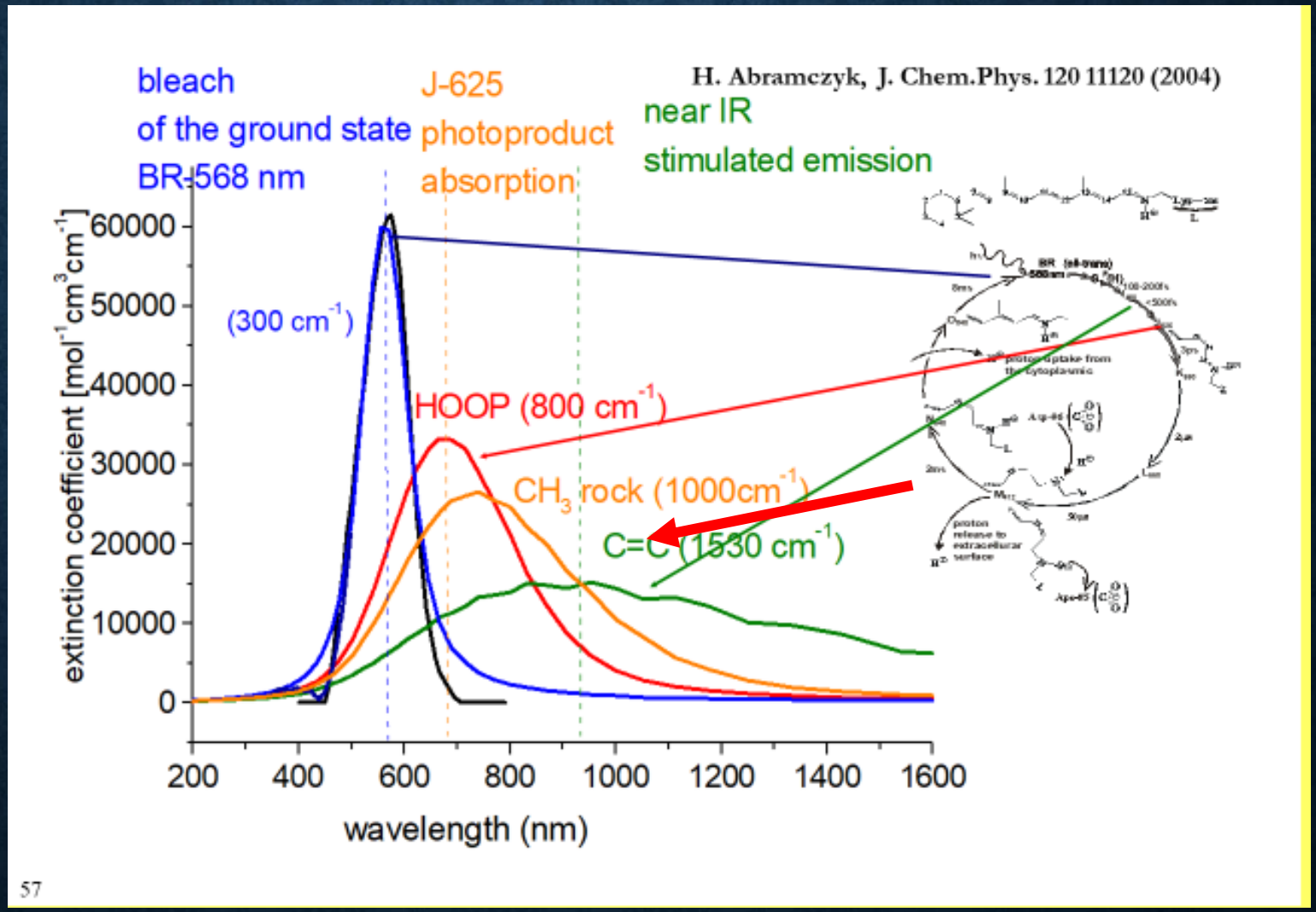

the high frequency mode (C=C stretching), not the torsional coordinate, i the primary accepting mode

H. Abramczyk, Femtosecond primary events in bacteriorhodopsin. Revision of commonly accepted interpretation of electronic spectra of transient intermediates, J. Chem. Phys. 120 11120 (2004)

PREVIOUS MODELS

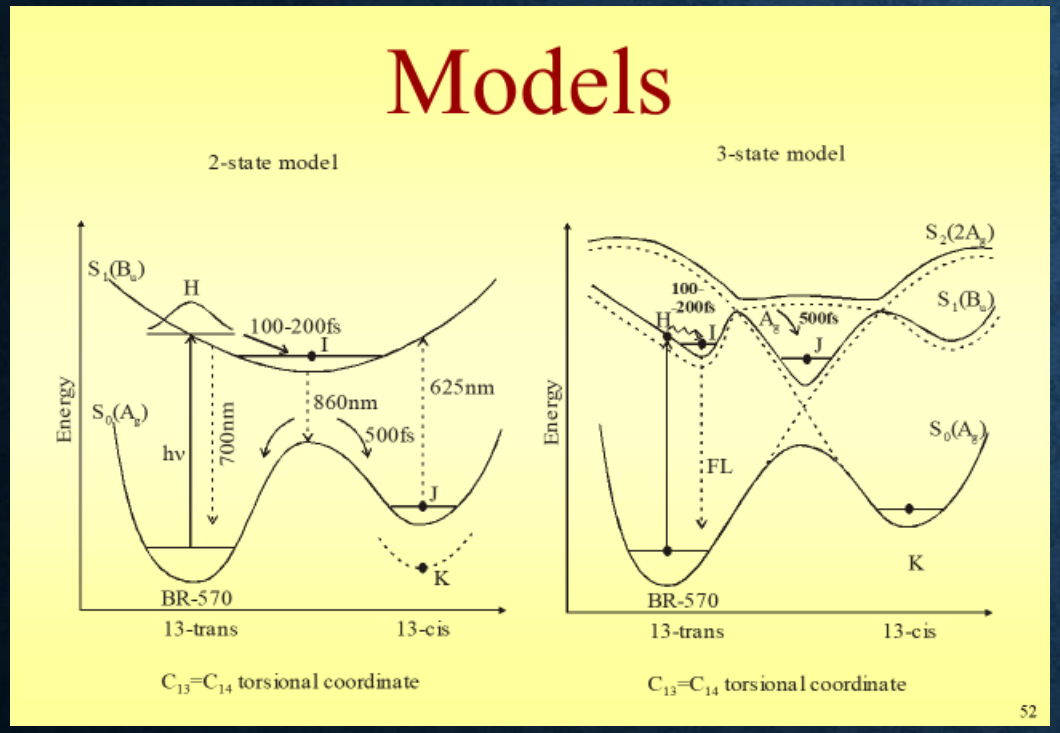

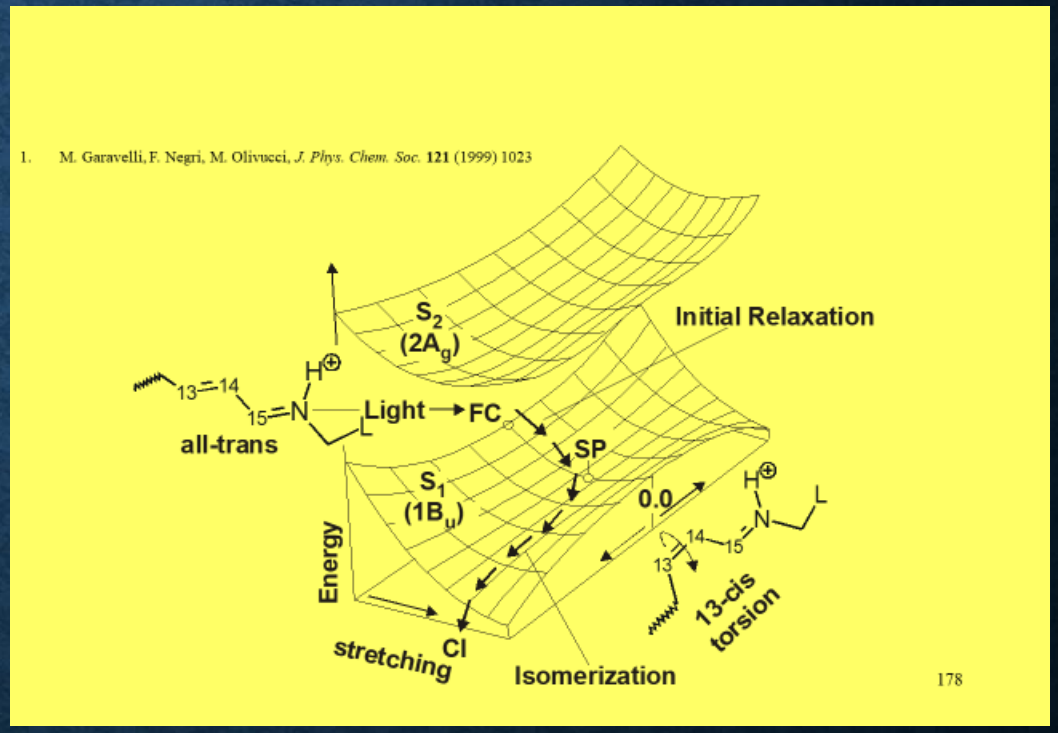

Despite the great diversity of traditional and modern approaches of experimental and theoretical methods applied to study the family of rhodopsins , which are responsible for vision processes, there is no generally accepted view on ultrafast primary events

CONCLUSIONS-1
PROPOSED MECHANISM OF PRIMARY EVENTS IN BR PHOTOCYCLE

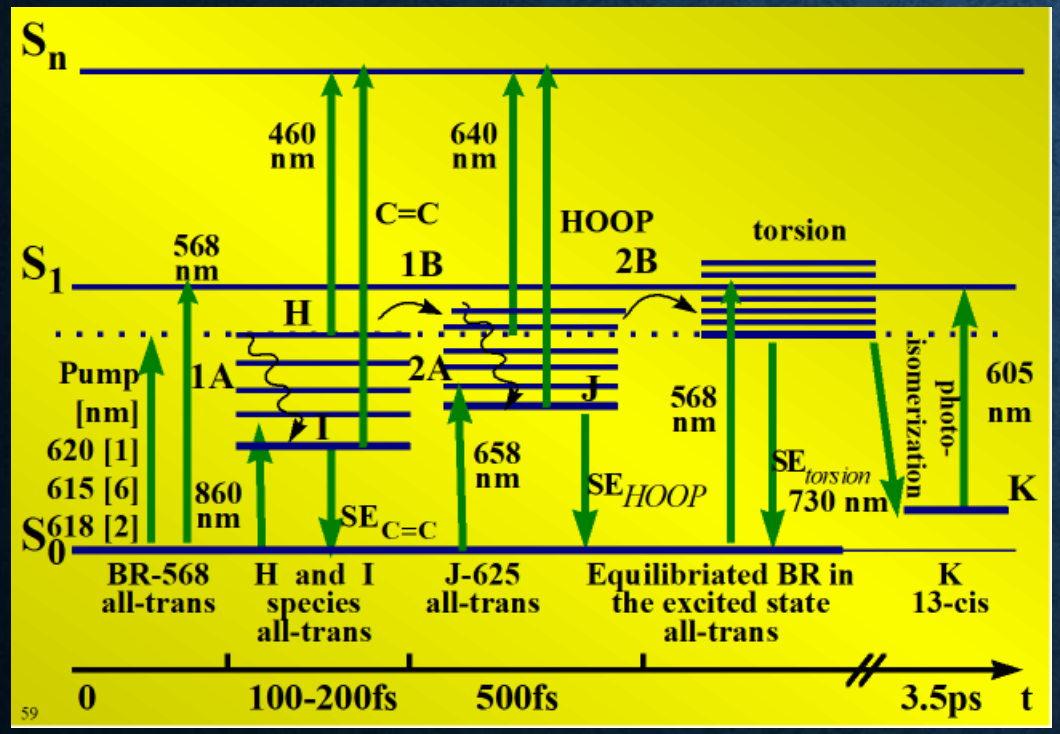

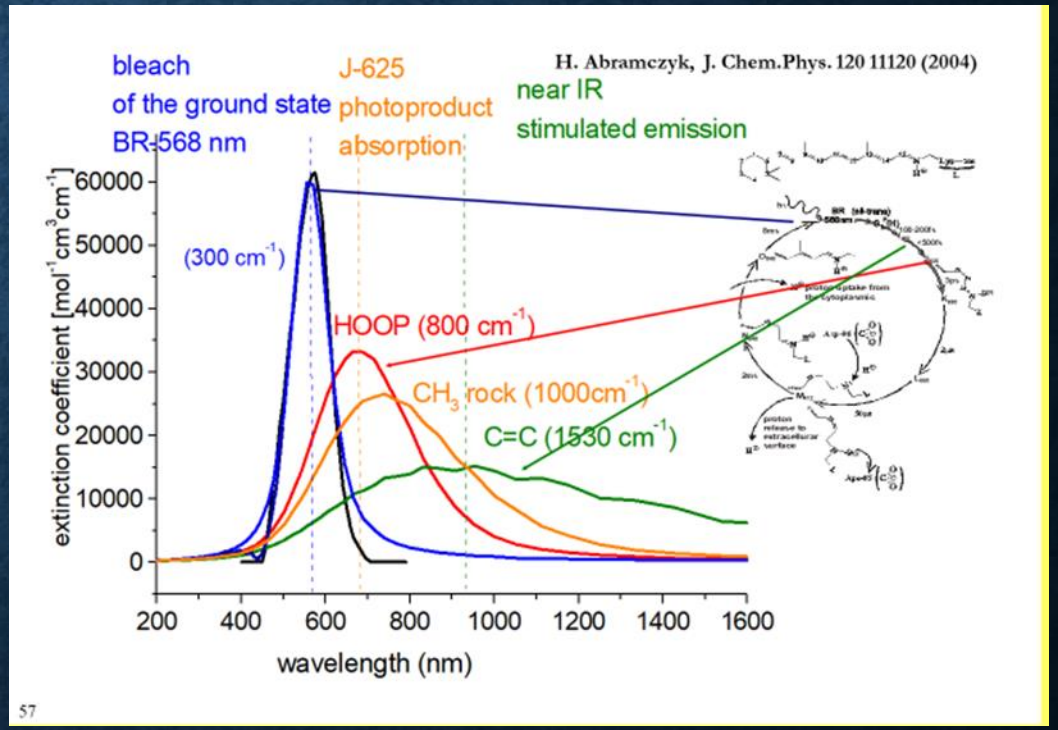

H. Abramczyk, Femtosecond primary events in bacteriorhodopsin. Revision of commonly accepted interpretation of electronic spectra of transient intermediates, J. Chem. Phys. 120 11120 (2004)

FREE RETINOIDS AND RETINOIDS BOUND TO PROTEINS

Is femtosecond dynamics of retinoids ,,free'' in solution different from that in retinoids bound to proteins?

Answering this question is very important , because femtosecond dynamics could monitor free retinol and retinol bound to proteins in cells providing information on the mechanism of retinol uptake and signalling by STRA6

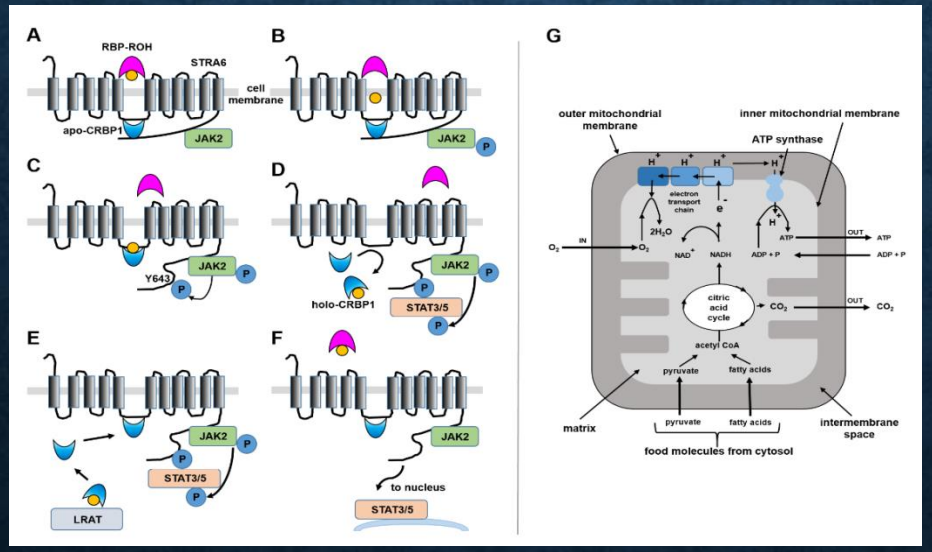

Model of the mechanism of retinol uptake and signalling by STRA6

RETINOIDS FREE IN SOLUTIONS

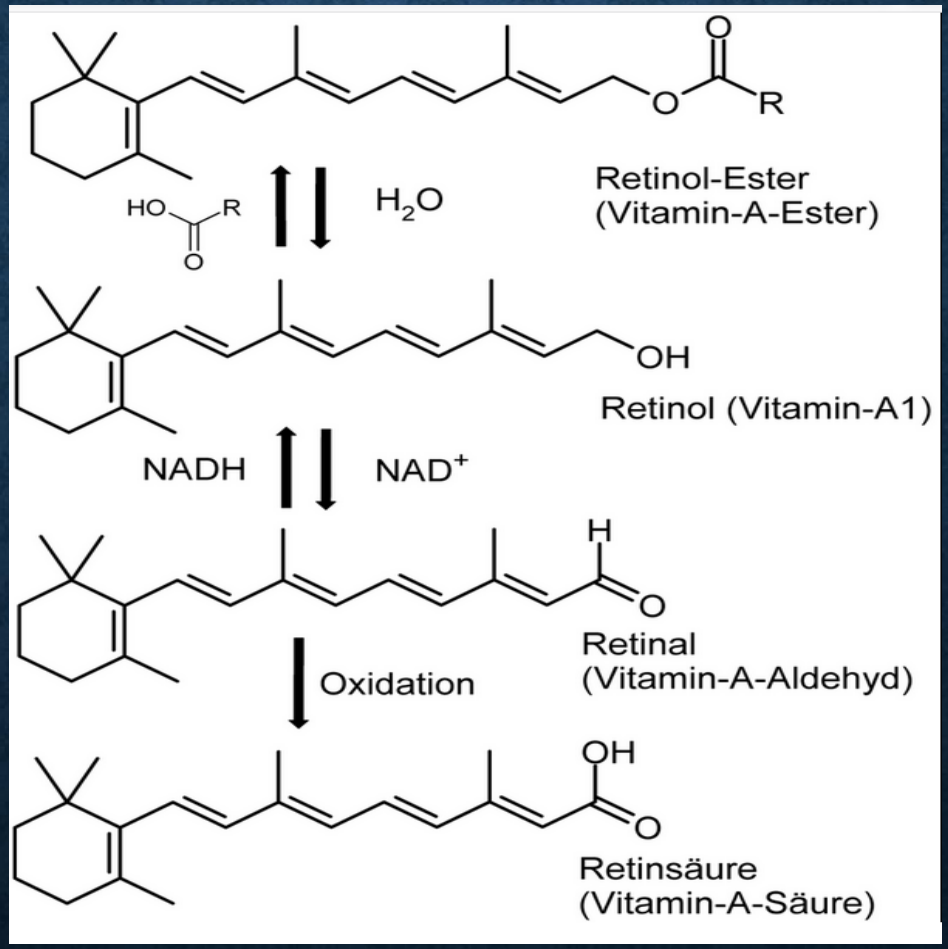

PUMP-PROBE TRANSIENT ABSORPTION FEMTOSECOND SPECTROSCOPY

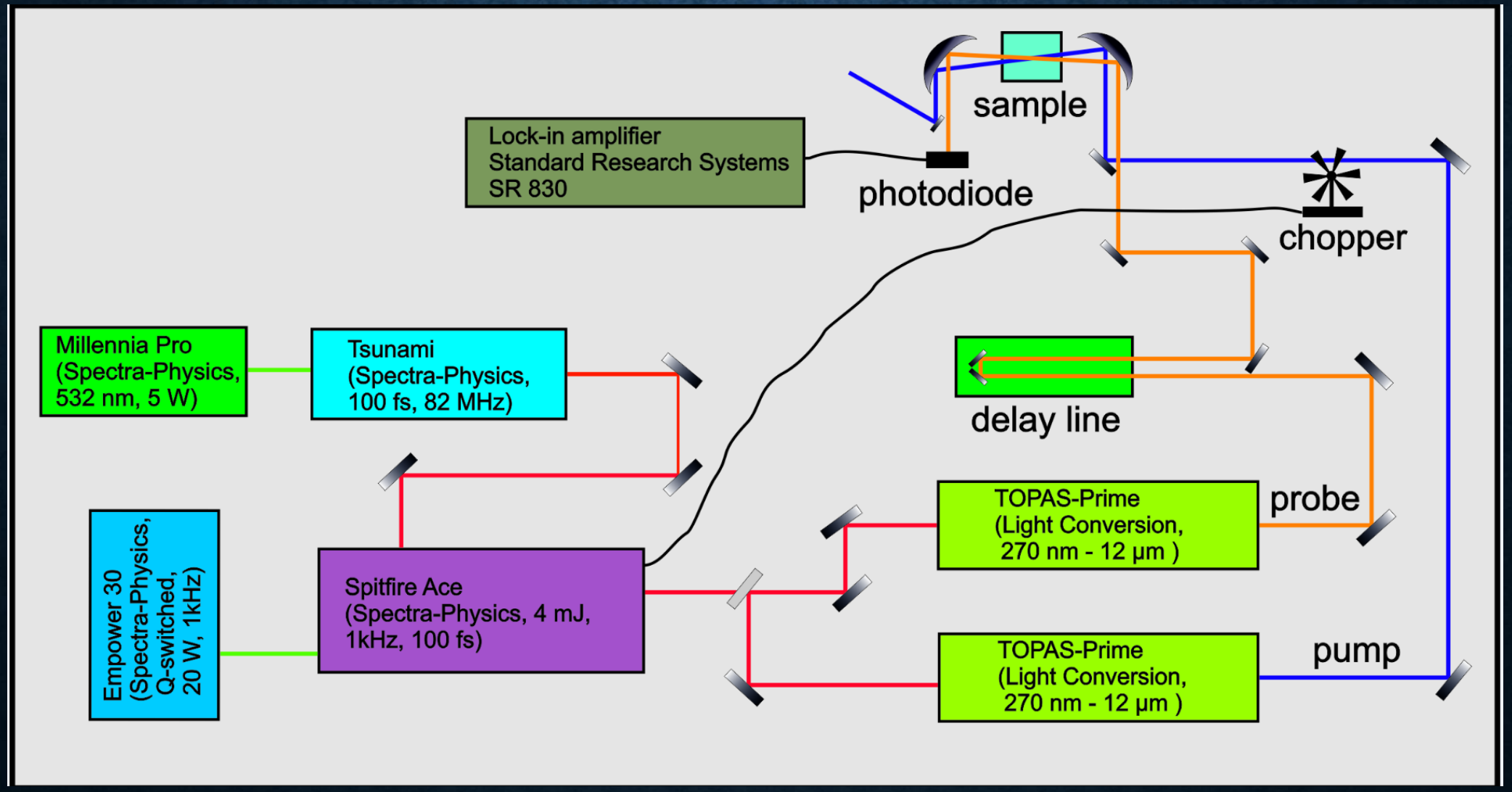

PUMP-PROBE TRANSIENT ABSORPTION FEMTOSECOND SPECTROSCOPY

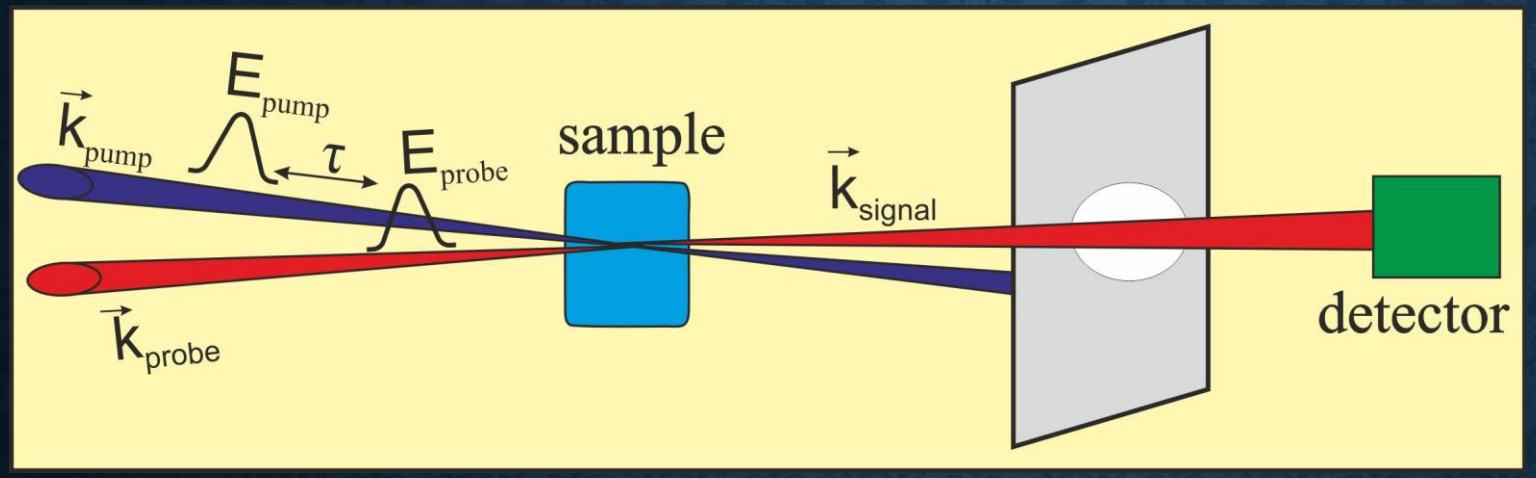

the measured pump-probe signal is proportional to the imaginary part of the polarization

$$\Delta I(\tau) = 2\omega_{sig}\ell \,\mathrm{Im}\left[E'_{pr}P^{(3)}(\tau)\right]$$

The pump-probe or transient absorption experiment is perhaps the most widely used third-order nonlinear experiment. It can be used to follow many types of time-dependent relaxation processes and chemical dynamics, and is most commonly used to follow population relaxation, chemical kinetics, or wavepacket dynamics and quantum beats.

PUMP-PROBE TRANSIENT ABSORPTION FEMTOSECOND SPECTROSCOPY

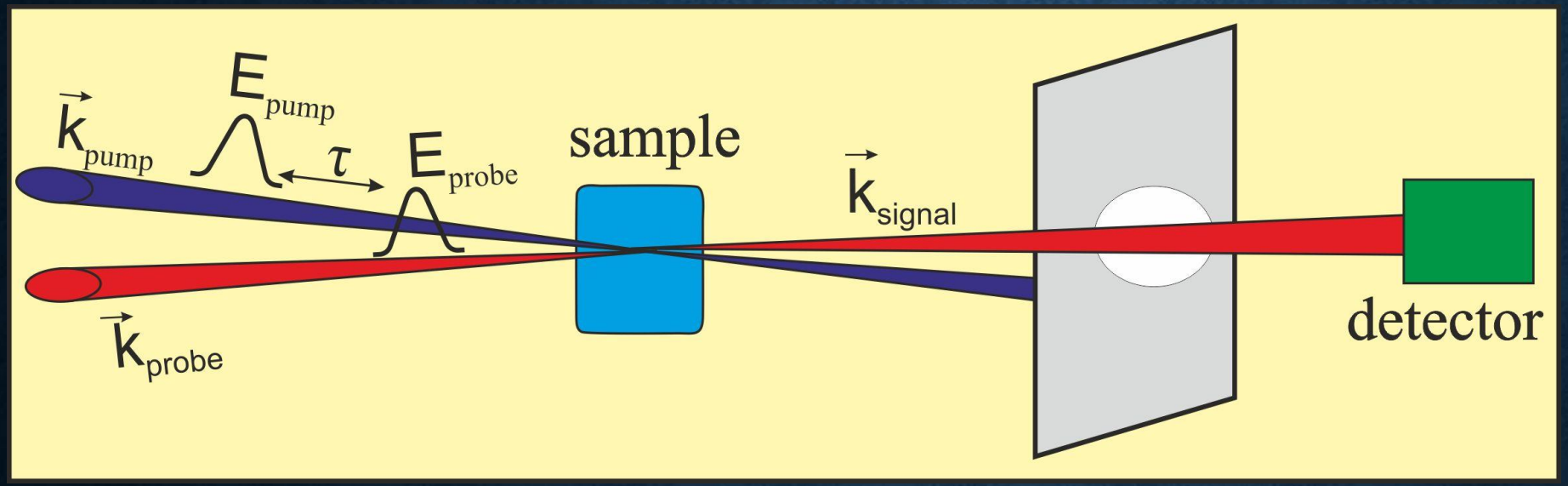

the measured pump-probe signal is proportional to the imaginary part of the polarization

$$\Delta I(\tau) = 2\omega_{sig}\ell \,\mathrm{Im}\left[E'_{pr}P^{(3)}(\tau)\right]$$

The principle is quite simple: two pulses separated by a delay τ are crossed in a sample: a pump pulse and a time-delayed probe pulse. The pump pulse Epu creates a non-equilibrium state, and the time-dependent changes in the sample are characterized by the probe-pulse Epr through the pump-induced intensity change on the transmitted probe, ΔI.

GROUND STATE BLEACHING OF RETINOIDS IN SOLUTION (N-HEXANE, MAGIC ANGLE)

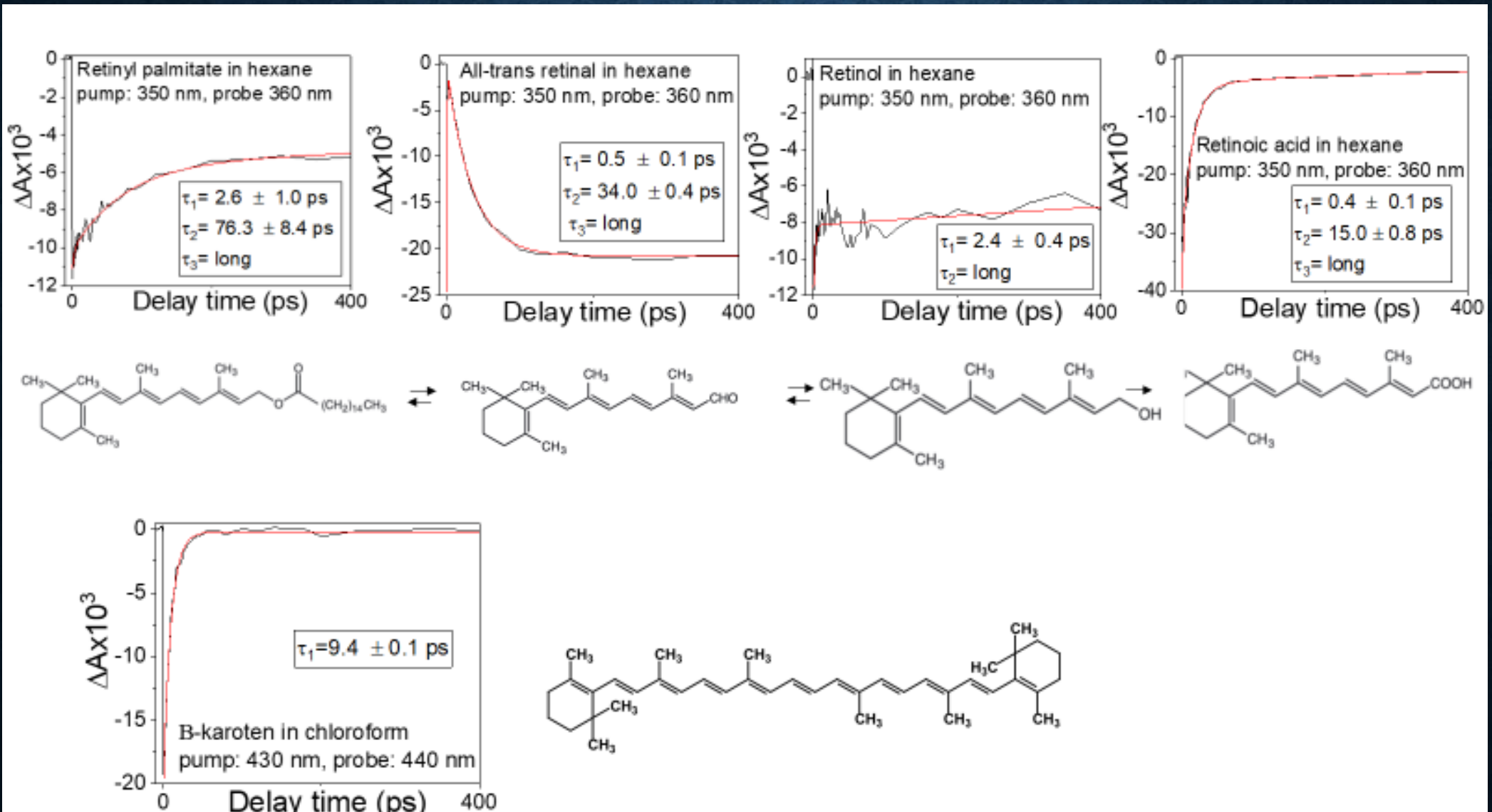

GROUND STATE BLEACHING OF RETINOIDS IN SOLUTION (CHLOROFORM)

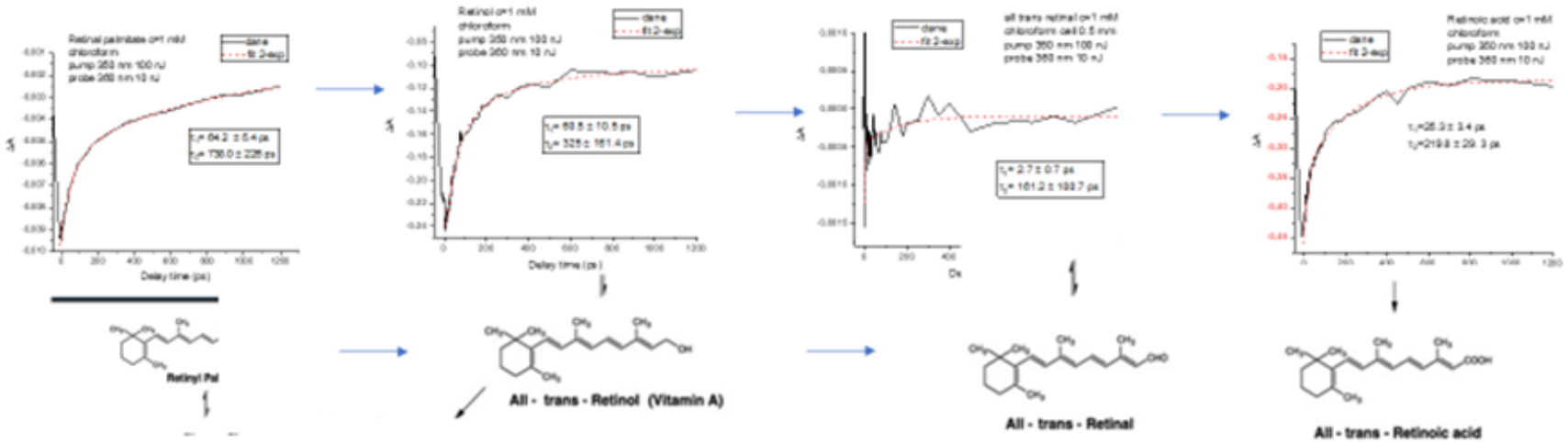

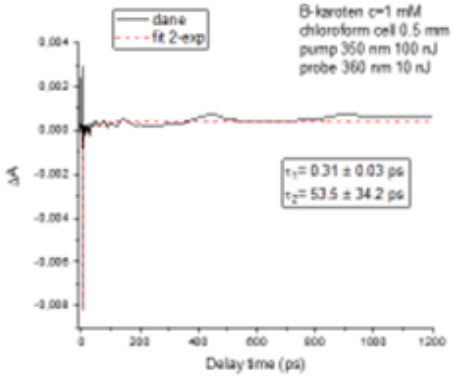

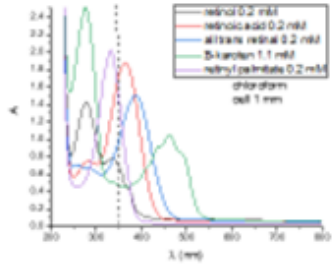

Pump 350 nm 100 nJ
Probe 360 nm 10 nJ

	t1	t2
B-karoten	0.31 ± 0.03 ps	53.5 ± 34.2 ps
Retinyl palmitate	64.2 ± 5.4 ps	738.0 ± 226 ps
All trans-retinal	2.7 ± 0.7 ps	161.2 ± 100.7 ps
Retinoic acid	25.3 ± 3.4 ps	219.8 ± 29. 3 ps
retinol	60.5 ± 10.5 ps	325 ± 161.4 ps

EXCITED STATE ABSORPTION OF RETINOIDS IN SOLUTION (N-HEXANE, MAGIC ANGLE)

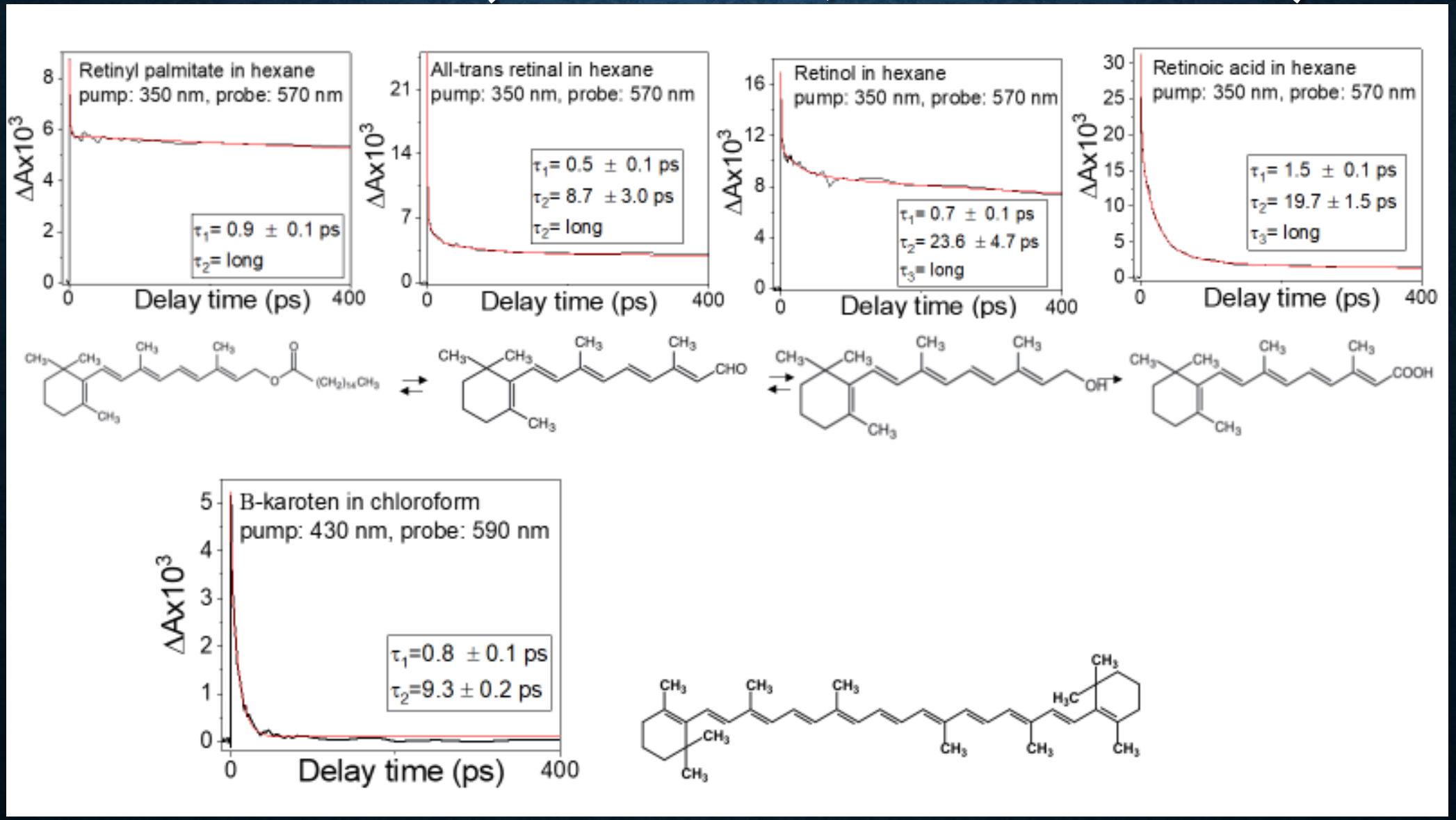

EXCITED STATE ABSORPTION OF RETINOIDS IN SOLUTION (CHLOROFORM)

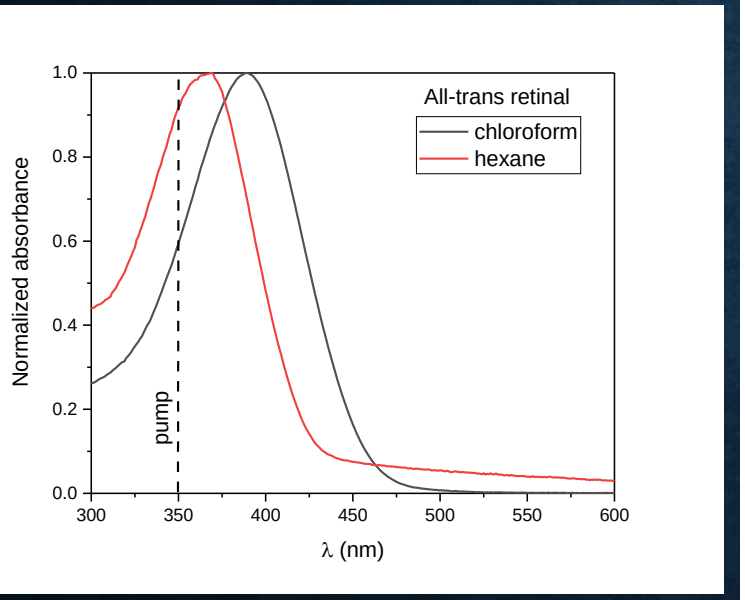

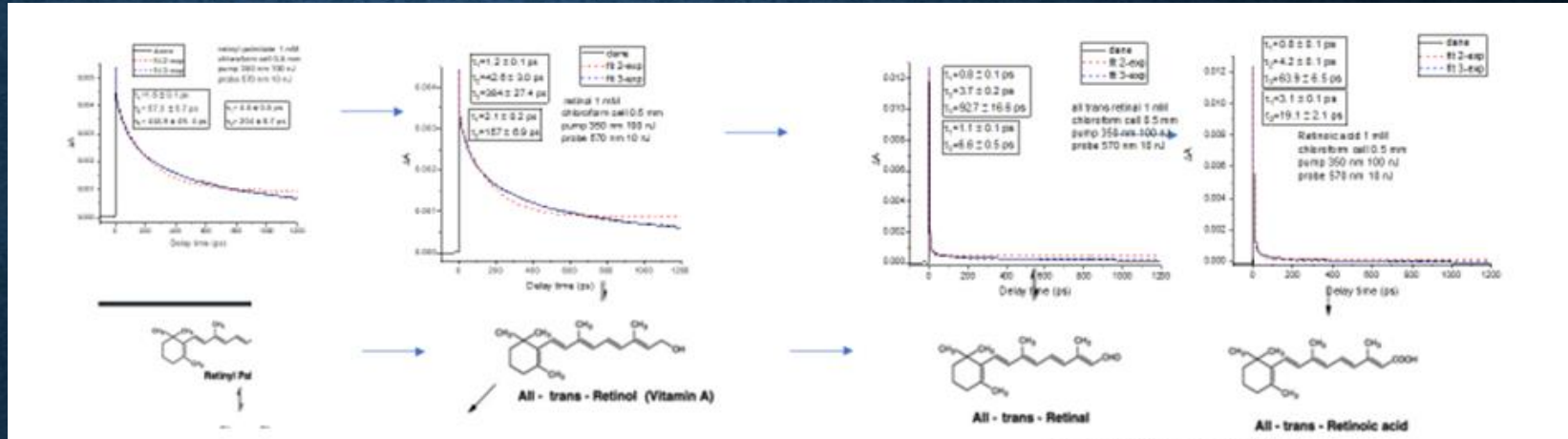

Pump 350 nm 100 nJ
Probe 570 nm 10 nJ

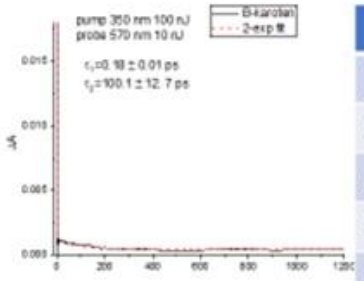

	t1	t2	t3
B-karoten	0.18 ± 0.01 ps	100.1 ± 12. 7 ps	
Retinyl palmitate	1.6 ± 0.1 ps	57.3 ± 5.7 ps	444.9 ± 49. 4 ps
All trans-retinal	0.8 ± 0.1 ps	3.7 ± 0.2 ps	92.7 ± 16.6 ps
Retinoic acid	0.8 ± 0.1 ps	4.2 ± 0.1 ps	63.9 ± 6.5 ps
retinol	1.2 ± 0.1 ps	42.6 ± 3.0 ps	384 ± 27.4 ps

B–CAROTENE

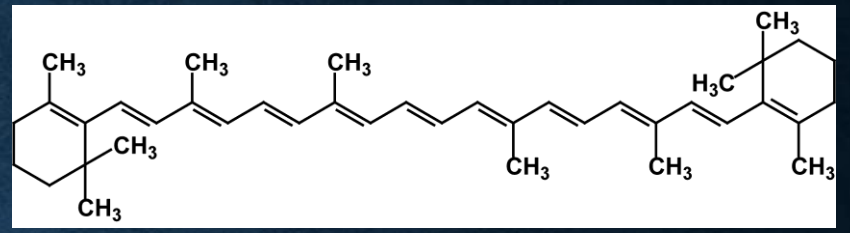

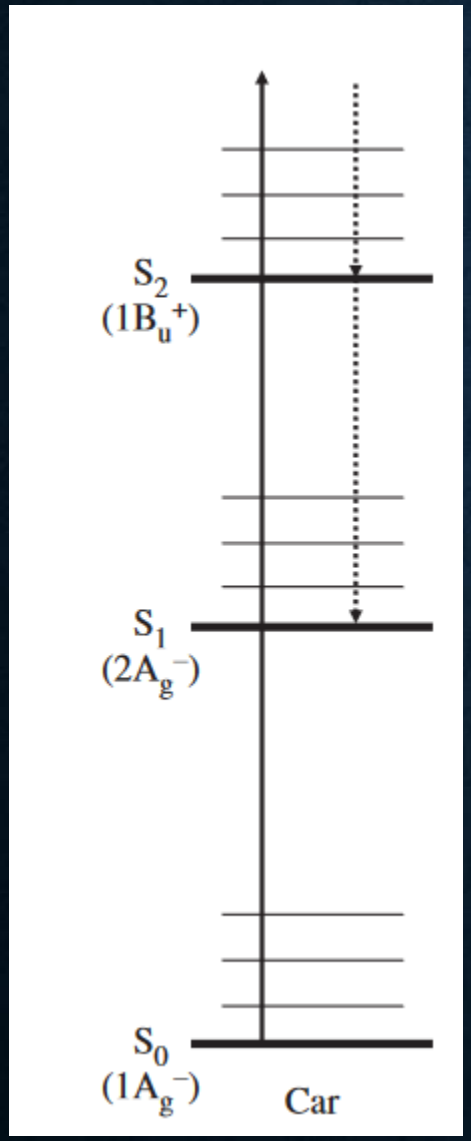

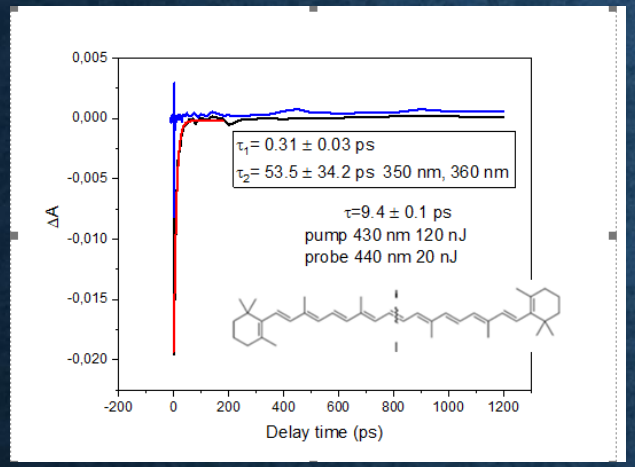

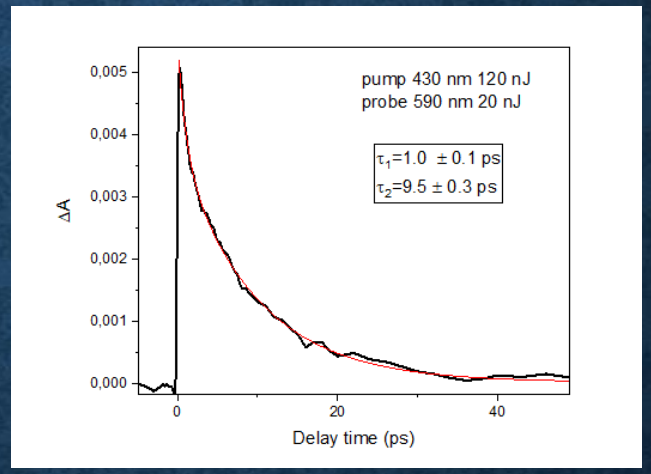

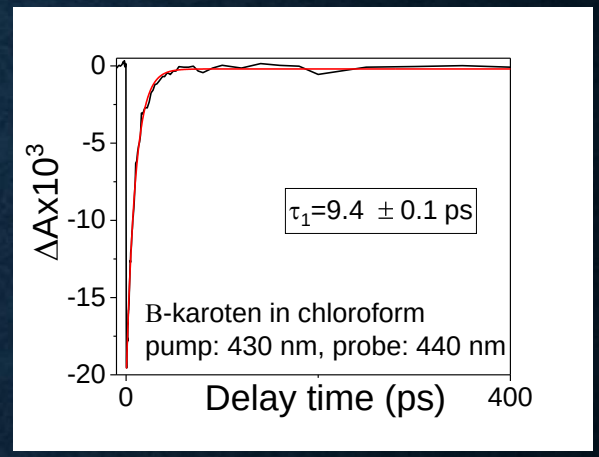

The bleaching results correspond well to the excited state absorption (ESA) of the S1 state shown in Figure. The ESA rises immediately the excitation and decays biexponentially with the times of 1 and 9.5 ps. The first one reflects vibrational relaxation in S1 state, the 9.5 ps reflects the decay to the S0 state corresponding perfectly to the lifetime of S0 state recovery within 9.4 ps.

ALL-TRANS RETINAL

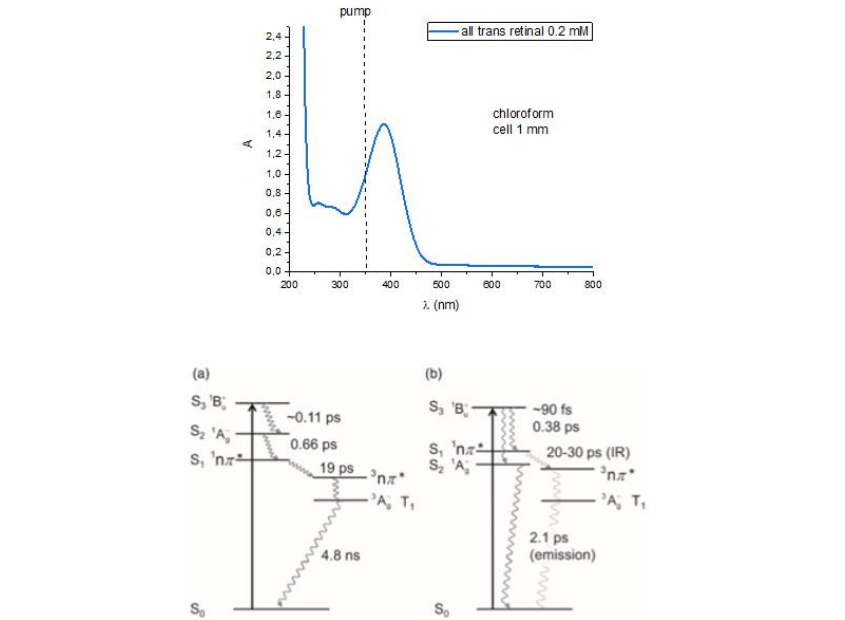

Scheme 1. Electronic structure of all-*trans*-retinal in (a) *n*-hexane or cyclohexane (nonpolar) and (b) acetonitrile (see Refs 3 and 7). Lifetimes representing state transitions are based on electronic transient absorption results although one for the weak ISC in (b) is based on transient infrared absorption.

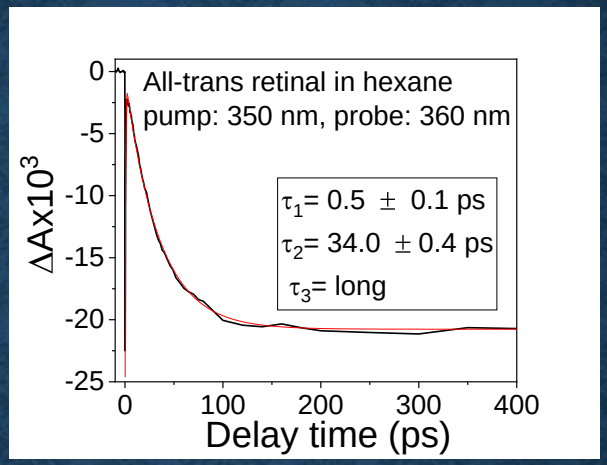

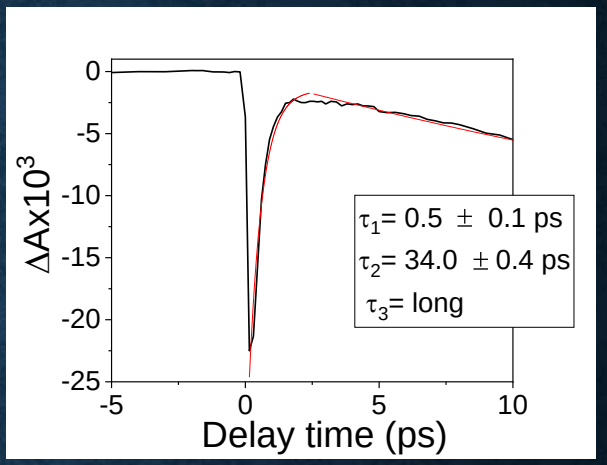

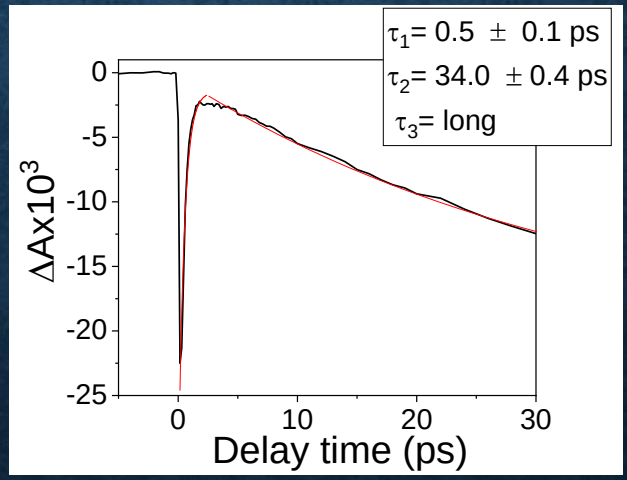

Fig. 7 shows the electronic structure levels for all-trans retinal . It consists of three excited singlet states in the near -UV-visible spectral region (Fig.2). The excited states S_2 $A_g(\pi\pi^*)$ and S_3 $B_u(\pi\pi^*)$ represent a polyene electronic structure, $S_1(n\pi^*)$ represents the aldehyde group of all-trans retinal.

ALL-TRANS RETINOL

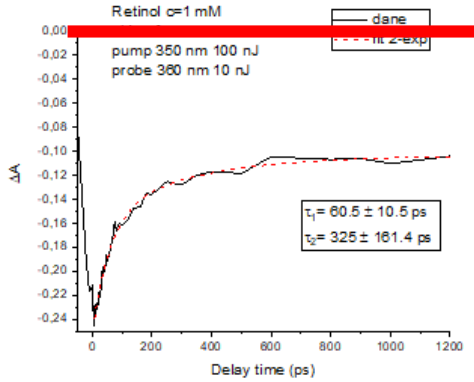

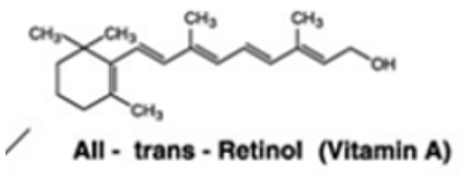

325 nm

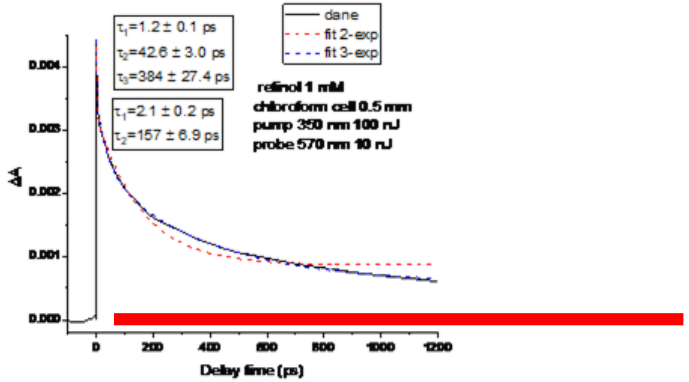

ULTRAFAST DYNAMICS OF METAL COMPLEXES OF TETRASULPHONATED PHTHALOCYANINES AT BIOLOGICAL INTERFACES OF THE HUMAN TISSUE

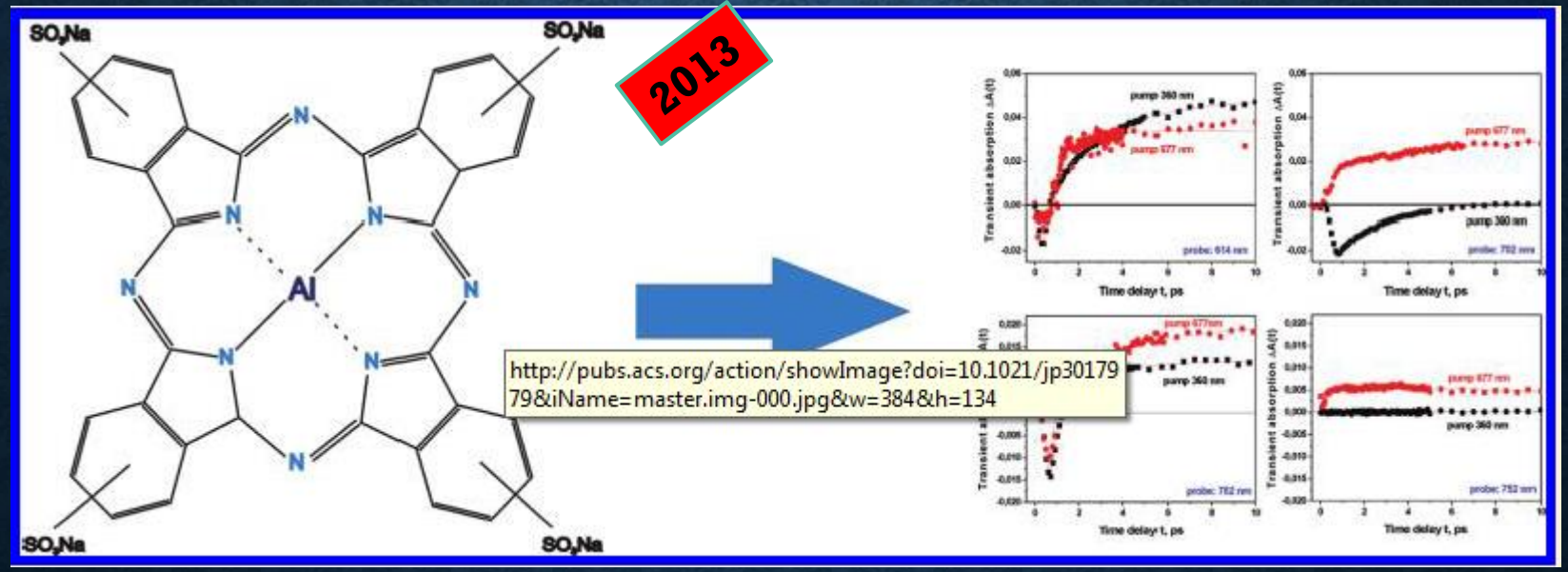

Arkadiusz Jarota, Marc Tondusson, Geoffrey Galle,Eric Freysz, and Halina Abramczyk , 2012

THE JOURNAL OF PHYSICAL CHEMISTRY A

Femtosecond spectroscopy of human breast tissues with aluminum phthalocyanine

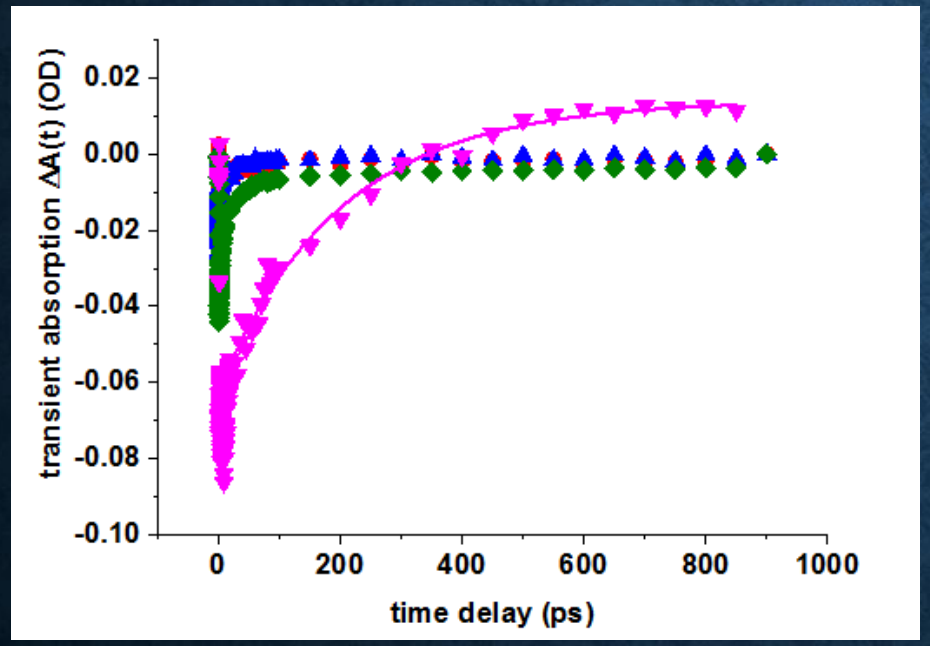

Normal tissue
130 ± 0.10 fs, 1.53 ± 0.19 ps, i 37.86 ± 5.25 ps Cancer tissue
110±0.10 fs, 1.34±0.16 ps, i 40.72±7.86 ps
Film
830±100 fs, 7.31±1.02 ps, i 56.03±6.58 ps
Solutions
232.52±81.00 ps, 5.09 ± 0.99 ps

pump 677 nm, probe 670 nm
P58

H. Abramczyk, B. Brozek-Pluska, E. Freysz, M. Tondusson, *J. Phys. Chem. C* 2013, 113, 4999.

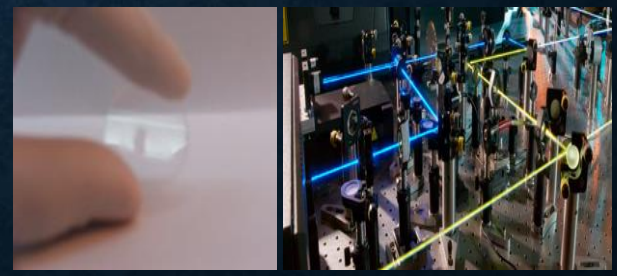

Femtosecond spectroscopy of human breast tissues with aluminum phthalocyanine

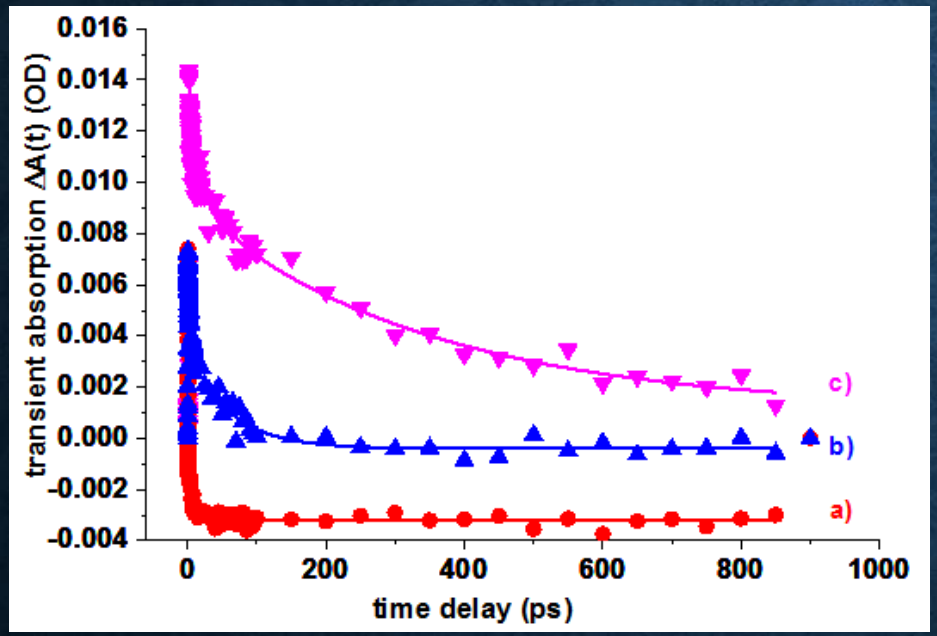

Cancer tissue
810±0.0.04 fs, 5.63±0.49 ps, i 59.90±1.85 ps
Normal tissue
176 ± 0.20 fs, 840 ± 0.42 fs, i 6.03 ± 1.92 ps
Solutions
345.81±107.00 ps, 2.37 ± 0.71 ps

pump 677 nm, probe 602 nm
P58

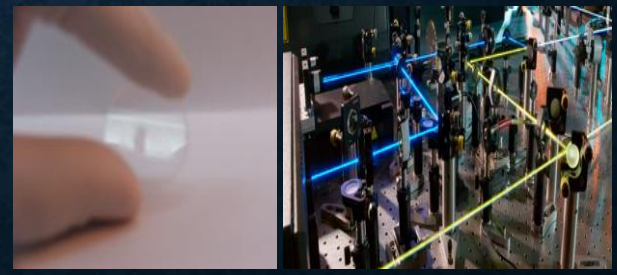

H. Abramczyk, B. Brozek-Pluska, E. Freysz, M. Tondusson,
J. Phys. Chem. C 2013, 113, 4999.

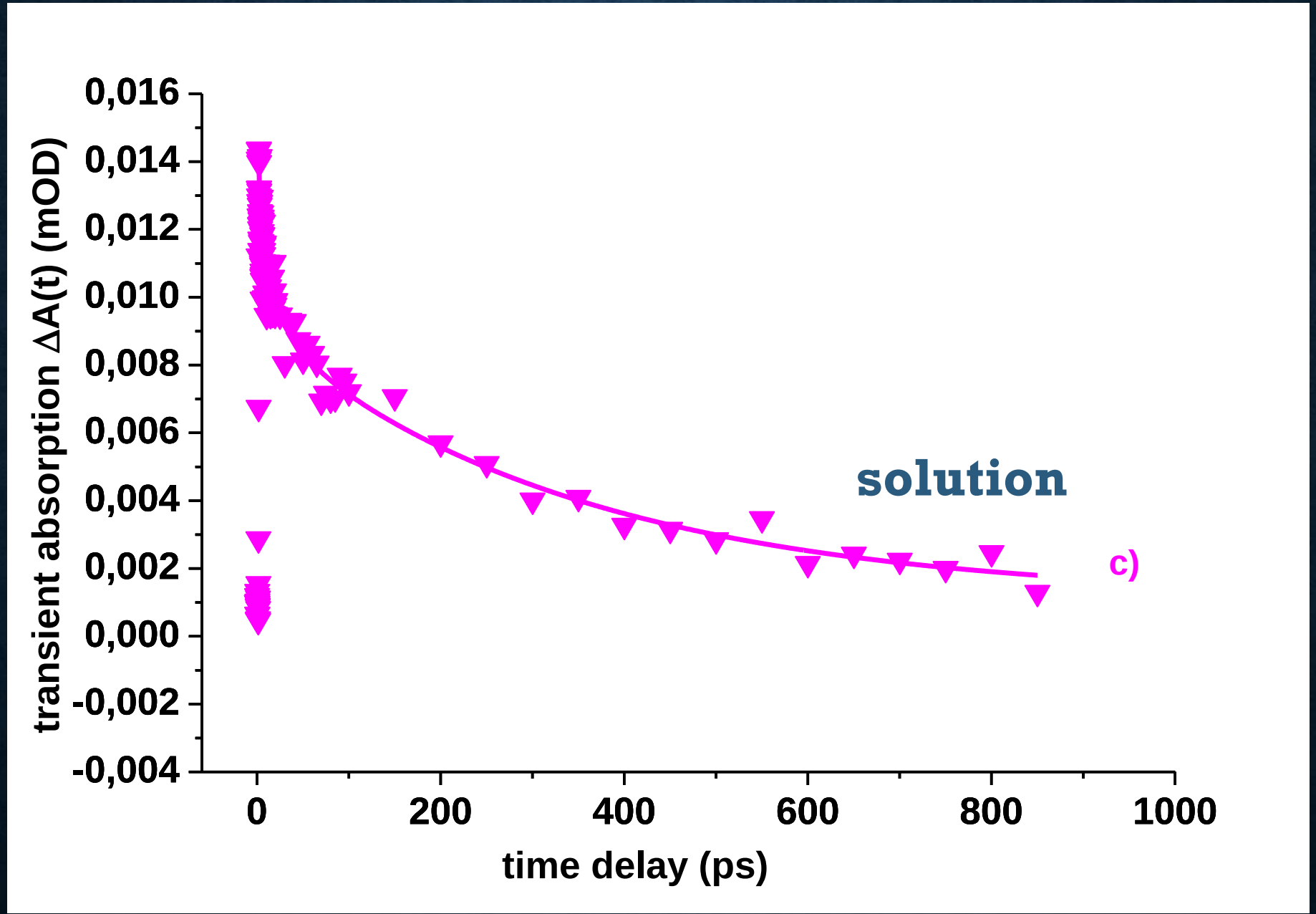

the results showed that the dynamics of the photosensitizer was markedly faster in the interfacial regions of the biological tissue than in solutions. Second, the photosensitizer localized in noncancerous tissue dissipates the energy through different pathways than that in cancerous breast tissue.

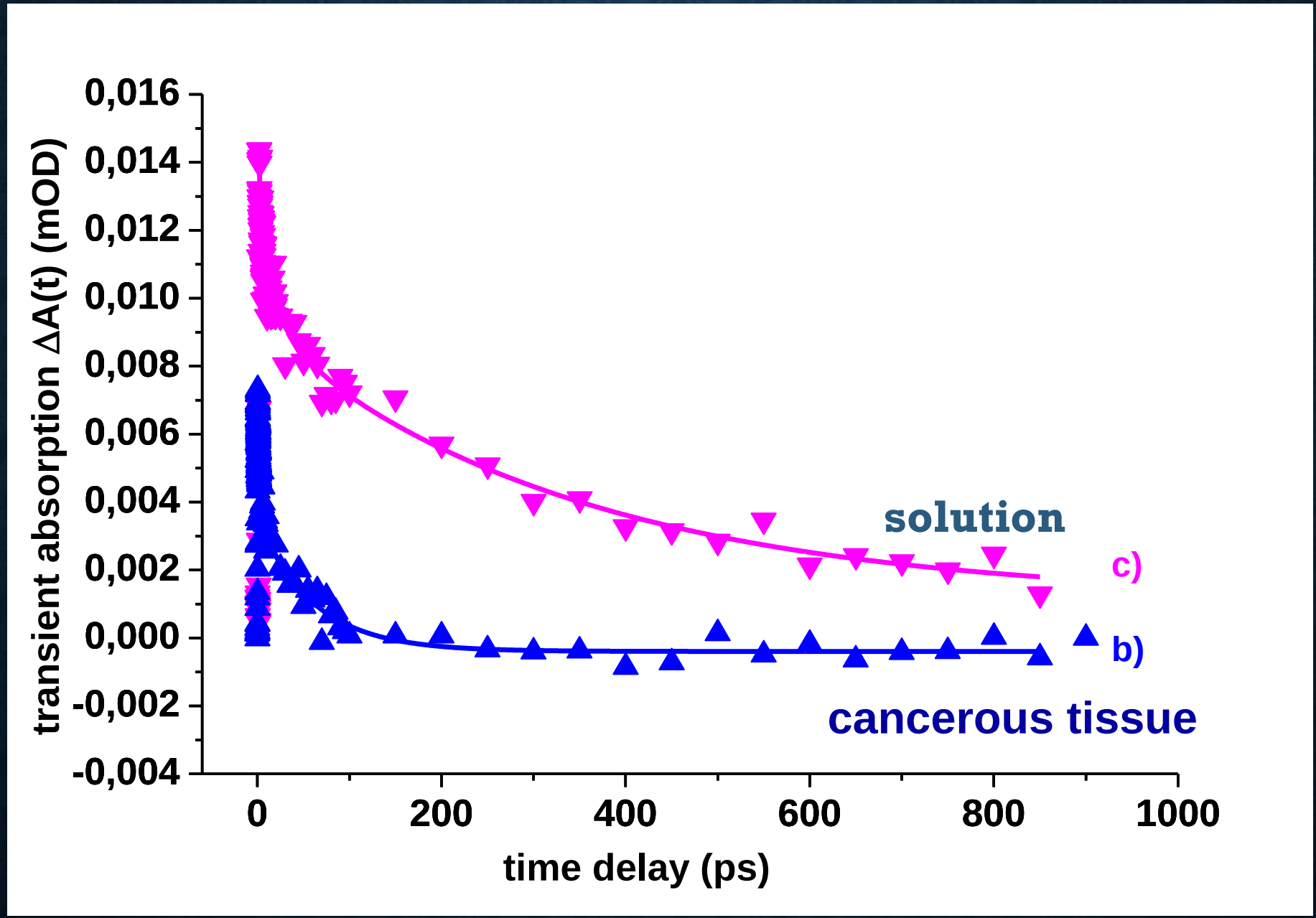

the results showed that the dynamics of the photosensitizer was markedly faster in the interfacial regions of the biological tissue than in solutions. Second, the photosensitizer localized in noncancerous tissue dissipates the energy through different pathways than that in cancerous breast tissue.

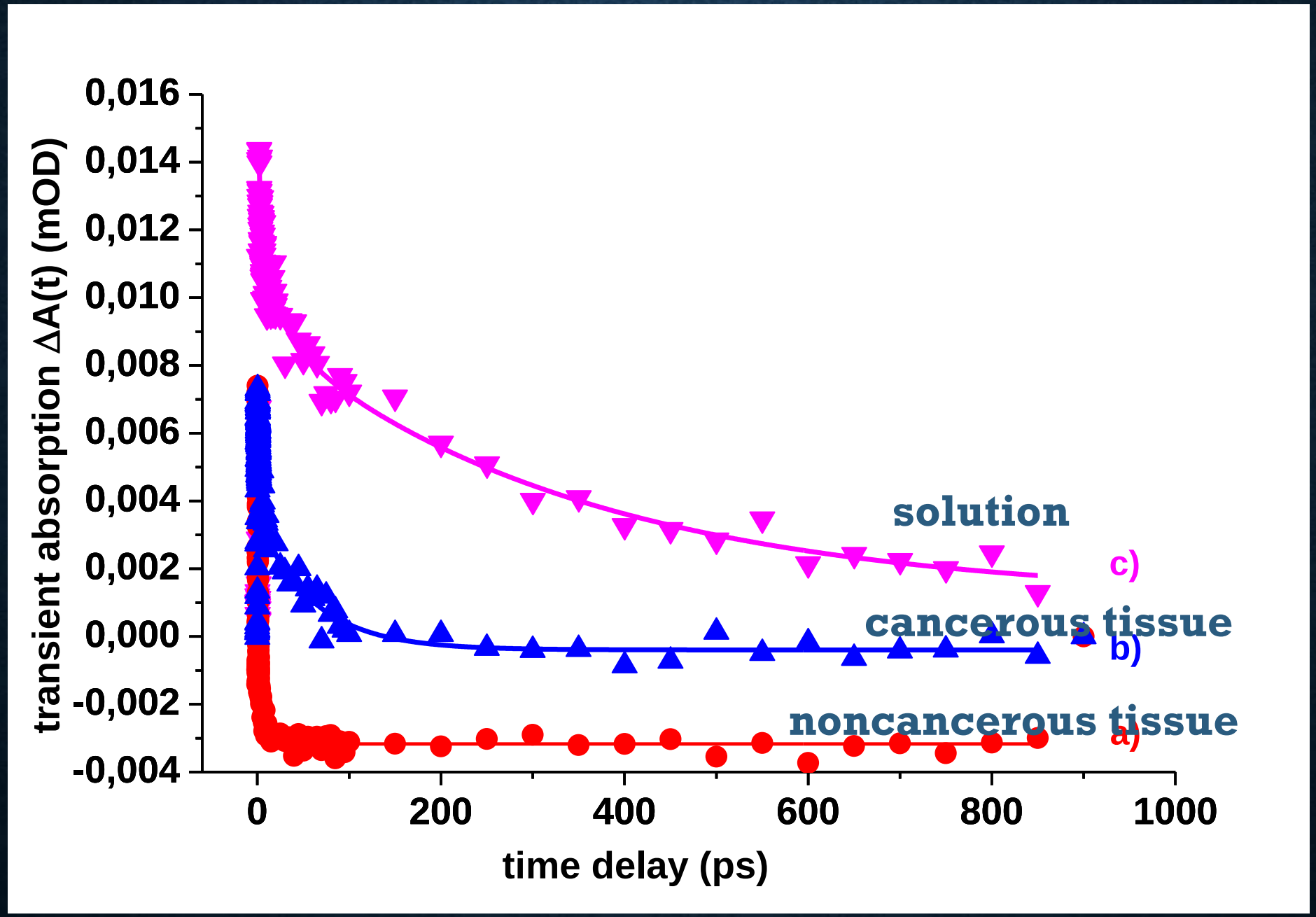

We have shown that the lifetimes characterizing both the ground state S_0 and the first excited state S_1 in the interfacial regions of noncancerous tissue are markedly shorter than those in cancerous tissue.

RAMAN SPECTRA OF RETINOIDS

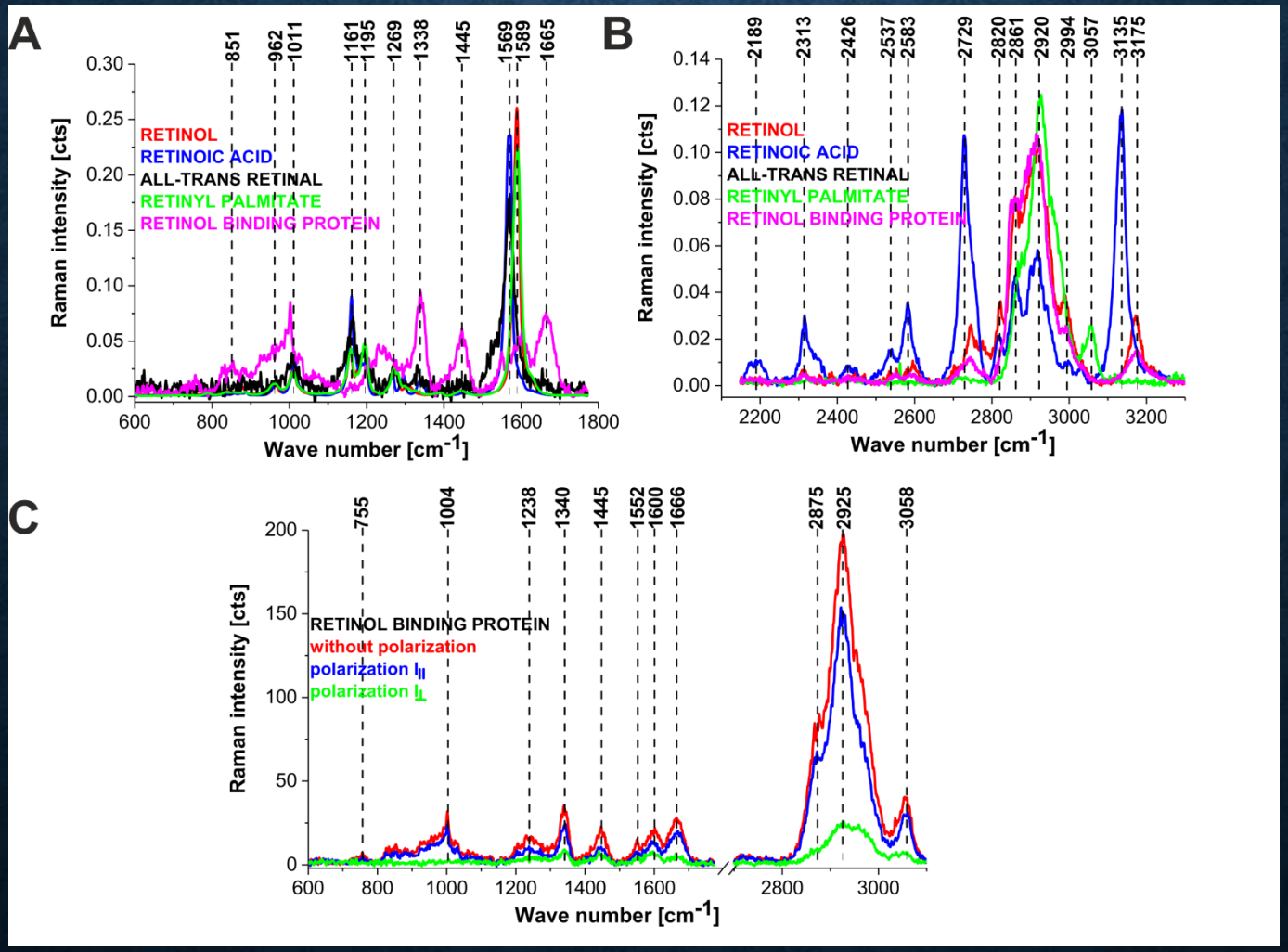

METHODS OF MOLECULAR AND LASER MICROSPECTROSCOPY IMAGING

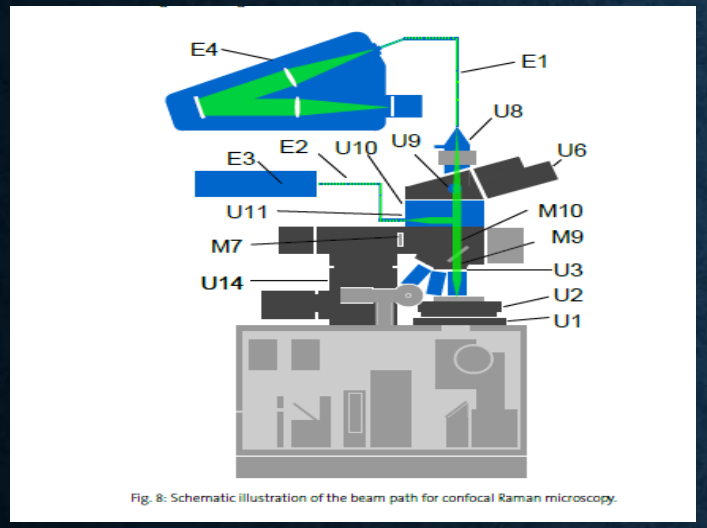

Fig. 8: Schematic illustration of the beam path for confocal Raman microscopy.

Raman imaging

IR imaging

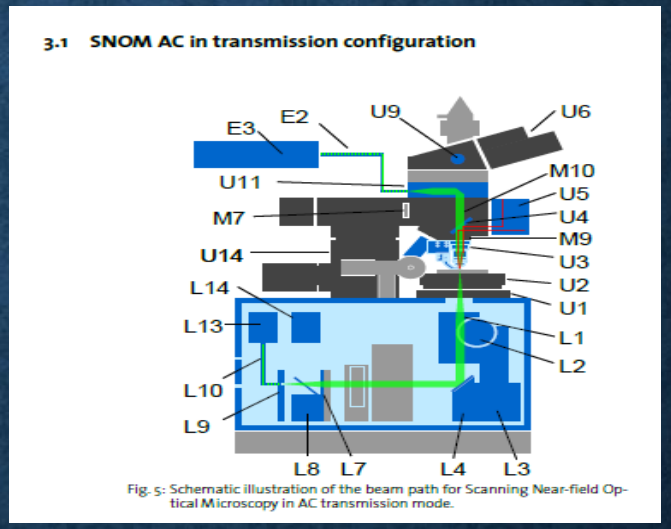

Fig. 5: Schematic illustration of the beam path for Scanning Near-field Optical Microscopy in AC transmission mode.

SNOM imaging

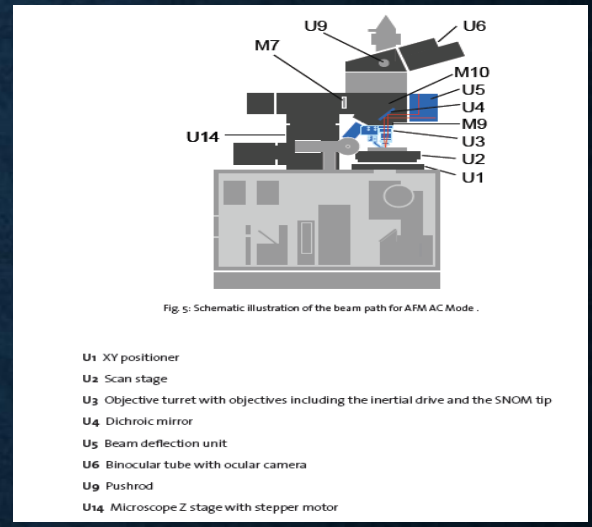

Fig. 5: Schematic illustration of the beam path for AFM AC Mode .

U1 XY positioner
U2 Scan stage
U3 Objective turret with objectives including the inertial drive and the SNOM tip
U4 Dichroic mirror
U5 Beam deflection unit
U6 Binocular tube with ocular camera
U9 Pushrod
U14 Microscope Z stage with stepper motor

AFM imaging

We do not need to disrupt cells to break open the cells and release the cellular structures

CONVENTIONAL MOLECULAR BIOLOGY

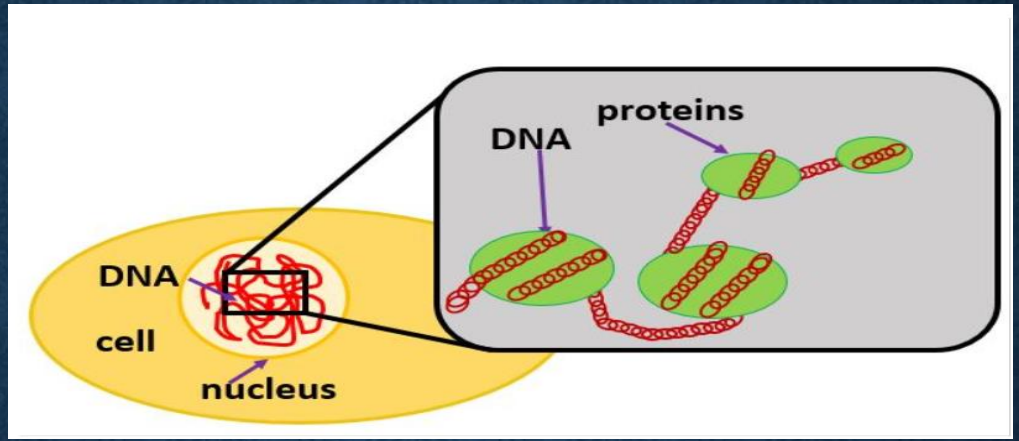

- **Isolation of DNA from Cells and Tissues**
- DNA can be extracted from many types of cells. The first step is to lyse or break open the cell. This can be done by grinding a piece of tissue in a blender. After the cells have broken open, a salt solution such as NaCl and a detergent solution containing the compound SDS (sodiumdodecyl sulfate) is added.

- **Isolation of Mitochondria from Cells and Tissues**
- Mitochondrial isolation protocols involve two processes – cell disruption to break open the cells and release the cellular structures, and differential centrifugation to recover fractions that are enriched for mitochondria

IN RAMAN IMAGING WE DO NOT NEED TO DISRUPT CELLS TO BREAK OPEN THE CELLS AND RELEASE THE CELLULAR STRUCTURES TO LEARN ABOUT THEIR BIOCHEMICAL COMPOSITION

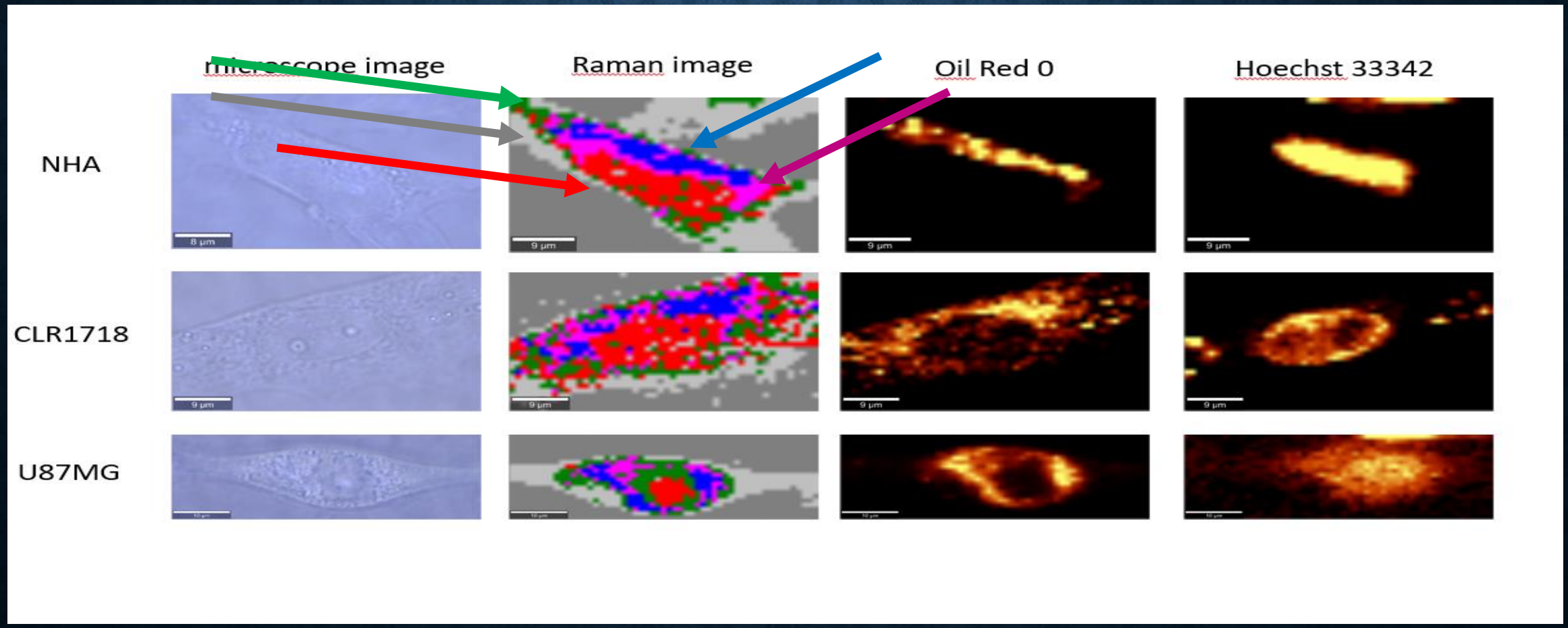

Abramczyk et al. LLSM, 2018

The real-time *in vivo* neurosurgical Raman system in our laboratory

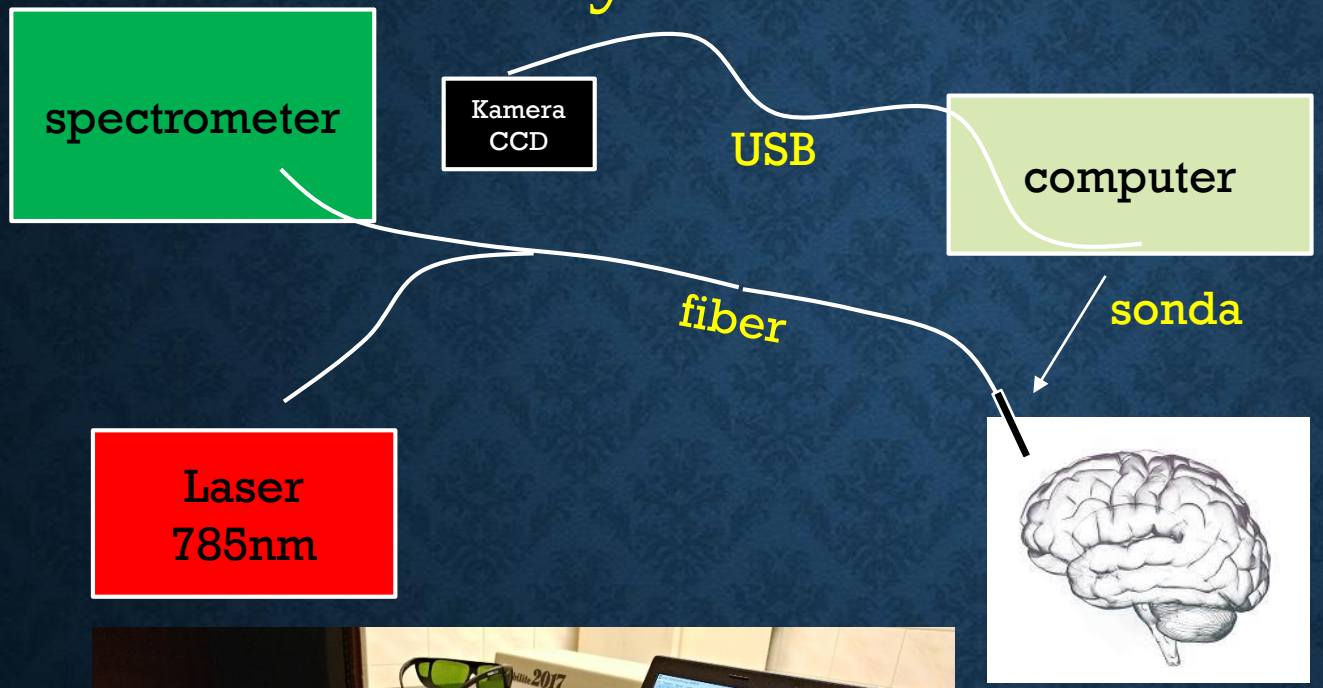

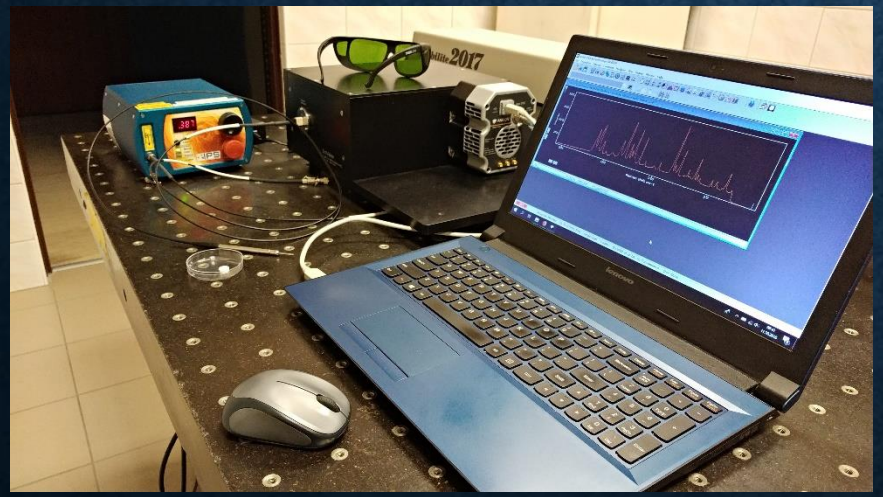

IN VIVO RAMAN OPTICAL BIOPSY ON RAT BRAIN IN LABORATORY OF LASER MOLECULAR SPECTROSCOPY

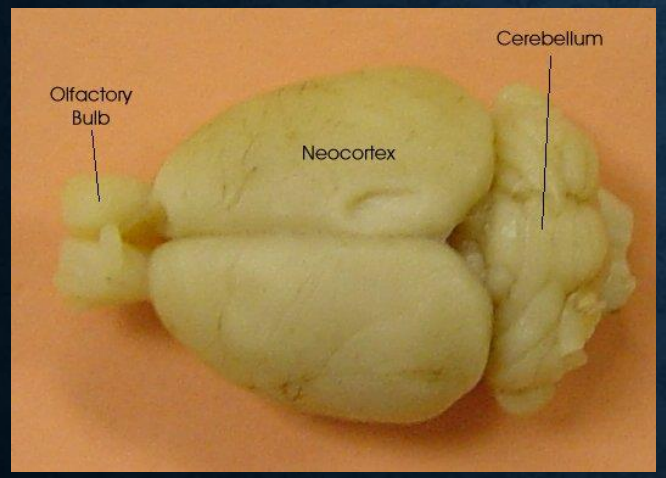

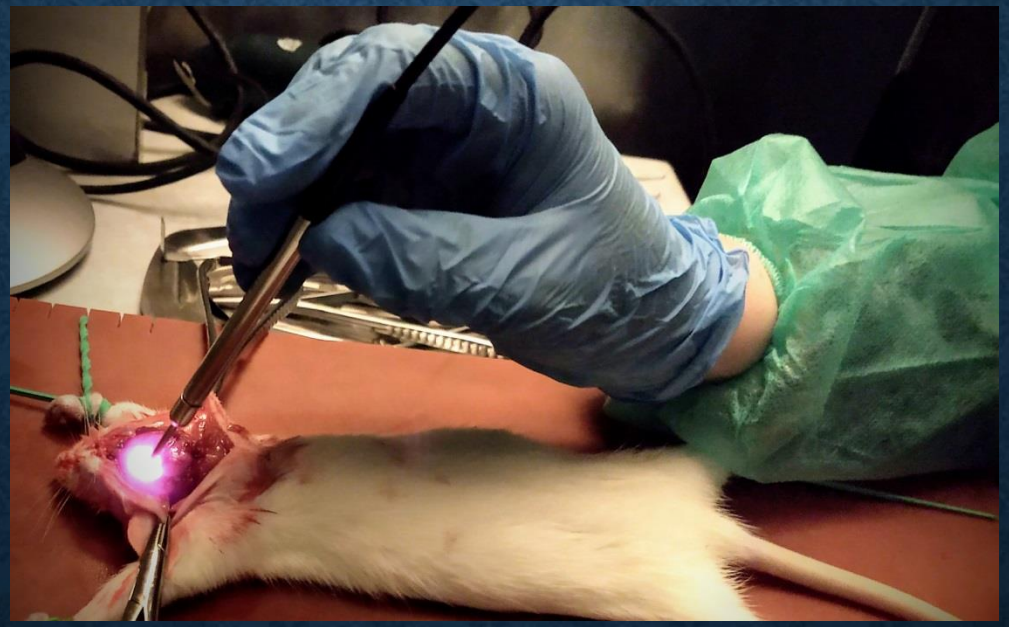

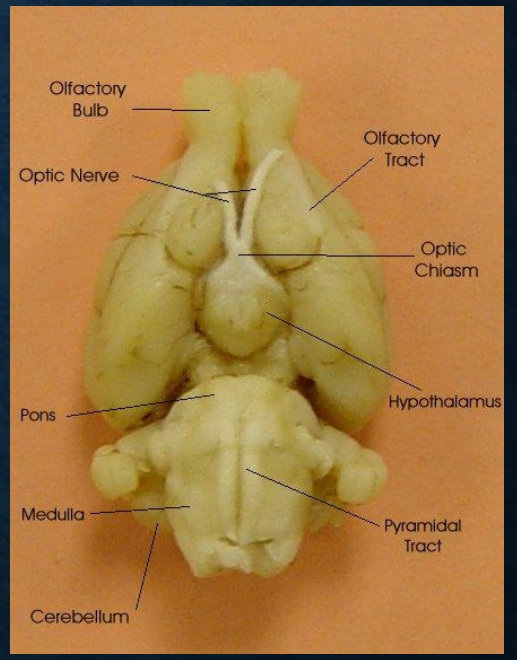

RAMAN SPECTROSCOPY GUIDES IN VIVO BRAIN OPTICAL BIOPSIES

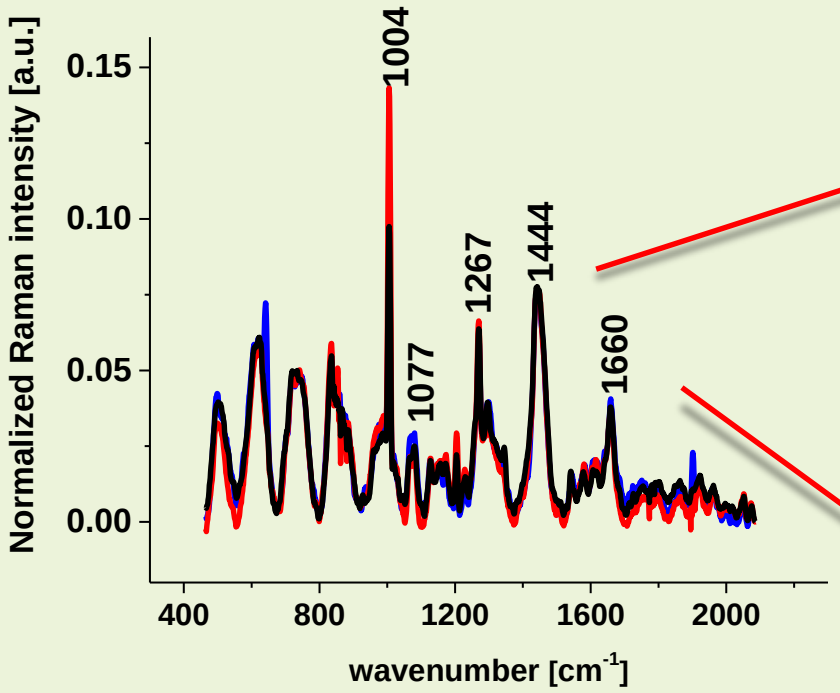

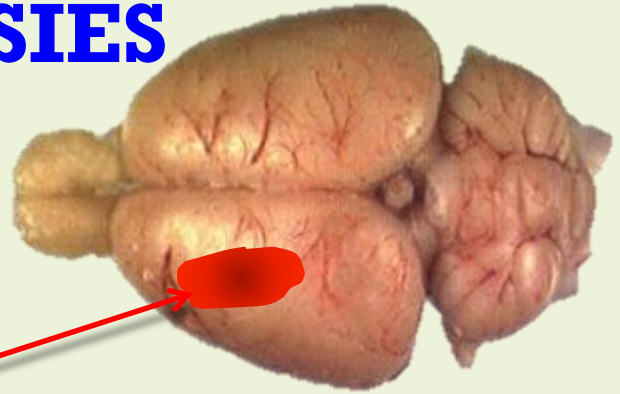

RAT BRAIN

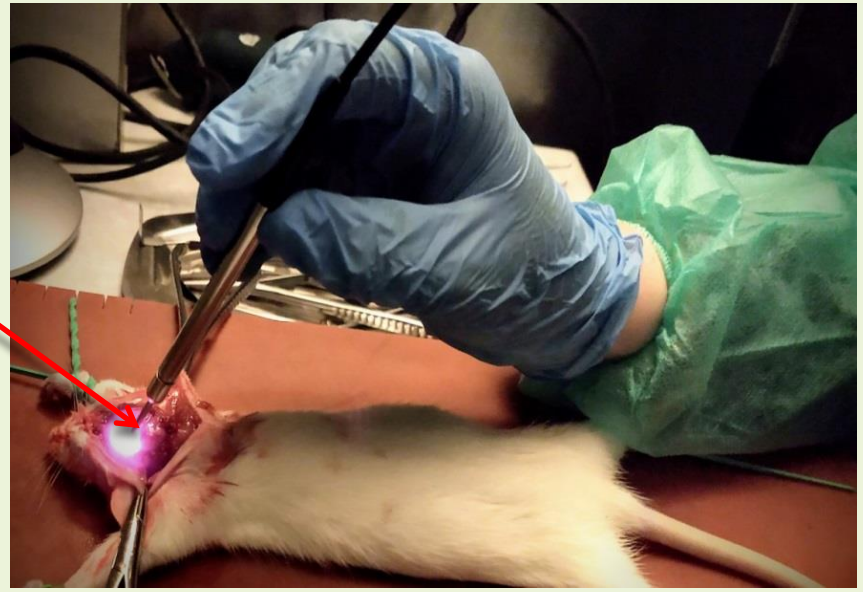

IN VIVO RAMAN OPTICAL BIOPSY IN RAT BRAIN IN LABORATORY OF LASER MOLECULAR SPECTROSCOPY

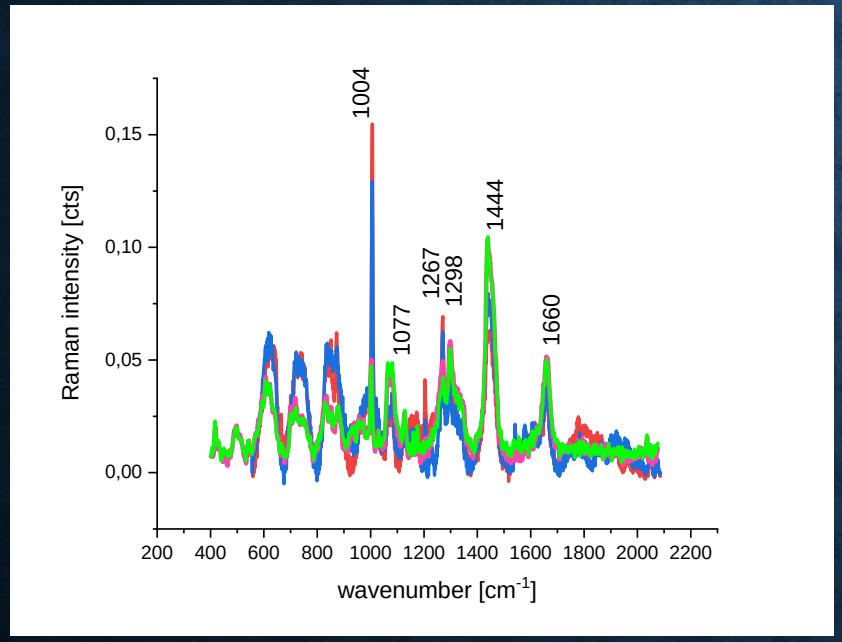

IN VIVO RAT BRAIN

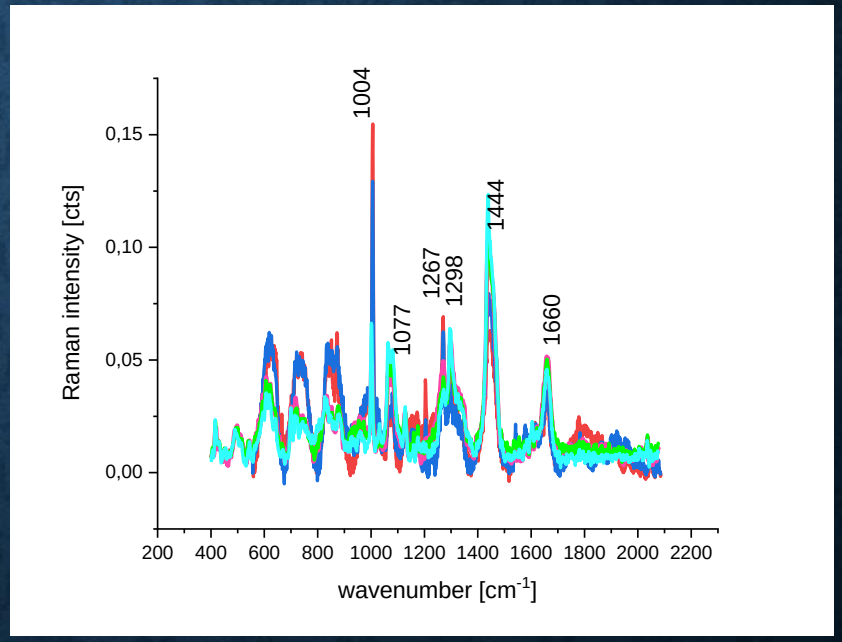

EX VIVO SWINE BRAIN

VISUALIZATION OF LIPISD DROPLETS CHEMISTRY

- While in some cases the morphology is a good indicator for metabolic changes in cells, it can be of equal importance to know cellular contents. In the case of LDs, changes in carbon saturation and chain length can be linked to diseases

TAG CHAIN LENGTH AND SATURATION MAPS IN SITU

- TAG saturation can be mapped in differentiated 3T3-L1 adipocytes from BCARS spectra using the ratio of 1650 cm-1 / 1450 cm-1 [232]. Di Napoli et al. show further that this ratio can be used both on phase-retrieved spectra and from raw CARS images along with 2930 cm-1 / 2885 cm-1 and 3010 cm-1 / 2855 cm-1 [233].

TAG CHAIN LENGTH AND SATURATION MAPS IN SITU

- The disadvantage of this ratio is that only one quantity for TAG chemistry, the number of double bonds, is determined while the chain length is not taken into consideration. In algae, it has been shown that the 1650 cm-1 / 1450
- cm- 1 from spontaneous Raman spectra can be correlated with number of double bonds and Nc=c/NCH2. This allows then the calculation of the chain length [235]. However, since the data is collected with spontaneous Raman spectroscopy, the measurements are slow causing low throughput.

TAG CHAIN LENGTH AND SATURATION MAPS IN SITU

- [232] H. A. Rinia, K. N. J. Burger, M. Bonn, and M. Müller, "Quantitative label-free imaging of lipid composition and packing of individual cellular lipid droplets using multiplex CARS microscopy.," Biophys. J., vol. 95, no. 10, pp. 4908–4914, 2008.
- [233] C. Di Napoli, I. Pope, F. Masia, P. Watson, W. Langbein, and P. Borri, "Hyperspectral and differential CARS microscopy for quantitative chemical imaging in human adipocytes," Biomed. Opt. Express, vol. 5, no. 5, pp. 1378–1390, 2014.
- [234] C. Di Napoli, I. Pope, F. Masia, W. Langbein, P. Watson, and P. Borri, "Quantitative Spatiotemporal Chemical Profiling of Individual Lipid Droplets by Hyperspectral CARS Microscopy in Living Human Adipose-Derived Stem Cells," Anal. Chem., vol. 88, no. 7, pp. 3677–3685, 2016.
- [235] H. Wu, J. V Volponi, A. E. Oliver, A. N. Parikh, B. A. Simmons, and S. Singh, "In vivo lipidomics using single-cell Raman spectroscopy.," Proc. Natl. Acad. Sci. U. S. A., vol. 108, no. 9, pp. 3809–14, 2011.
- [236] I. W. Schie, L. Nolte, T. L. Pedersen, Z. Smith, J. Wu, I. Yahiatène, J. W. Newman, and T. Huser, "Direct comparison of fatty acid ratios in single cellular lipid droplets as determined by comparative Raman spectroscopy and gas chromatography.," Analyst, vol. 138, no. 21, pp. 6662–6670, 2013. [

LIPID DROPLETS IN NORMAL MCF10A EPITHELIAL CELLS OF BREAST vs MILDLY MALIGNANT MCF7 AND AGRESSIVELY MALIGNANT MDA-MB-231

MCF10A - normal cells

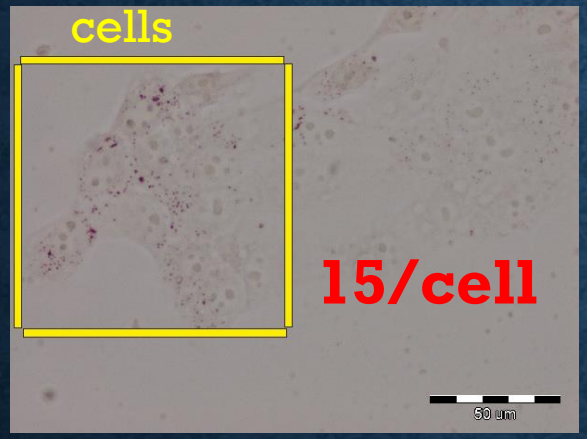

MCF7 - mildly malignant

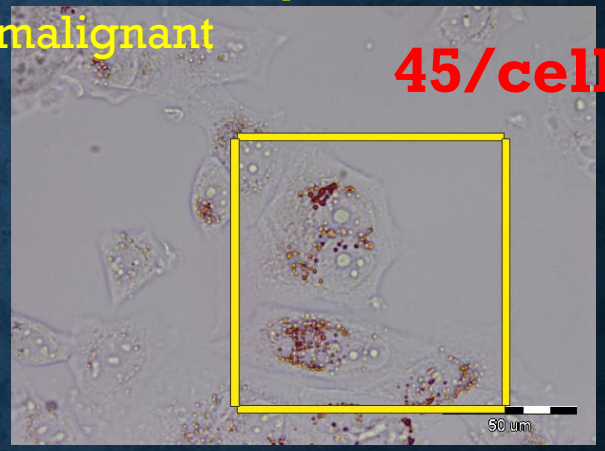

MDA-MB-231 - Agressively malignant

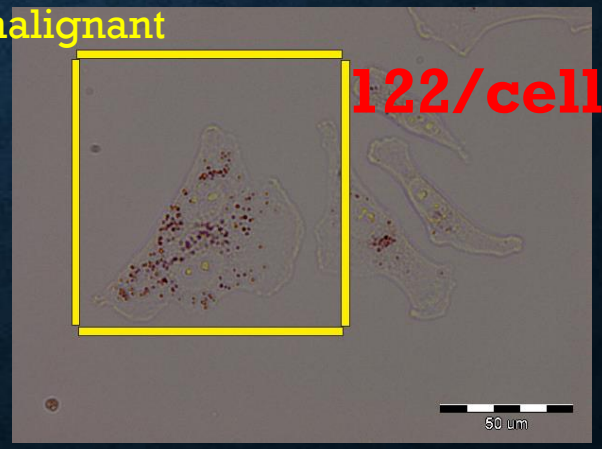

The goal of our study will be to assess the impact of cancer aggressiveness on the amount of cytosolic lipid droplets and their chemical composition in non-malignant and malignant human epithelial cell lines.

Abramczyk et al. Analyst, 2015

LIPID DROPLETS IN ASTROCYTES VS GLIOBLASTOMA U89

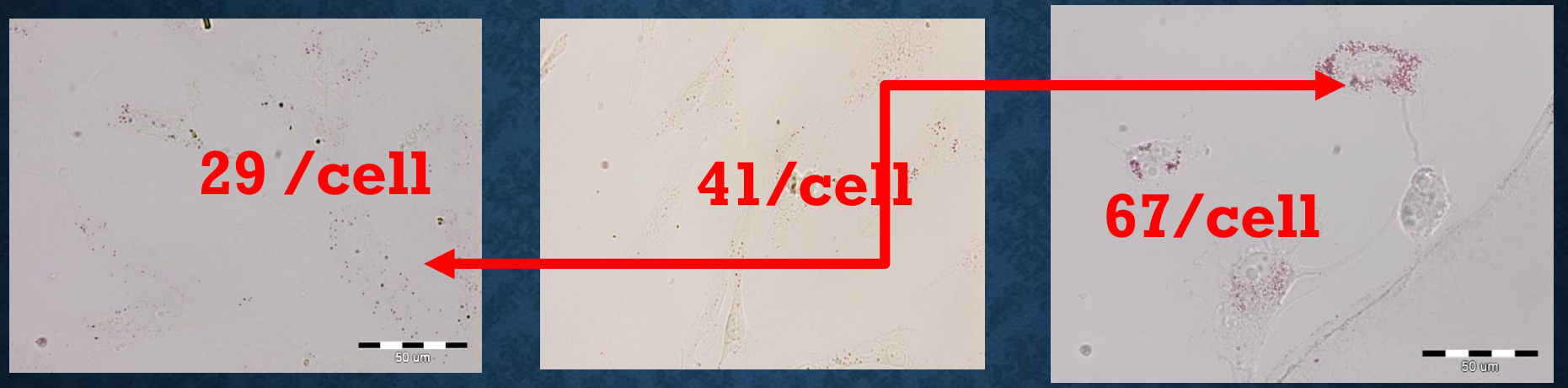

Astrocytes –normal cells

Astrocytoma –malignant cells

Glioblastoma U89- highly malignant cells

- Cancer cells contain increased numbers of lipid droplets compared with normal cells.
- Increased amount of lipid droplets correlates with increased aggressiveness of cancer.
- The increased amount of cytoplasmic lipid droplets in the human cancer cells may be closely related to increased rate of lipid synthesis in cancerous tissues.

Abramczyk et al. LLSM, 2018

THE SPATIAL DISTRIBUTION OF RETINOIDS IN NORMAL ASTROCYTES AND GLIOBLASTOMA CELLS

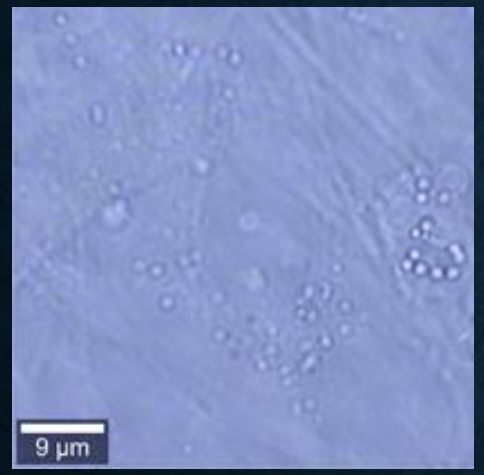

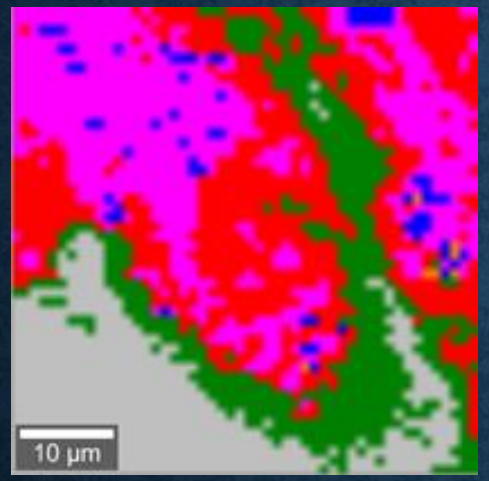

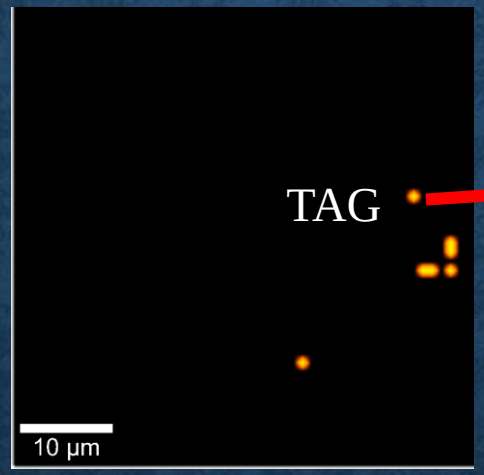

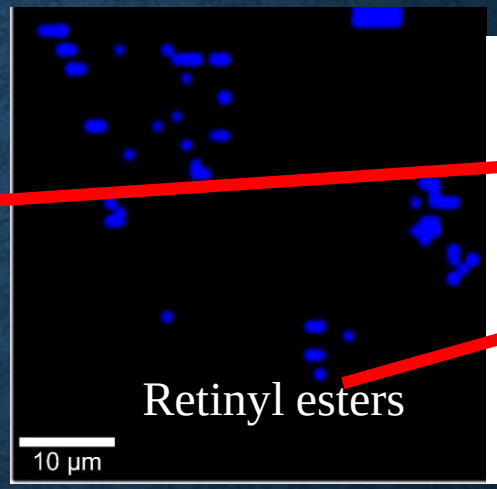

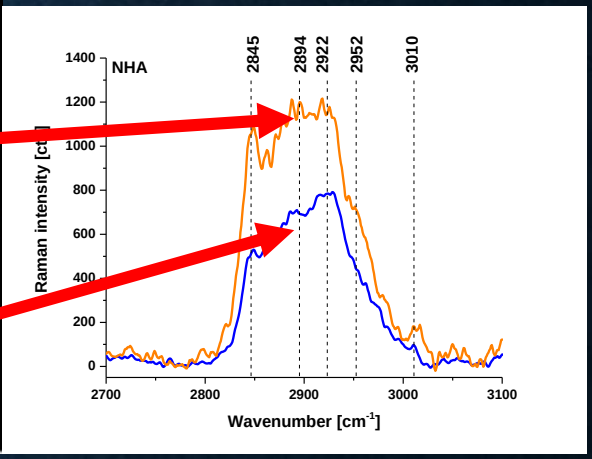

NORMAL ASTROCYTES

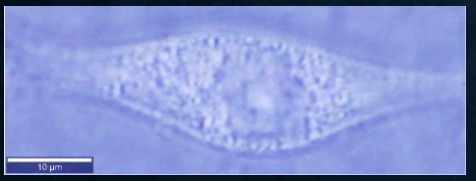

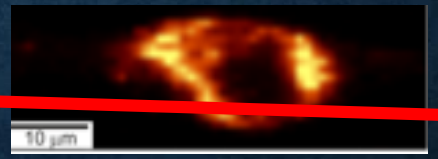

TAG

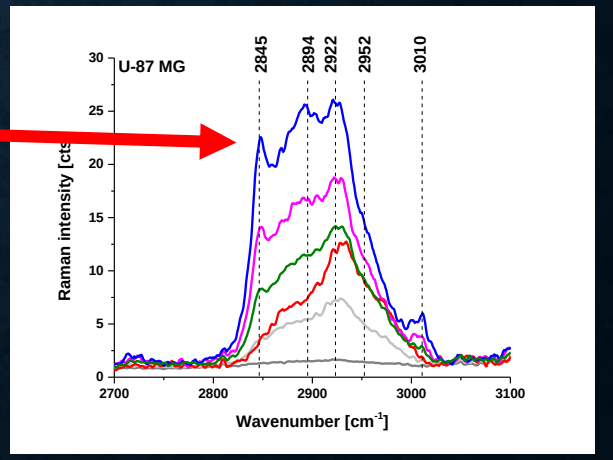

GLIOBLASTOMA

THE SPATIAL DISTRIBUTION OF RETINOIDS IN GLIOBLASTOMA CELLS: RETINOIDS IN MITOCHONDRIA, LIPID DROPLETS, NUCLEUS

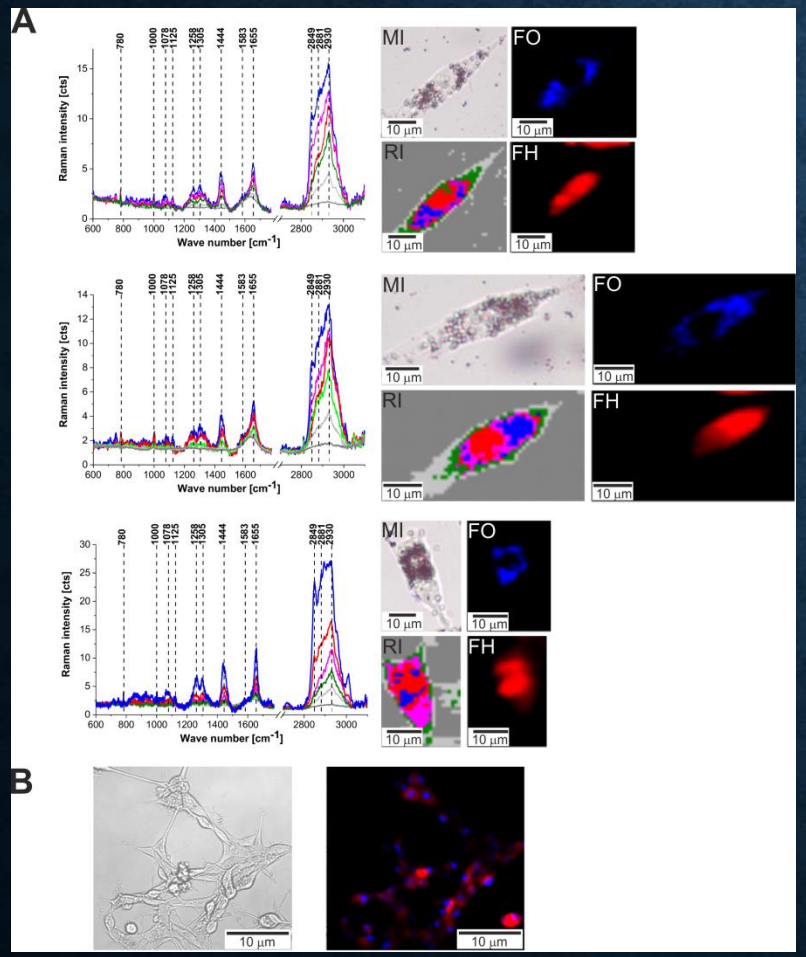

In Raman imaging we do not need to disrupt cells to break open the cells and release the cellular structures to learn about their biochemical composition in lipid droplets, nucleus, mitochondria

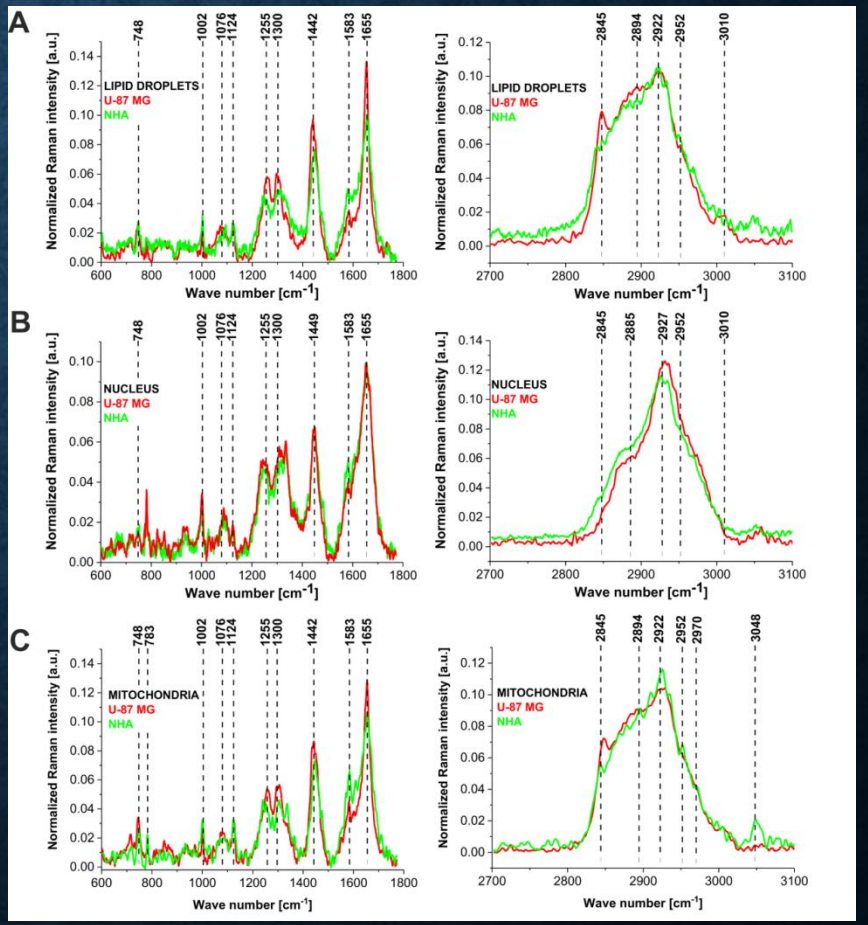

THE SPATIAL DISTRIBUTION OF RETINOIDS IN NORMAL ASTROCYTES AND GLIOBLASTOMA. RESONANCE RAMAN AND POLARIZATION SPECTRA

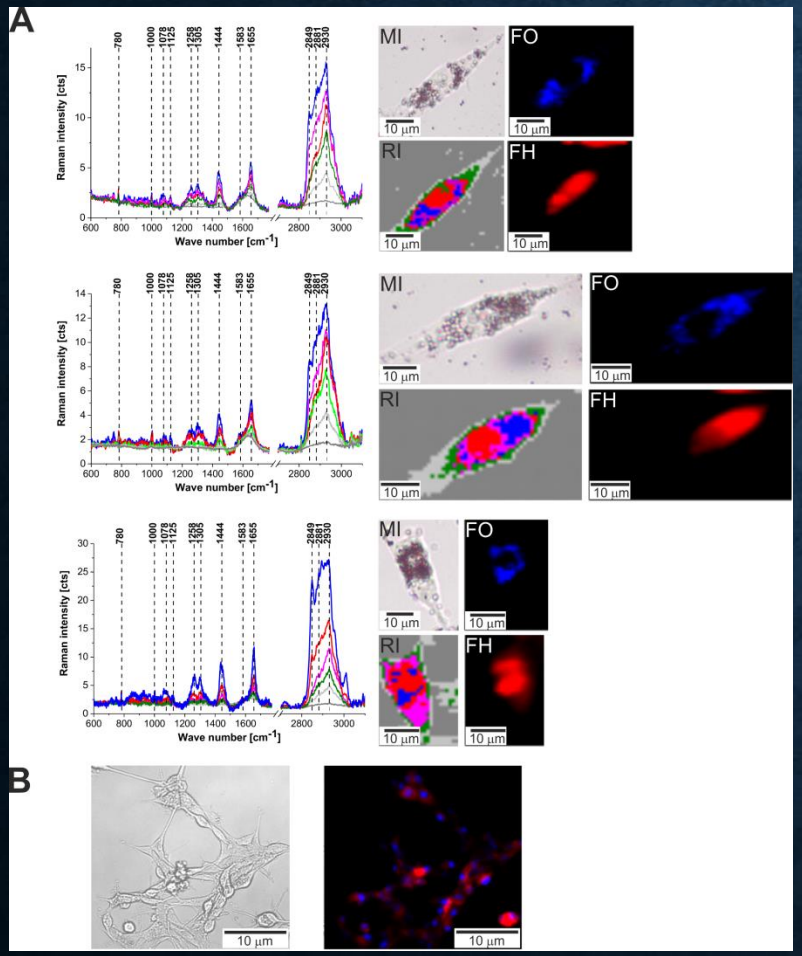

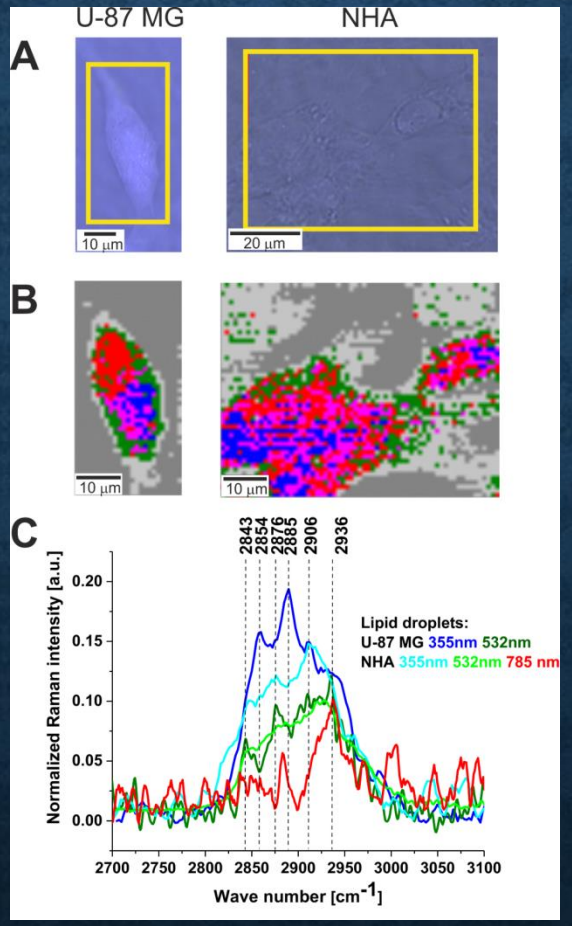

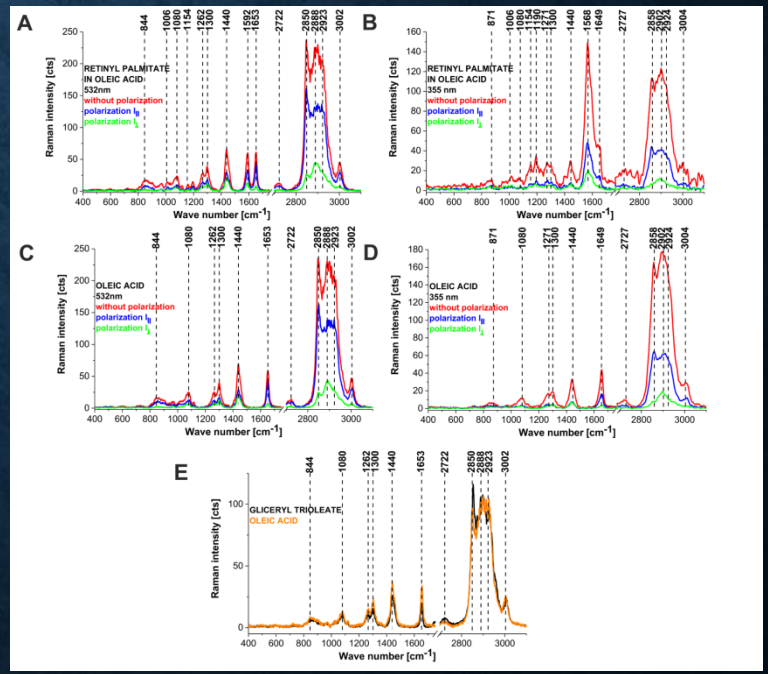

RAMAN IMIGINGTHE SPATIAL DISTRIBUTION OF RETINOIDS IN MEDULLOBLASTOMA (HUMAN BRAIN TISSUE) GRADE IV

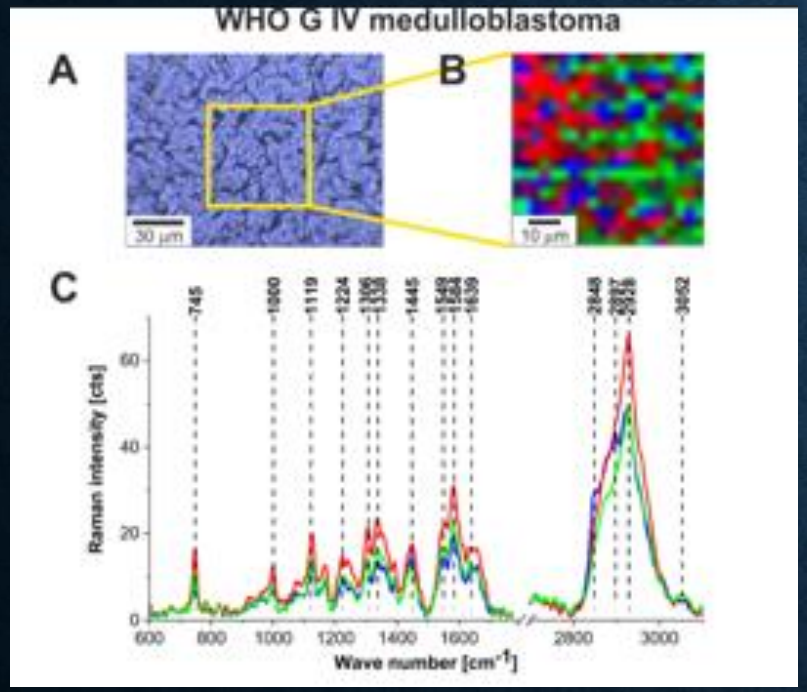

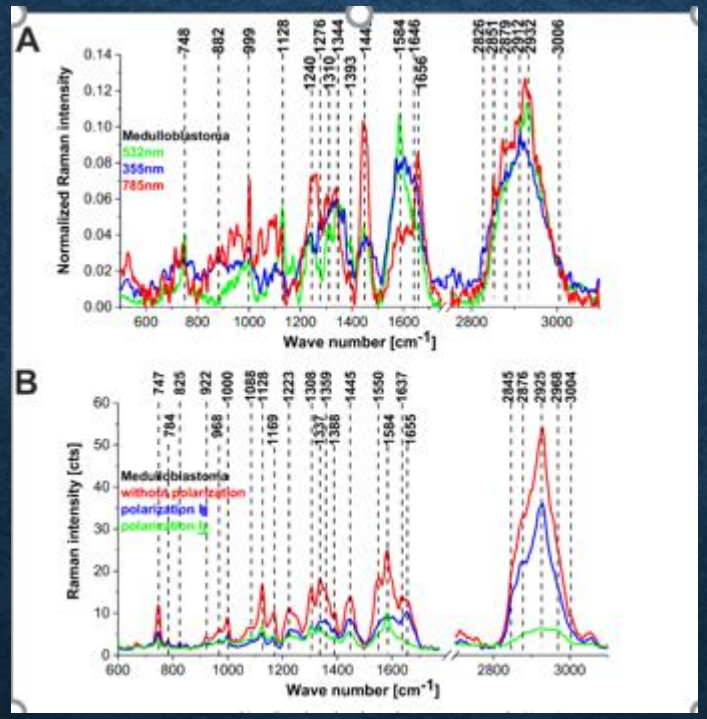

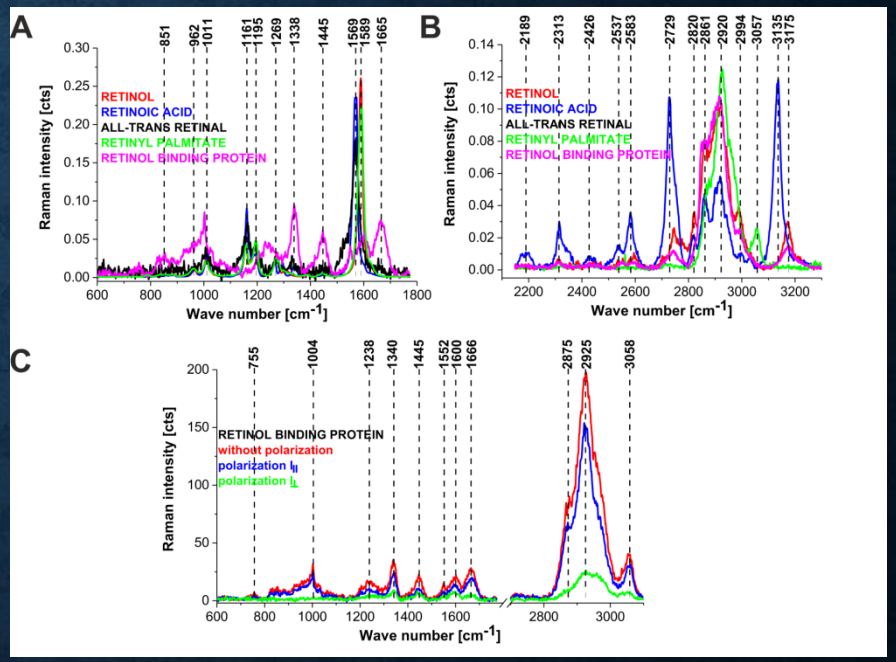

RAMAN AND MRI IMIGING THE SPATIAL DISTRIBUTION OF RETINOIDS IN ASTROCYTOMA (HUMAN BRAIN TISSUE) GRADE II/III

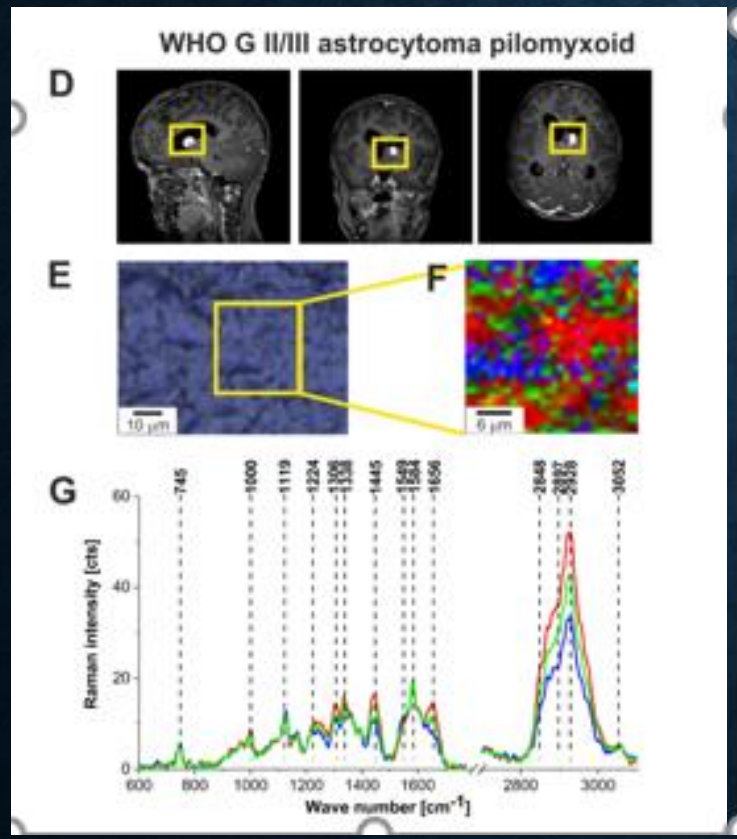

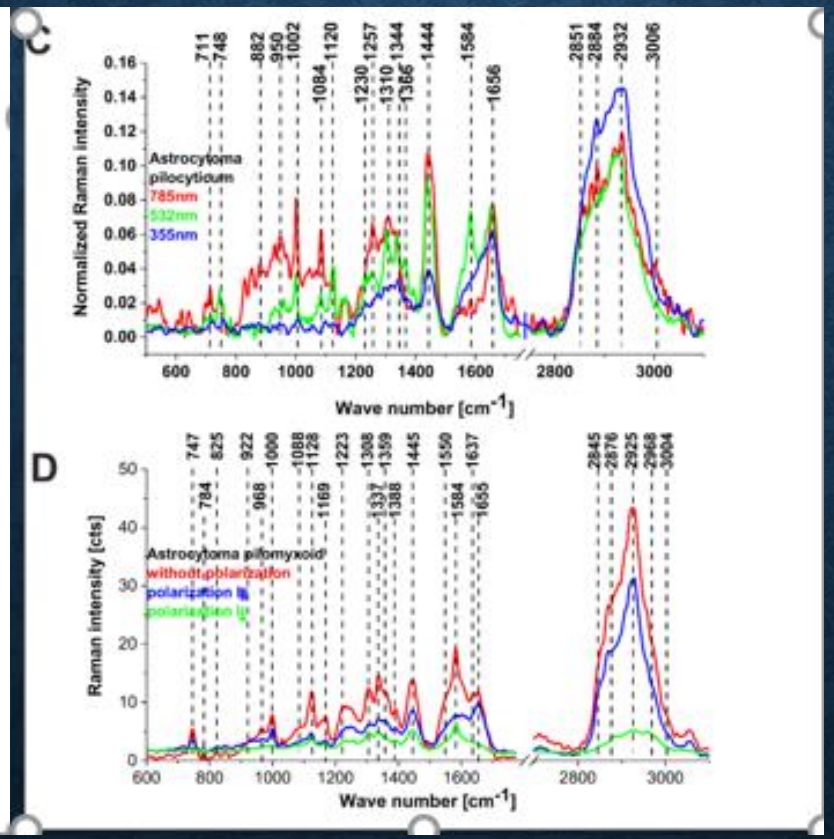

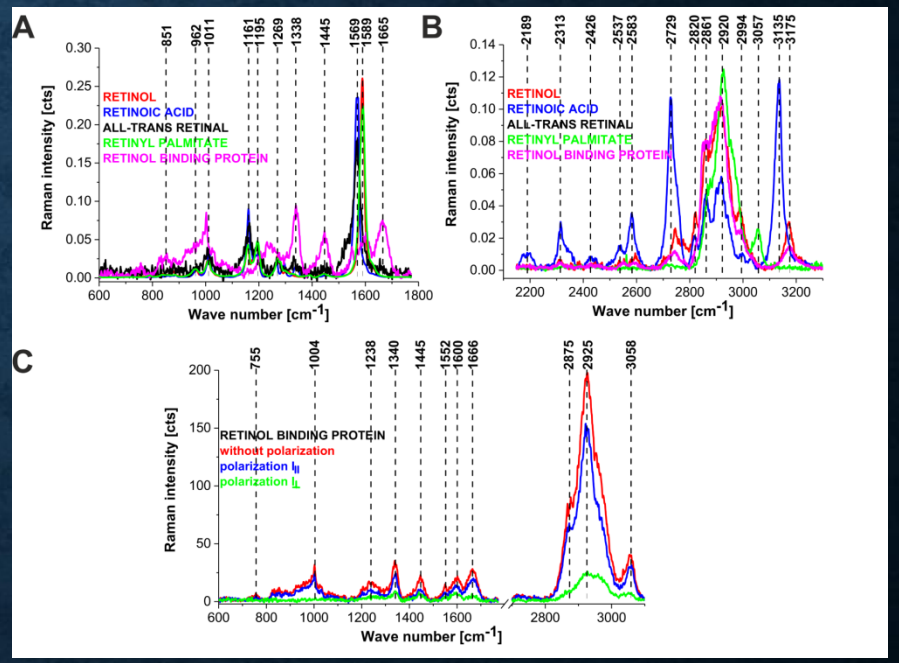

CONCLUSION

- Two types of lipid droplets in normal astrocytes and cancer cells of glioblastoma with distinct chemical compositions, biological functions and vibrational properties have been found.

- The two types of lipid droplets are related to different functions - energy storage and signalling. Their expression and biochemical composition depend on cancer aggressiveness.

- The first group is dominantly filled with TAGs and is involved in energy storage.
- The second group is mainly filled with retinyl esters and retinol binding proteins and is involved in signalling, especially JAK2/STAT6 pathway signalling.

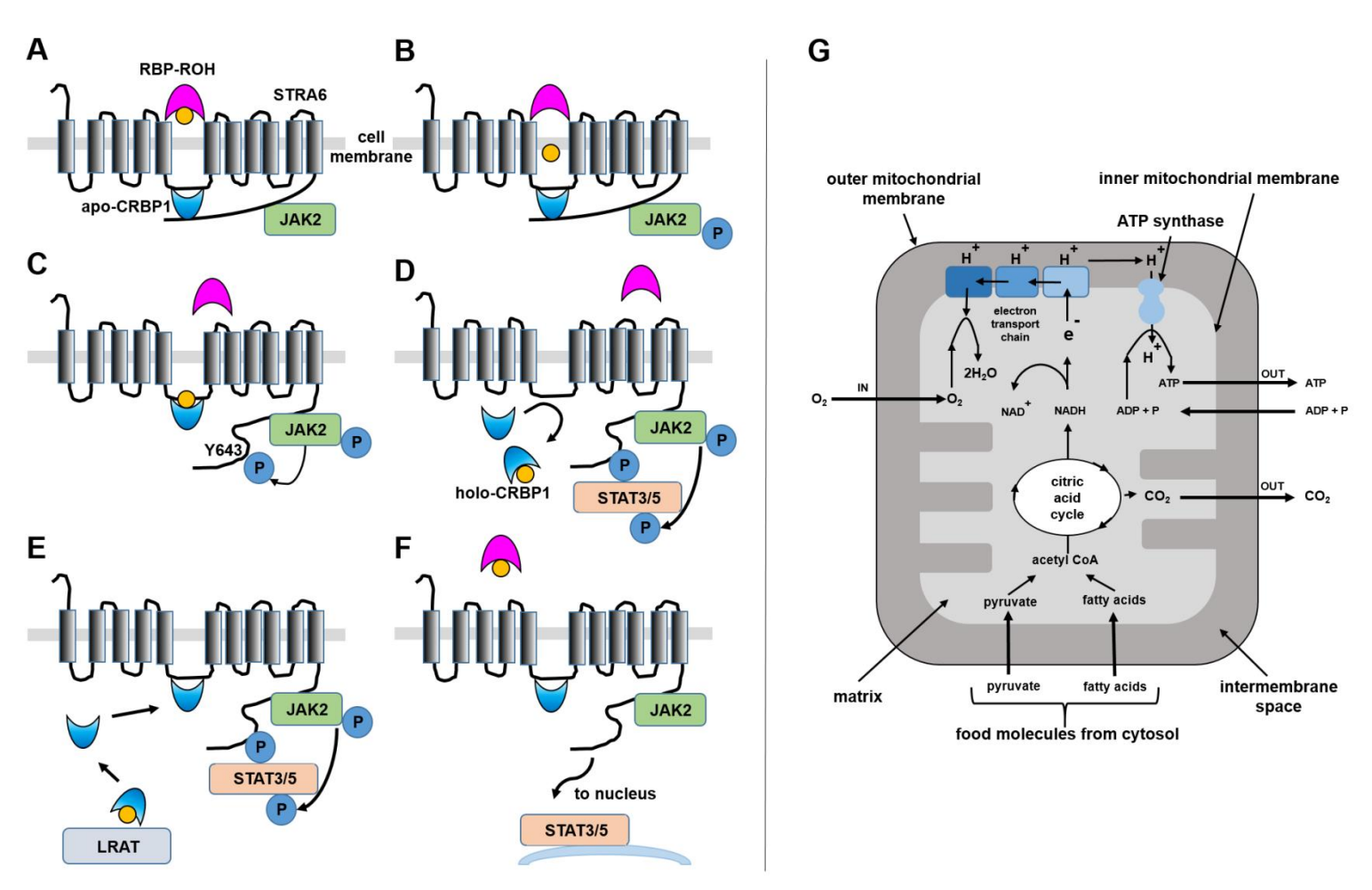

GENERAL CONCLUSION

Raman imaging, together with ultrafast time resolved spectroscopies are revealing functional aspects of retinoids at a new molecular level. These multidisciplinary approaches for free and protein bound retinoids combined with suitable cell cultures, ex vivo tissues, animal models can be especially helpful in translating these findings into therapeutic options for further development in animals and eventually in humans.

TIME RESOLVED SPECTROSCOPY AND STIMULATED RAMAN SPECTROSCOPY

stimulated Raman spectroscopy [158–161]. These methods should be able to help resolve the ongoing problems of understanding the pattern of carotenoid excited singlet states and their involvement in light harvesting. They should be able to resolve the key issues of which absorption changes reflect discrete electronic states and which come from different vibrational ones. Sorting this out will hopefully remove many of the current controversies.